

Università degli Studi di Pavia
Facoltà di Ingegneria
Corso di Laurea Specialistica in Ingegneria Biomedica
Universitat Politècnica de Catalunya

**CARDIOVASCULAR SYSTEM:
A ONE-DIMENSIONAL FLUID DYNAMIC
ANALYSIS USING FINITE ELEMENT METHOD**

Relatore: Chiar.mo Prof. Ferdinando Auricchio

Tutor UPC: Chiar.mo Prof. Eugenio Oñate Ibañez de Navarra

**Tesi di Laurea di:
Fabio MUSSI**

Anno Accademico 2004-2005

*Alla mia famiglia e a Maira,
luce e conforto nei momenti bui.*

This project has been realized at **CIMNE**, *Ciéntro Internátional de Metodos Numéricos en Ingeniería*, UPC, Campus Nord, building C1, C. Jordi Girona, 1-3. 08034 *Barcelona*, Spain
(Phone: 93 205 70 16 Fax: 93 401 65 17 E-mail: cimne@cimne.upc.edu
Web: <http://www.cimne.upc.es>)



Contents

1	Introduction	2
1.1	Cardiovascular System	4
1.1.1	Vascular system	4
1.1.2	Classification of arterial vessels	6
1.1.3	Function of arteries	7
1.1.4	Heart	10
1.2	Rheology of blood	12
1.3	Hemodynamics	14
1.3.1	The one-dimensional model	15
2	Problem formulation	18
2.1	Governing equations	18
2.1.1	Mass conservation equation	20
2.1.2	Momentum equation	21
2.2	Vessel wall mechanical modelling	24
2.3	The final model	26
2.4	Characteristic analysis	27
2.5	Boundary conditions	30
2.6	Numerical discretization	31
2.7	Bifurcation treatment	37
3	Implementation of the numerical solver	39
3.1	Geometry of the model	41
3.2	Definition of materials	42
3.3	Boundary and bifurcation conditions	42
3.4	General configuration of the problem	46
3.4.1	General data	46

3.4.2	Numerical integration data	48
3.5	The numerical solver	50
4	Numerical results	54
4.1	Inlet profiles	54
4.2	Case I: model of a single artery	55
4.3	Case II: 55 artery network	58
4.3.1	Terminal resistance	58
4.3.2	Ascending-descending aorta	61
4.3.3	Flow distribution	64
5	Conclusion and future prospects	70
A	The GiD software	72
A.1	GiD basics	73
A.2	Problem type customization	75
A.2.1	Configuration files	78
A.3	Post-process data files	80
B	Finite element code <i>Arteries-1D.exe</i>	81
B.1	Input-output data files	81
B.2	Finite element code flowchart	82
	Bibliography	90

List of Figures

1.1	Schematic representation of cardiovascular system, including arterial and venous circulations	4
1.2	Schematic representation of artery layers. From http://hemodynamics.ucdavis.edu/	5
1.3	Heart anatomy. Image taken from http://sci2135d1-pm68.morris.umn.edu/pzmyers/MyersLab/	10
1.4	Cardiac cycle notes. AV stands for atria-to-ventricles valves. Image taken from http://sci2135d1-pm68.morris.umn.edu/pzmyers/MyersLab/teaching/Bi104/	11
1.5	Relationship between shear rate and shear stress in a non-newtonian fluid	13
2.1	Sketch of a single compliant vessel	19
2.2	One-dimensional cylindric domain for a single arterial vessel and detail of the circular section $\mathcal{S}(t, z)$	19
2.3	Velocity profiles for blood flow in arteries considering several values of γ	22
2.4	Infinitesimal portion \mathcal{T} of Ω_c	23
2.5	Diagram of characteristics in the (z, t) plane. The solution on the point R is obtained by the superimposition of the two characteristics W_1 and W_2	29
2.6	Sketch of the two characteristics entering the domain.	31
2.7	One-dimensional linear mesh	33
2.8	Sketch of a 1D shape function	34
2.9	Domain decomposition for a generic bifurcation containing one inlet vessel and two outgoing vessels.	37
3.1	Flowchart describing the execution of a GiD problem type	40
3.2	Comparison between a 3D vessel geometry and the 1D representation used in GiD problem type	42
3.3	Scheme of a bifurcation containing three vessels. As we note each vessel has its own local reference axis (pink color), rotated with respect to the global reference system (red color).	45

3.4	GiD windows containing material properties. Left window: vessel types belonging to arterial network defined [25],[34] and [33]. Right window: customizable vessel with user-defined properties	46
3.5	Connectivities between the 55 main arteries of the human body. From [22]	47
3.6	GiD window for boundary conditions assignment.	48
3.7	Bifurcation assignment window	49
3.8	Inlet known pressure profiles. Left graph: polynomial-interpolated function based on physiological data. Right graph: half-sine wave profile. Data referred to a single cardiac cycle.	50
3.9	GiD general data window	50
3.10	Correspondence between 1D and 3D representation of a single vessel into GiD problem type.	51
3.11	Windows for the assignment of numerical analysis parameters.	52
3.12	GiD window for monitoring numerical calculation	53
4.1	Lower image: input flow rate profile for the 1D model. Upper image: flow rate profile out of the left ventricle. From http://www.zoo.ufl.edu/courses/pcb4723/	56
4.2	Result visualization through GiD post-process interface. In this case we consider mean sectional values of flow rate in a certain time instant.	57
4.3	Comparison between the solutions, related to blood flow propagation into a 80 cm length Thoracic aorta, obtained using straightforward Galerkin and Taylor-Galerkin schemes. We imposed a known pressure profile at the inlet and no terminal resistance has been applied.	58
4.4	Comparison between flow rate waveforms obtained using different velocity profiles; $\gamma = 2$ the parabolic one and $\gamma = 9$ for the power law profile. Taylor-Galerkin scheme applied. Again we imposed a known pressure profile at the inlet and no terminal resistance has been applied.	59
4.5	Scheme of the resistive model adopted to simulate reflecting outlet conditions	59
4.6	GiD representation of the 55 artery network	60
4.7	Flow rate values at four locations (A,B,C,D sections) in the aorta. Comparison between 1D-model profiles, obtained applying/not applying terminal resistance, and MRI imaging data.	62
4.8	Flow rate profiles at the root of the ascending aorta (section A).	63
4.9	Flow rate profiles at the top of the ascending aorta (section B).	63
4.10	Flow rate profiles in the aortic arch (section C).	64

4.11	Flow rate profiles in the beginning of the descending aorta (section D).	64
4.12	Flow rate profiles in Brachiocephalic artery (No. 3 in table 3.2).	66
4.13	Flow rate profiles in left carotid artery (No. 15).	66
4.14	Flow rate profiles in left subclavian artery I (No. 9).	67
4.15	Flow rate profiles in Thoracic Aorta (No. 18).	67
4.16	Flow rate profiles in abdominal aorta V (No. 41).	68
4.17	Flow rate profiles in right common iliac artery (No. 43).	68
4.18	Flow rate profiles in left common iliac artery (No. 42).	69
A.1	Flowchart describing the execution of a GiD problem type	76
A.2	Problem type flowchart including file configuration.	77
A.3	Interaction between pre process and solver by means of the template <code>.bas</code> file	79
A.4	Post-process file creation	80
B.1	Left figure: sketch of a 3D-mesh section. The number of radial nodes can be settled into GiD preprocess (see fig. 3.9 in chapter 3). Right figure: side wall meshing for a generic vessel. The element are triangular and link nodes belonging to different radial sections.	84

List of Tables

- 3.1 Physiological data of the 55 main arteries used in the one-dimensional model. From [34][25] and [33]. Part 1 of 2, vessels from 1 to 29 43
- 3.2 Physiological data of the 55 main arteries used in the one-dimensional model. From [34][25] and [33]. Part 2 of 2, vessels from 30 to 55 44

- 4.1 Values of terminal resistance for the 55 artery model. Data taken from [33]. 61
- 4.2 Table containing flow rate values for those arteries involved in the evaluation of blood distribution. 65

- B.1 Main program flowchart: input data are read and allocated in memory, while the definition of initial conditions allow to start calculating the approximated solution. 87
- B.2 Solver routine flowchart. 88
- B.3 Runge-Kutta and FEM routines 89

Chapter 1

Introduction

The correct blood circulation is a necessary condition for the adequate supply of oxygen and other substances to all tissues, which, in return, is synonymous with cardiovascular health, survival of surgical patients, longevity and quality of life. It is also well known that some very frequent cardiovascular diseases, like hypertension or congestive heart failure, are related to the behavior of blood flow. Diseases of the arterial wall, such as arteriosclerosis, are the leading cause of death in western society. Many studies have shown that there is a correlation between 'disturbed' blood flow patterns in large arteries and the development of arterial disease; however, the specific causative link between blood flow and arterial disease remain partially unknown. This is in part due to the significant complexity of arterial blood flow patterns.

It is therefore extremely important to obtain as many informations as possible about blood circulation and interactions that blood flow develops interacting with vessel walls. A powerful device is represented by the employment of mathematical models which may reproduce the characteristics of such a physical system at different levels of accuracy. On one hand we can obtain high levels of precision, e.g. through of three-dimensional blood flow models, but on the other hand it is useful to implement simplified models in order to study the pressure and flow rate propagation of blood through the circulatory system. Such models may be convenient because they allows both to reduce the computational costs and to consider a greater number of vessels into the models with respect to the 3D models.

The purpose of this project is to create a numerical solver in order to simulate the general patterns of pressure and blood flow waves that propagate into the cardiovascular system. To obtain such a result we used a simplified one-dimensional

formulation for the physical system governing the blood circulation into the main arterial vessels.

This project is organized as follows:

- In this chapter we will present general informations about the cardiovascular system physiology, describing heart and blood vessel main structures. Then we will focus on hemodynamics, explaining the functions of circulatory system and introducing the role played by computational models applied to blood dynamics; to this purpose we will briefly present the state of art concerning the one-dimensional formulation of blood flow in arteries;
- In Chapter 2 we will discuss the mathematical formulation of the 1D model for blood flow in arteries; first the equations related to the conservation of mass and momentum for a single one-dimensional vessel will be derived, together with an algebraic pressure-area relation and suitable boundary conditions. Then we will present the numerical space-time schemes for the discretization of such equations. Once the mathematical model for one single vessel has been obtained, we will apply it to the case of a vessel bifurcation.
- In Chapter 3 we will show how we implemented the one-dimensional model through a pre-post process FEM software, GiD¹: the numerical solver will be programmed in FORTRAN90 and then imported into a GiD problem type. Such a software will be used also for input data management and for the analysis of results;
- In Chapter 4 we will show the results obtained by numerical simulation of the 1D model using GiD and we will discuss what we have obtained comparing it with physiological data and other studies present in literature;
- In the appendices, we will give some notes about GiD, the software developed at CIMNE and used in this project to program the numerical solver for the one-dimensional blood flow model. Moreover we will present the FORTRAN90 source codes used to implement the FEM solver for the blood flow model.

¹GiD is an interactive graphical interface for definition, preparation and visualization of all the data related to a numerical solution. See Appendix A for details

1.1 Cardiovascular System

The cardiovascular system is the transport system of the body which, by means of blood, carries oxygen and nutrients to the body and carries away waste substances (e.g. carbon dioxide) to the kidneys for excretion; it is composed by a pulsatile pump, the *heart*, and a branched network of vessels, the *vascular system*, which drive blood through tissues and organs.

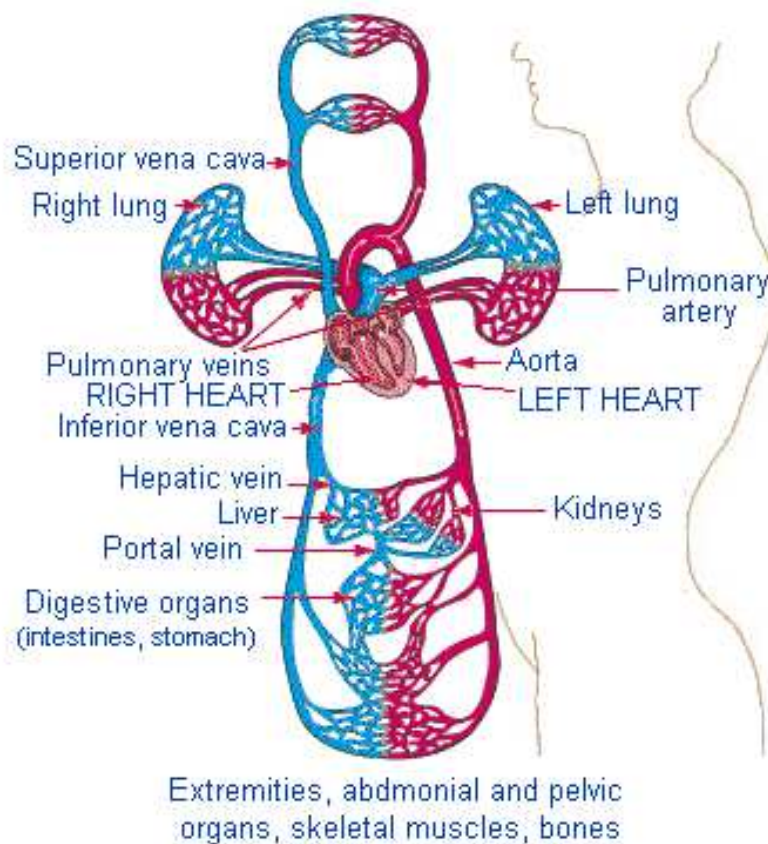


Figure 1.1: Schematic representation of cardiovascular system, including arterial and venous circulations

1.1.1 Vascular system

Vascular system can be divided in two kinds of vessel: arteries and veins. The former pumps blood away from the heart, while the latter carries blood toward the heart. Arteries (fig.1.2) are often classified relating to their tasks and main tissue

components. The biggest arteries in the circulatory system are called *conduction* or *elastic arteries*; average size arteries are called *muscular* or *distribution arteries*, whilst the smallest ones are defined as *arterioles*. Veins classification is generally based only on the vessel dimension and includes *small veins*, *average dimension veins* and *large veins*.

A complete but very thin squamous epithelial cell layer, called *endothelium*, covers both heart internal surface (so called *cardiac endothelium*) and vessels internal coating (*vascular endothelium*). The subdivisions of veins and arteries present different quantities of smooth muscular and connective tissue, organized in specific layers that can vary depending on the class of vessels considered.

The most internal layer of arteries and veins the *tunica intima*. It is composed by a continuous lining of endothelium (simple squamous epithelium), which contains a thin connective tissue layer (sub-endothelial connective tissue) adjoint with endothelium. Sometimes in this case we can find a certain thickness layer composed by an elastic fibre provided with little gaps (*internal elastic lamina*). The intermediate layer, called *tunica media*, is usually the thickest of the three layers and is typically composed by smooth muscular (especially in arteries), elastic fibres, collagen fibres, amorphous intracellular substances and cells that produce such materials. The external layer, called *tunica adventitia*, is an outer connective tissue sheath, but also can contain smooth musculature in bigger veins. In this case the connective tissue is composed by collagen fibres, elastic fibres, intracellular substances and cells that produce such materials.

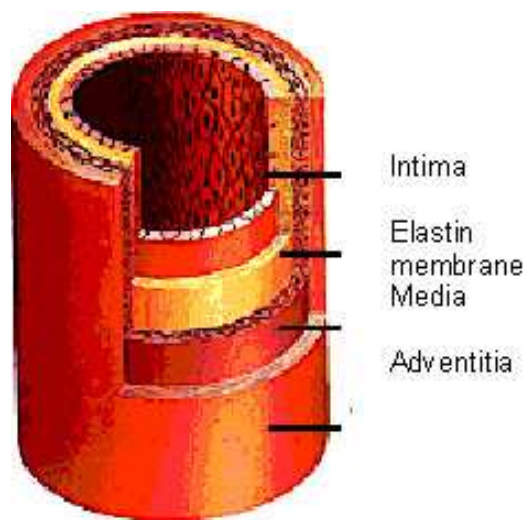


Figure 1.2: Schematic representation of artery layers. From <http://hemodynamics.ucdavis.edu/>

1.1.2 Classification of arterial vessels

Conducting or elastic arteries

They are large vessels, with very strong and relatively elastic walls, whose function is to drive the bulk of blood outgoing from the heart to the regions of the body where it has to be distributed.

Such vessels must withstand a great head of pressure to pump blood against the peripheral system resistance caused by the distal arterial network. Then the elastic fibers composing the wall allow some stretching and narrowing of the vessel in response to the incoming pressure, and the collagen fibers limit the stretch permitted.

Elastic arteries include aorta, pulmonary arteries, common carotid, subclavian artery and common iliac arteries. The lumen of such arteries is very large but their walls appear to be very thin compared to the vessel diameter (ratio about 1:10).

Distribution or muscular arteries

Once the blood has reached the region of distribution (e.g. the limbs) it will be handled by smaller, but still fairly large, *distribution* or *muscular* arteries, which send it to the next sub-regions composed by smaller arteries.

Such vessels, like femoral, renal and ulnar arteries, are mainly composed by smooth musculature with smaller quantities of elastic tissue; the smooth muscle of the wall makes them very extensible, and also provides for a counter force to be exerted. In fact as the vessel expands, smooth muscle cells are stretched; reacting to this they begin to contract.

The contraction mechanism of the conduction arteries dampens out the pulsations of the flow to provide a steady supply of blood at normal pressure into the following arterial bed composed by arterioles and capillaries.

Arterioles

Arterioles represent the smallest branches in the arterial network. Given that the transition between different artery types is gradual and not the same for all the situations, researchers have come to set several definitions of an arteriole. Some of them define it as an artery with a diameter equal or less than $300\ \mu\text{m}$ having one, three or four smooth muscular cell layers, which are disposed in a circular way into

the tunica media. Other researchers sustain that arterioles have a diameter included from 40 to 200 μm and they use also the ratio between wall thickness and lumen diameter as a tool to define an arteriole: in normal conditions this ratio is about 1:2.

The arterioles offer a considerable resistance to blood flow because of the decreasing of section with respect to the upstream vessels. This area of high resistance to the blood flow serves several functions: first, together with the conduction arteries, it converts the pulsatile ejection of blood from the heart into a steady flow through the capillaries; second, if no resistance were present and a high pressure persisted into the capillary bed, there would be a considerable loss of blood volume into the tissues because of the exchange of fluid across the capillary walls.

Capillaries

Capillaries are blood vessels without any kind of covering and are simply shaped as endothelial pipes. The surface area of capillaries, in human beings, is about 6000 m^2 . They usually have a diameter between 7 and 10 μm , barely sufficient as leukocytes and erythrocytes could flow through the vessel lumen. The total area of a capillary transversal section is about 800 times greater than the aorta transversal section. The flow through capillaries is about 0.4 mm/sec compared with the 320 mm/sec flow evaluated into the aorta. Pressure in capillaries can reach values up to 35 mm Hg in arterial tips but can decrease up to 10 mm Hg in venous tips.

1.1.3 Function of arteries

As already written, the different types of artery in the vascular system have a different amount of elastic tissue; for this reason the vessel stiffness, expressed by the elastic modulus is not the same in every vessel.

Applied to the wall of an artery, this infers a structural property. The functional consequence of having elastic tissue in the wall is that these arteries can expand to accommodate added volume. This behaviour of the vessel walls reflects itself on the pressure and flow waves of blood during circulation into the vascular system.

The pressure in a vessel, for example the aorta, significantly changes with increasing distance from the heart. The peak of the pressure pulse delays downstream indicating wave propagation along the aorta with a certain wave speed. Moreover,

the shape of the pressure pulse changes and shows an increase in amplitude, a steepening of the front and only a moderate fall of the mean pressure.

This wave phenomenon is a direct consequence of the distensibility of the arterial wall, allowing a partial storage of the blood injected from the heart due to an increase of pressure and the elastic response of the vessel. The cross-sectional area of the vessels depends on the pressure difference over the wall. This pressure difference is called the *transmural pressure* and can be denoted by p_{tr} . This transmural pressure consists of several parts. First, there exists a hydrostatic component proportional to the blood density ρ , the gravity acceleration g and the height h . Next, a time dependent part p_0 and a periodic time dependent part, $p \sim$. So, the transmural pressure takes the following form

$$p_{tr} = \rho gh + p_0 + p_{\sim} \quad (1.1)$$

The relationship between transmural pressure and cross-sectional area A of the vessel is in most cases non-linear and may be rather complicated. Moreover it varies from one vessel to the other. For negative transmural pressure values the vessel can even collapse. Important quantities with respect to this relationship are the *compliance* or alternatively the *distensibility* of the vessel. Compliance may be defined as the partial derivative between the cross-sectional area A and pressure p :

$$C = \frac{\partial A}{\partial p} \quad (1.2)$$

The distensibility D is defined as the ratio of the compliance and the cross-sectional area and hereby is given by:

$$D = \frac{1}{A} \frac{\partial A}{\partial p} = \frac{C}{A} \quad (1.3)$$

For thin walled tubes, with radius a and wall thickness h , without considering longitudinal strain, distensibility can be derived as follows:

$$D = \frac{2a}{h} \frac{1 - \sigma^2}{E} \quad (1.4)$$

where σ denotes the Poisson ratio and E the Young modulus. From 1.4 we can see that besides the properties of the vessel material (E, σ) also its geometrical properties (a, h) play an important role.

The flow is driven by the pressure gradient and hereby determined by the propagation of the pressure wave. Normally the pressure wave may have a pulsating progress. In order to describe such flow phenomena it can be possible to make a distinction between *steady* and *unsteady* part of the considered pulse. Assuming that

the unsteady part can be described by means of linear theory, we can introduce the concept of pressure and flow waves which are superpositions of several harmonics:

$$p_{\sim} = \sum_{n=1}^N p_n e^{ni\omega t} \quad Q_{\sim} = \sum_{n=1}^N Q_n e^{ni\omega t} \quad (1.5)$$

Here p_n and Q_n are the complex Fourier coefficients and hereby p_{\sim} and Q_{\sim} are the complex pressure and the complex flow, σ denotes the angular frequency of the basic harmonic. Actual pressure and flow can be obtained by taking the real part of these complex functions. Normally spoke 6 to 10 harmonics are sufficient to describe the most important features of the pressure wave.

As mentioned before the blood flow is driven by the force acting on the blood induced by the pressure gradient. The relation of these forces to the resulting motion of blood is expressed through the *longitudinal impedance*:

$$Z_l = \frac{-\frac{\partial p}{\partial x}}{Q} \quad (1.6)$$

The longitudinal impedance is a complex number defined by complex pressures and complex flows. It can be calculated by frequency analysis of the pressure gradient and the flow that have been recorded simultaneously. As it expresses the flow induced by a local pressure gradient, it is a property of a small (infinitesimal) segment of the vascular system and depends on local properties of the vessel. The longitudinal impedance plays an important role in the characterisation of vascular segments. It can be measured by a simultaneous determination of the pulsatile pressure at two points in the vessel with a known small longitudinal distance apart from each other together with the pulsatile flow.

A second important quantity is the *input impedance* defined as the ratio of the pressure and the flow at a specific cross-section of the vessel:

$$Z_i = \frac{p}{q} \quad (1.7)$$

The input impedance is not a local property of the vessel but a property of a specific site in the vascular system. If some input condition is imposed on a certain site in the system, then the input impedance only depends on the properties of the entire vascular tree distal to the cross-section where it is measured and is often referred to as a characteristic impedance. In general the input impedance at a certain site depends on both the proximal and distal vascular net.

The compliance of an arterial segment is characterized by the *transverse impedance* defined by:

$$Z_t = \frac{p}{\frac{\partial Q}{\partial x}} = -\frac{p}{\frac{\partial A}{\partial t}} \quad (1.8)$$

This quantity expresses the flow drop due to the storage of the vessel caused by the radial motion of its wall (being A the cross-sectional area) at a given pressure.

1.1.4 Heart

The heart is the muscular organ of the circulatory system; approximately the size of a clenched fist, it acts as a double pump driving blood, feeding and wasting products along the two distinct circulations, the *pulmonary circuit* and the *systemic circuit* (see figure 1.1). In order to maintain these two circuits separate, heart is divided in two distinct parts, each one having two chambers (fig. 1.3).

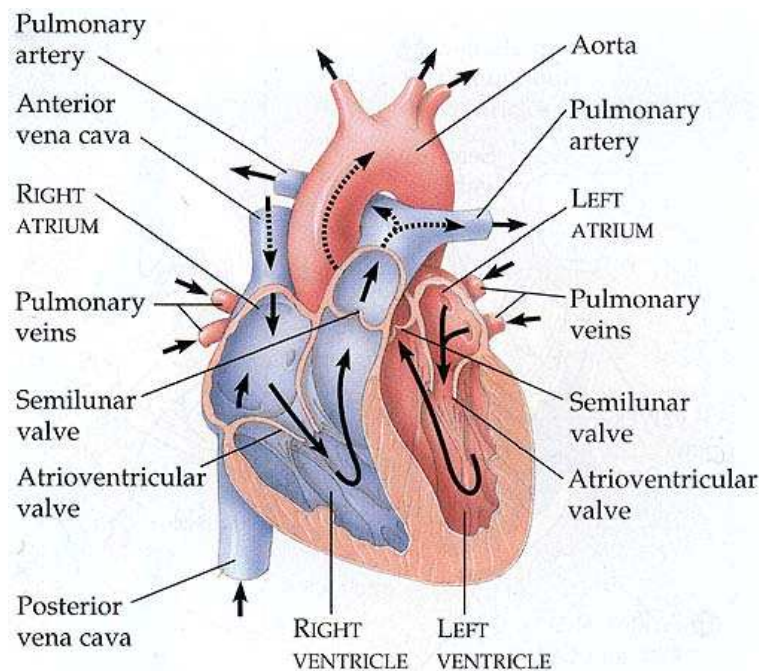


Figure 1.3: Heart anatomy. Image taken from <http://sci2135d1-pm68.morris.umn.edu/pzmyers/MyersLab/>

The right side of the heart has to pump blood, through the vessels belonging to the *pulmonary circuit*, to oxygenate blood in lungs. Left side of the heart provide the blood pumping to the vessels which compose the *systemic circuit*.

Blood pumping is provided through the alternation of a contraction phase, called *systole*, with a relaxation phase, the *diastole*; the repetition of these two phases rep-

resents a *beat* or *cardiac cycle* (fig.1.4), which is the simplest parameter to evaluate the heart activity. The average pumping rate of the left ventricle is about 70 bpm (beats per minute), which corresponds to a period of about 0.85 seconds for each cardiac cycle.

Since each side of the heart has an atrium and a ventricle, we have two valves for each side, an inlet one and an outlet one. Venous blood comes to the right atrium from the two cava veins, the superior vein and the inferior vein. Then blood flows through *tricuspid valve* into the right ventricle, where is pumped during systole phase trough another valve, the *semi-lunar valve*, and goes along pulmonary arteries finally reaching lungs. Oxygenated blood then returns from lungs to the left atrium passing trough the pulmonary veins; once the atrium is filled, the *mitral* or the *bicuspid valve* opens and blood can reach the left ventricle. From this location blood passes through the aortic *semilunar valve* and enters the aorta where it will be distributed to the whole body going along the systemic circulation.

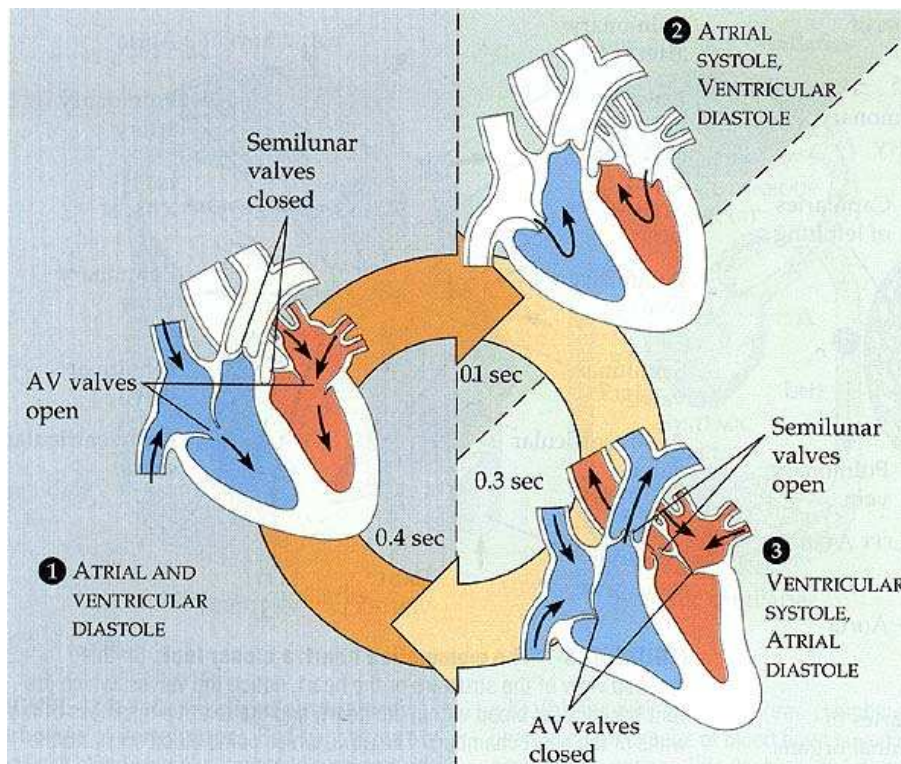


Figure 1.4: Cardiac cycle notes. AV stands for atria-to-ventricles valves. Image taken from <http://sci2135d1-pm68.morris.umn.edu/pzmyers/MyersLab/teaching/Bi104/>

1.2 Rheology of blood

Blood volume is composed by formed elements (about 45%) and *plasma* (about 55%). The plasma is a diluted electrolyte solution containing about 8 percent by weight of three major types of proteins: fibrinogen, globulin and albumin in water. Fibrinogen is involved in blood coagulation through a process of polymerization that transform fibronogen into fibrin. Globulin is a carrier of lipids and other water soluble substances and also contains antibodies that resist from the attacks of bacteria and virus. Albumin is the main contributor to the total colloid osmotic pressure of plasma and play an important role in the balance of water metabolism.

The formed elements in blood consists of 95% red blood cells, 0.13% white blood cells and about 4.9% platelets. The white blood cells, also known as leucocytes consist of monocytes, lymphocytes, and basophils. Monocytes that leave the circulation and enter the tissues develop into macrophages. Neutrophils, monocytes, and macrophages are collectively known as phagocytes since they can engulf and ingest bacteria and other foreign particles. Platelets are cells without a nucleus; they can repair the damaged vessel walls and also can help blood through thrombus formation. The majority of the formed elements are red blood cells that consist of hemoglobin surrounded by flexible red cell membrane. The primary function of hemoglobin in the red blood cell is to transport oxygen from the lungs to the living tissue of the body.

Because of its heterogeneous composition, blood rheology, that is the relationship between the strain and stress tensors, is hard to define. In fact rheologic behaviour of blood depends on several factors like pressure, temperature, and vessel geometry which values can vary in time; moreover the effects caused by trauma or inflammatory processes can change even more the normal behaviour of blood flow. Several studies have been made in order to give a mathematical description of blood behaviour; we may now consider its main characteristic.

Indicate with \mathbf{T} the stress tensor and with \mathbf{D} the strain tensor: $\mathbf{D} = [D_{ij}] = [\frac{1}{2}(u_{i,j} + u_{j,i})]$, where \mathbf{u} is the fluid velocity field. We can define the constitutive relationship between \mathbf{T} and \mathbf{D} as follows:

$$\mathbf{T} = -p\mathbf{I} + \mathbf{S}(\mathbf{D}) \quad (1.9)$$

where \mathbf{I} is the identity Kronecker tensor, p is the pressure, $p\mathbf{I}$ is the *isotropic* stress tensor component and $\mathbf{S}(\mathbf{D})$ is the *deviatoric* component. If the relationship between

\mathbf{S} and \mathbf{D} is linear, and \mathbf{S} takes zero values when the fluid is at rest, then we have a *newtonian* fluid. However in generic conditions this relationship is not linear and the deviatoric component does not vanish if the fluid has zero velocity. In this case we assume the fluid as *non newtonian* and it has the following characteristic:

For what concerns the blood we can expose its main rheological characteristics as follows:

Pseudo-elastic behaviour. Like non-newtonian fluids, blood shows a non linear relationship between shear stress and shear rate. For this kind of fluids we may define the *apparent viscosity* as the ratio between shear stress and shear rate. If apparent viscosity decreases when shear rate increases, we have a pseudo-plastic fluid; otherwise we have a dilatant fluid (fig. 1.5).

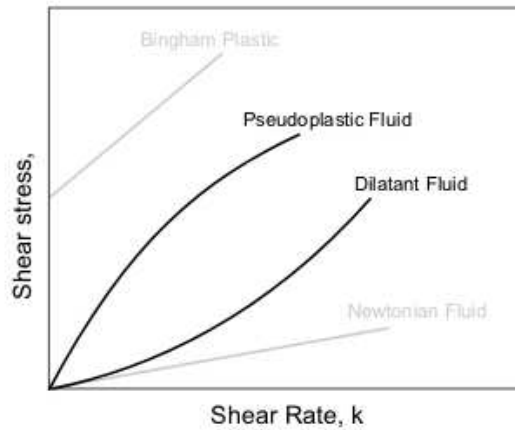


Figure 1.5: Relationship between shear rate and shear stress in a non-newtonian fluid

Micro-circulation effects. Blood rheologic properties may change when vessel diameter reduces to a dimension comparable with the one of a red blood cell. In fact, when the diameter is less than $12 \mu m$, blood cannot be considered as a continuous anymore. When the vessel diameter assumes values less than $500 \mu m$, it is experimentally possible to observe a reduction in apparent viscosity. This behaviour is called *Fahraeus-Lindqvist effect* and is essentially due to two causes: first, when blood is carried away into a vessel smaller than the coming one, the plasma will easily flow away, while the blood formed components will be slowed down because of collisions between them and the vessel wall near the entrance. This phenomenon will decrease the red blood cell concentration (*hematocrit*) and, consequently, the apparent viscosity. Second, we can experimentally observe that hematocrit assumes higher values in the central lumen region than near the walls. For this reason, owing

to a vessel branching which causes a diameter reduction, the region close to the walls becomes more relevant than the central zone and there will be a decreasing of hematocrit and apparent viscosity. However this characteristic doesn't concern with big and middle size arteries, and it will not be considered during the model implementation.

All these rheologic characteristics are essentially due to the presence of red blood cells. In fact the plasma can be considered as a newtonian fluid, and white blood cells and platelets represent a small percentage of the blood volume and their microscopical effect on rheology may be neglected. When the red blood cells concentration is less than 12% of the total weight, blood has a newtonian behaviour.

For middle and big arteries, in physiologic conditions, the rheological newtonian model for blood is considered acceptable for a first level approximation. In fact we can experimentally discover that for values of \mathbf{D} in the proximity of artery walls, viscosity is independent from any value of \mathbf{D} . Since for our 1D model we consider only big and middle arteries, by default we will treat blood as a newtonian fluid with density $1.021 \times 10^3 \text{ kg m}^{-3}$ and viscosity equals to $0.004 \text{ kg m}^{-1} \text{ s}^{-1}$ (at $37 \text{ }^\circ\text{C}$), characterized by the following constitutive law:

$$\mathbf{T} = -p\mathbf{I} + 2\mu\mathbf{D} \quad (1.10)$$

where μ is the viscosity of the fluid.

1.3 Hemodynamics

Hemodynamics is an important field of cardiovascular physiology dealing with blood pumping and circulation through the cardiovascular system. Classical hemodynamics deals with in vivo and in vitro measurements of pressure, flow and resistance. The direct extrapolation of such quantities is difficult since the blood circulation is within the living body of human beings and so there must be a compromise between the accuracy of measurements and their invasive level. Also the employ of straightforward calculations can hardly handle the complicated dynamic phenomena of blood flow. Hence, computational simulation had become necessary and has been proved to be valid.

Computational Hemodynamics applies numerical techniques to support the investigators of physiological and pathological phenomena concerning blood flow in the cardiovascular system. In recent years, the development of computational methods

together with the increasing computing hardware performances have enabled computational Hemodynamics to become an important tool for analyzing the behavior of blood flow in vessels.

The mathematical modeling of hemodynamics problems, like the study of blood flow and its mechanical and biochemical interactions with the vessel walls is very complex. Together with the equations describing the motion of an incompressible fluid, we have to consider advection diffusion equations for the dynamics of soluted lipids, oxygen and drugs; moreover, specific interaction models for the osmosis of these substances with the wall may be taken into account. Finally, we have to define a structural model that describes the mechanical behaviour of the vessel wall coupled with the blood flow.

The development of a numerical solution for such hemodynamics problems must take into account some compromises related to several aspects; at one hand we have to provide all those informations about the problem that will be essential for the comprehension of the involved phenomena. On the other hand it is necessary to allow a numerical treatment of the model at reasonable computational costs. For this purpose the choice of the model may be oriented either to an accurate modelization of a localized system or a heavily simplified representation of a more global physical system; the former case implies the application of 2D/3D models with the coupling fluid-structure [29][3], while the latter refers to consider the whole system as a network of compartments whose features are treated as *mean* or *lumped* parameters [14]

A possible compromise between these approaches is represented by the one-dimensional wave propagation model, which involves solving the governing equations of blood flow in a one-dimensional domain and assumes that dominant component of the blood flow velocity is oriented along the vessel axis.

1.3.1 The one-dimensional model

The one-dimensional modelling, and its application to the human arterial system, was introduced for the first time by Euler in 1775[2] who derived the partial differential equations expressing the conservation of momentum and mass for an inviscid fluid. In order to close the problem, he suggested two possible, but experimentally not realistic, constitutive equations which describe the behaviour of an elastic wall with changes in the luminal pressure. Euler did not recognise the wave-like nature

of the flow and was not able to find a solution for his system of equation.

The wave nature of the arterial flow was first described by Young[36] who derived the wave speed in analogy to Newton theory of the speed of sound in air. In 1877 Moens[13] and Kortweg[8] independently published analyses of flow in thin-walled elastic vessels, deriving what is now known as the Moens-Kortweg equation for the wave speed. Riemann[20], in the 1860, provided the analytical solution for the general equations for 1D model when he introduced the method of characteristics; such tool was first applied to arterial flow more than 50 years ago by Anliker and co-workers[26][27] and Skalak[23].

The system of equations derived by Euler is composed by non-linear partial differential equations analogous to the shallow-water equations of hydrodynamics or the one-dimensional inviscid equations of gas dynamics. However, under physiological conditions of the arterial system, such equations are only weakly non-linear and therefore many characteristics of the flow may be captured using a linearised system. This is the approach of Womersley[35] (1957) who linearised the two dimensional equations for the flow in straight, circular elastic pipes and obtained the wave solution by Fourier techniques. This linear analysis has become the "standard" model of waves in arteries and is found in most hemodynamics books. The success of the linearised model and the apparently periodic nature of the arterial system has convinced most researchers since Womersley to analyse arterial flow in the frequency domain rather than the time domain, using the "electrical analogy" pressure-voltage and flow-current.

Although the body of work using the frequency domain is considerable, many aspects of the physiological waveforms have yet to be understood; moreover there are some limiting aspects concerning the solution of such a problem in the frequency domain. Firstly the frequency domain may lead to the implicit assumption that the arterial system is in a state of permanent "steady oscillation" that may continue even when the forcing from the heart is stopped. However, the characteristic speed of wave propagation is sufficiently fast that the time scale to propagate information through the whole arterial system is much smaller than the duration of the cardiac cycle. It is generally observed, in resting conditions, that flow in large arteries appears at rest during late diastole. Secondly, the aortic valve is an essentially non-linear element dividing the cardiac cycle into systole and diastole. Since the frequency domain cannot distinguish between these two phases of ht cardiac cycle, an identical systolic behaviour of the ventricle during systole (and the arterial system

during diastole) could be masked simply by changes in the fundamental frequency.

An alternative approach to simulate the one-dimensional arterial system is to work in a space-time domain instead of a frequency analysis;...

Chapter 2

Problem formulation

In chapter I we gave a preliminary base of knowledge about the cardiovascular system, introducing both the physiological background and possible models to be used for the numerical characterization of its functioning. In this chapter we focus on the mathematical formulation related to the one-dimensional model of the vascular network, accounting for several aspects: firstly, the derivation of the governing equations for this kind of model is detailed accounting for geometrical and physical assumptions, definition of the computation domain and attribution of suitable boundary conditions. Secondly, the governing system we obtained is numerically solved by means of time-space integration schemes adopting the finite element theory. Such schemes will be further implemented into a numerical solver which, coupled with GiD¹ pre-post process interface permits to calculate the numerical solution of the problem and to display the obtained results.

2.1 Governing equations

The governing equations for 1D blood flow model in arteries can be derived considering a single vessel (fig. 2.1). Since we are adopting a one-dimensional formulation, several simplifying hypothesis must be taken into account; starting from the geometry, we can assume the arterial vessel as a long, straight cylinder of length L (fig. 2.1). Doing this, we decided not to consider local curvatures so that the axial coordinate z represents also the preferential direction of the blood motion. The new cylindrical domain Ω_c , described using a cylindrical coordinate

¹See appendix A.

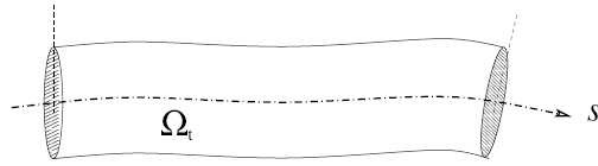


Figure 2.1: Sketch of a single compliant vessel

system (r, θ, z) , is defined as follows:

$$\Omega_c = \{(r, \theta, z) : 0 \leq r \leq R(z, t), \theta \in [0, 2\pi), z \in (0, L)\}$$

for $\forall t > 0$, indicating with \mathbf{e}_r , \mathbf{e}_θ and \mathbf{e}_z the radial, circumferential and axial unit vectors.

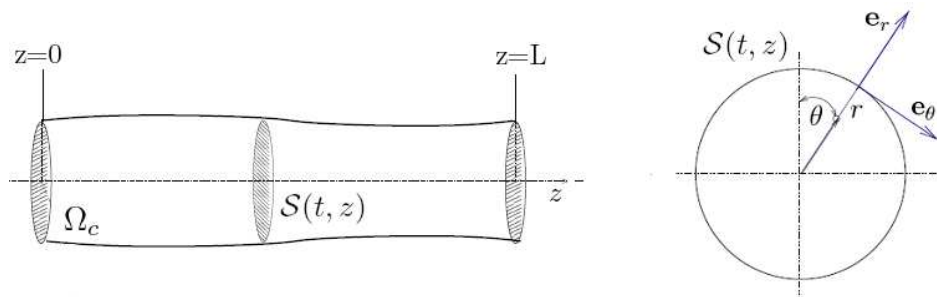


Figure 2.2: One-dimensional cylindric domain for a single arterial vessel and detail of the circular section $\mathcal{S}(t, z)$

The assumption of a cylindrical geometry for the vessel is not the only simplifying hypothesis adopted for the one-dimensional model; since we wish to study how pressure and flow waves propagate into the arterial system without considering hemodynamic details, we analyze the blood flow in terms of *transversally averaged* area and flow rate calculated on the vessel section; mean sectional values anyway give a good description of the wave propagation in arteries [15][28] and allow to avoid considering the radial and angular components of velocity.

Following this approach we assume axial symmetry for all the components involved (area, velocity and pressure), which are functions of z and t only, and radial displacements along the radial direction solely. The latter hypothesis means that each axial section \mathcal{S} remains circular at all times, i.e., for $z \in [0, L]$ and $t > 0$ we have:

$$\mathcal{S} = \mathcal{S}(z, t) = \{(r, \theta, z) : 0 \leq r \leq R(z, t), 0 \leq \theta \leq 2\pi\}$$

At each point of the section surface we may write $\boldsymbol{\eta} = \eta \mathbf{e}_r$, where $\eta = R - R_0$ is the displacement with respect to a reference radius R_0 ².

2.1.1 Mass conservation equation

Considering the vessel defined in fig. 2.2, the principle of mass conservation requires that the rate of change of mass within the domain Ω_c plus the net mass flux out of the domain is zero. Since we consider transversally averaged values for area and axial velocity, they may be defined as:

$$A(t, z) = \int_{\mathcal{S}(t,z)} d\sigma = \pi R^2(t, z) \quad (2.1)$$

$$u_z(t, z) = \bar{u}(t, z) s \left(\frac{r}{R(t, z)} \right) \quad , \quad \bar{u}(t, z) = \int_{\mathcal{S}(t,z)} u_z d\sigma \quad (2.2)$$

$$Q(t, z) = A(t, z) \bar{u} \quad (2.3)$$

where \bar{u} is the mean velocity on each section and $s : \mathbf{R} \rightarrow \mathbf{R}$ is a *velocity profile function*. We assumed this profile does not vary in time, thinking s as representative of an average flow configuration.

Denoting the vessel volume as $V(t) = \int_0^L A dz$, and assuming there are no infiltrations through the side walls, the mass conservation can be written as

$$\rho \frac{dV(t)}{dt} + \rho Q(L, t) - \rho Q(0, t) = 0 \quad (2.4)$$

where ρ is the blood density. If infiltration does occur we must add a source term to this equation [32][31].

To determine the one-dimensional equation of mass conservation, we insert $V(t) = \int_0^L A dz$ into (2.4) and, since we can write

$$Q(L, t) - Q(0, t) = \int_0^L \frac{\partial Q}{\partial z} dz,$$

we obtain

$$\rho \frac{d}{dt} \int_0^L A(z, t) dz + \rho \int_0^L \frac{\partial Q}{\partial z} dz = 0.$$

As we assume L independent of time, we can include the time derivative inside the integral to have

$$\rho \int_0^L \left\{ \frac{\partial A}{\partial t} + \frac{\partial Q}{\partial z} \right\} dz = 0$$

²As reference state we indicate a generic steady state of the 1D system, where we have the section $A = A_0 = \pi R_0^2$ and the blood mean velocity $\bar{u} \approx 0$

Since we have not specified the vessel length L , the domain is arbitrary and so the above equation must be true for any value of L . We therefore obtain the differential equation for the mass conservation related to the one-dimensional model:

$$\frac{\partial A}{\partial t} + \frac{\partial Q}{\partial z} = 0 \quad (2.5)$$

2.1.2 Momentum equation

The momentum equation states that the rate of change of momentum within the integration domain Ω_c plus the net flux of the momentum out of the domain itself is equal to the applied forces on the domain and can be expressed over an arbitrary length L as

$$\frac{d}{dt} \int_0^L \rho Q dz + (\alpha \rho Q u)_L - (\alpha \rho Q u)_0 = F \quad (2.6)$$

where F is defined as the applied forces in the z -direction acting on the domain; again we have not considered flux losses through the side walls of Ω_c . The equation (2.6) includes a *momentum-flux correction coefficient* α , also called *Coriolis coefficient*, which accounts for the fact that the momentum flux calculated with averaged quantities (\bar{u}) does not consider the non-linearity of sectional integration of flux momentum. So we may assume

$$\int_S \rho \bar{u}^2 d\sigma \equiv \alpha \rho \bar{u}^2 A = \alpha \rho Q \bar{u} \quad \Rightarrow \quad \alpha(z, t) = \frac{\int_S \bar{u}^2 d\sigma}{A \bar{u}^2} = \frac{\int_S \bar{s}^2 d\sigma}{A}$$

In general α may vary in time and space, yet in our model is taken constant as a consequence of (2.2). There are several choices for the profile law s ; one is the classical parabolic function $s(y) = 2(1 - y^2)$, corresponding to the Poiseuille solution for steady flows in circular tubes. Another profile law often used for blood flow in arteries [24] is a power law of the type

$$s(y) = \gamma^{-1}(\gamma + 2)(1 - y^\gamma) \quad (2.7)$$

Figure 2.3 shows the profile trend adopting several values for γ .

To complete the equation (2.6) we need to define the applied forces F which typically involve a pressure and a viscous force contribution, i.e.

$$F = (PA)_0 - (PA)_L + \int_0^L \int_{\partial S} \hat{P} n_z ds dz + \int_0^L f dz \quad (2.8)$$

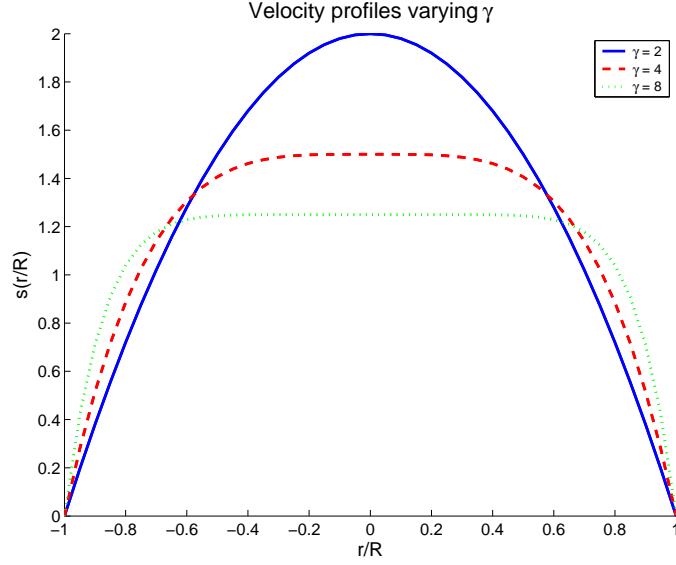


Figure 2.3: Velocity profiles for blood flow in arteries considering several values of γ

where $\partial\mathcal{S}$ represents the boundary of the section \mathcal{S} , n_z is the z -component of the surface normal and f stands for the friction force per unit of length. The pressure force acting on the side walls, given by the double integral, can be simplified since we assumed both constant sectional pressure and axial symmetry of the vessel; so we have

$$\int_0^L \int_{\partial\mathcal{S}} \hat{P} n_z ds dz = \int_0^L P \frac{\partial A}{\partial z} dz \quad (2.9)$$

If we finally combine equations (2.6),(2.8) and (2.9) we obtain the momentum conservation for the computation domain expressed as

$$\begin{aligned} \frac{d}{dt} \int_0^L \rho Q dz + (\alpha \rho Q u)_L - (\alpha \rho Q u)_0 &= (PA)_0 - (PA)_L + \\ &+ \int_0^L P \frac{\partial A}{\partial z} dz + \int_0^L f dz \end{aligned} \quad (2.10)$$

To obtain the one-dimensional differential equation for the momentum we note that

$$(\alpha \rho Q u)_L - (\alpha \rho Q u)_0 = \int_0^L \frac{\partial(\alpha \rho Q u)}{\partial z} dz$$

$$(PA)_0 - (PA)_L = - \int_0^L \frac{\partial(PA)}{\partial z} dz$$

which, inserted into (2.10), taking L independent of time and ρ constant, gives

$$\rho \int_0^L \left\{ \frac{\partial Q}{\partial t} + \frac{\partial(\alpha Qu)}{\partial z} \right\} dz = \int_0^L \left\{ -\frac{\partial(PA)}{\partial z} + P \frac{\partial A}{\partial z} + f \right\} dz$$

Once again this relationship is satisfied for an arbitrary length L and therefore can only be true when the integrands are equal. So the one-dimensional equation for the momentum conservation becomes

$$\frac{\partial Q}{\partial t} + \alpha \frac{\partial}{\partial z} \left(\frac{Q^2}{A} \right) = -\frac{A}{\rho} \frac{\partial P}{\partial z} + \frac{f}{P}. \quad (2.11)$$

The viscous term in the equation (2.8) may be also expressed as a function of the velocity profile $s(y)$. Considering an infinitesimal portion \mathcal{T} of the domain Ω_c

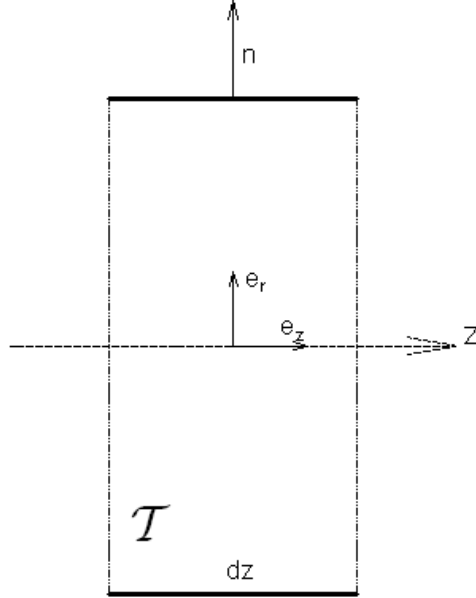


Figure 2.4: Infinitesimal portion \mathcal{T} of Ω_c

(fig. 2.4), we can write:

$$\int_0^L f dz \Rightarrow \mu \int_{\mathcal{T}} \Delta u_z = \mu \int_{\partial \mathcal{T}} \nabla u_z \cdot \mathbf{n} = \mu \left[\int_{S^-} \frac{\partial u_z}{\partial z} + \int_{S^+} \frac{\partial u_z}{\partial z} + \int_{\Gamma_{\mathcal{T}}} \nabla u_z \cdot \mathbf{n} \right]$$

The term $\partial u_z / \partial z$ is assumed to be much smaller than the others, and moreover we may split \mathbf{n} into its radial and axial components, $\mathbf{n}_r = n_r \mathbf{e}_r$ and $\mathbf{n}_z = n_z \mathbf{e}_z$. Consequently we have

$$\int_{\mathcal{T}} \Delta u_z = \int_{\Gamma_{\mathcal{T}}} (\nabla u_z \cdot \mathbf{n}_z + \nabla u_z \cdot \mathbf{e}_r n_r) d\sigma$$

Again the term $\nabla u_z \cdot \mathbf{n}_z$ may not be considered, being proportional to $\partial u_z / \partial z$. Recalling the relation (2.2) we obtain

$$\int_{\mathcal{T}} \Delta u_z = \int_{\Gamma_{\mathcal{T}}} \nabla u_z \cdot \mathbf{e}_r n_r d\sigma = \int_{\Gamma_{\mathcal{T}}} \frac{\bar{u}}{R} s'(1) \mathbf{n} \cdot \mathbf{e}_r d\sigma \approx 2\pi \bar{u} s'(1)$$

because $n_r d\sigma$ can be expressed as $2\pi R dz$. Passing this term to the limit as $dz \rightarrow 0$ and substituting it with f/ρ into the equation (2.11) we finally obtain

$$\frac{\partial Q}{\partial t} + \alpha \frac{\partial}{\partial z} \left(\frac{Q^2}{A} \right) = -\frac{A}{\rho} \frac{\partial P}{\partial z} + K_r \bar{u}$$

where

$$K_r = -2\pi \nu s'(1)$$

is the *friction parameter* for our one-dimensional system, which depends on the kinematic viscosity $\nu = \frac{\mu}{\rho}$ of the fluid and the velocity profile s .

2.2 Vessel wall mechanical modelling

Once we obtained the two governing equations (2.5) and (2.11), it is possible to write the one-dimensional system as

$$\frac{\partial A}{\partial t} + \frac{\partial Q}{\partial z} = 0, \quad z \in (0, L), \quad t > 0 \quad (2.12a)$$

$$\frac{\partial Q}{\partial t} + \frac{\partial}{\partial z} \left(\alpha \frac{Q^2}{A} \right) + \frac{A}{\rho} \frac{\partial P}{\partial z} + K_R \frac{Q}{A} = 0, \quad z \in (0, L), \quad t > 0 \quad (2.12b)$$

where the unknowns are A , Q and P . As we can notice the number of variables is greater than the number of equations (three unknowns for the two equations (2.5) and (2.11)); therefore one equation more is needed in order to solve this system. For this reason we introduce an algebraic relationship between area and pressure, deriving it from a mechanical model for the vessel wall displacement. In this project we considered the generalised string model [18], which can be expressed as

$$\rho_w h_0 \frac{\partial^2 \eta}{\partial t^2} - \tilde{\gamma} \frac{\partial \eta}{\partial t} - \tilde{a} \frac{\partial^2 \eta}{\partial z^2} - \tilde{c} \frac{\partial^3 \eta}{\partial t \partial z^2} + \tilde{b} \eta = (P - P_{ext}) \quad (2.13)$$

where η is the radial displacement defined previously and P_{ext} is the pressure external to the vessel, here taken constant.

Each term of the equation (2.13) has its own physical significance: the first one is the inertia term, proportional to the wall acceleration. The second term is a Voigt-type, viscoelastic term, proportional to the radial displacement velocity. The third term is related to the longitudinal pre-stress state of the vessel wall, and accounts for the longitudinal tensions acting on arteries. The fourth term is another viscoelastic term while the last term is the elastic response function. Besides ρ_w is the vessel density, h_0 is the wall thickness, \tilde{a} , \tilde{b} and \tilde{c} are three positive coefficients. We can develop the last term of (2.13) being

$$\eta = R - R_0 \implies \eta = \frac{\sqrt{A} - \sqrt{A_0}}{\sqrt{\pi}}, \quad \text{with } A_0 = \pi R_0^2$$

and

$$\tilde{b} = \frac{Eh_0}{kR_0^2} = \frac{\pi Eh_0}{kA_0}, \quad \text{with } k = 1 - \xi^2$$

where E is the Young modulus of elasticity and ξ represents the Poisson ratio, typically taken to be $\xi = 0.5$ (then $k = 0.75$) since biological tissue is practically incompressible.

It is known that, under physiological conditions, the elastic response of the main arteries is the dominating effect, while the other inertial and viscoelastic terms give a negligible contribution. Consequently, a first model which relates pressure and area may be

$$P - P_{ext} = \tilde{b}\eta = \beta_1 \frac{\sqrt{A} - \sqrt{A_0}}{A_0} \quad (2.14)$$

where

$$\beta_1 = \frac{Eh_0\sqrt{\pi}}{1 - \xi^2}$$

is a function of z through the Young modulus, $E(z)$. In general, the algebraic relationship may be expressed as

$$P = P_{ext} + \mathcal{F}(A; A_0, \boldsymbol{\beta}) \quad (2.15)$$

where we outlined that the pressure will depend not only on A , but also on A_0 and on a set of coefficients $\boldsymbol{\beta} = \{\beta_1, \beta_2, \dots, \beta_n\}$ which accounts for the physical and mechanical characteristics of the arterial vessel. Both A_0 and $\boldsymbol{\beta}$ are given functions of z , but they do not vary in time. It is required that \mathcal{F} be at least a C^1 function of its arguments and be defined for each positive value of A and A_0 . In addition we must have, for all the allowable values of A , A_0 and $\boldsymbol{\beta}$ that

$$\frac{\partial \mathcal{F}}{\partial A} > 0, \quad \text{and } \mathcal{F}(A_0; A_0, \boldsymbol{\beta}) = 0$$

There are several examples of algebraic pressure-area relationship for one-dimensional models of arterial flow [9][24]; here we assumed the relationship (2.14), where $\boldsymbol{\beta} = \{\beta_1\}$ and, for the sake of simplicity, $P_{ext} = 0$. Then function \mathcal{F} can be written as

$$\mathcal{F}(A; A_0, \beta_1) = \beta_1 \frac{\sqrt{A} - \sqrt{A_0}}{A_0} \quad (2.16)$$

2.3 The final model

The derivation of the above pressure-area dependence allows to close our one-dimensional system (2.12), replacing the pressure term with the algebraic relationship (2.14). To this purpose we also introduce the following quantity

$$c_1 = c_1(A; A_0, \boldsymbol{\beta}) = \sqrt{\frac{A}{\rho} \frac{\partial \mathcal{F}}{\partial A}} \quad (2.17)$$

which represents the propagation speed of waves along the cylindrical vessel.

The two-equation system we finally obtained may be written in a *quasi-linear* form, using the matrix notation. So we have

$$\frac{\partial \mathbf{U}}{\partial t} + \mathbf{H}(\mathbf{U}) \frac{\partial \mathbf{U}}{\partial z} + \mathbf{B}(\mathbf{U}) = 0, \quad z \in (0, L), \quad t > 0 \quad (2.18)$$

where

$$\begin{aligned} \mathbf{U} &= \begin{bmatrix} A \\ Q \end{bmatrix} \\ \mathbf{H}(\mathbf{U}) &= \begin{bmatrix} 0 & 1 \\ \frac{A}{\rho} \frac{\partial \mathcal{F}}{\partial A} - \alpha \bar{u}^2 & 2\alpha \bar{u} \end{bmatrix} = \begin{bmatrix} 0 & 1 \\ c_1^2 - \alpha \left(\frac{Q}{A}\right)^2 & 2\alpha \frac{Q}{A} \end{bmatrix} \\ \mathbf{B}(\mathbf{U}) &= \begin{bmatrix} 0 \\ -K_R \frac{Q}{A} + \frac{A}{\rho} \frac{\partial \mathcal{F}}{\partial A_0} \frac{dA_0}{dz} + \frac{A}{\rho} \frac{\partial \mathcal{F}}{\partial \boldsymbol{\beta}} \frac{d\boldsymbol{\beta}}{dz} \end{bmatrix} \end{aligned} \quad (2.19)$$

In our modelling, A_0 and β_1 are taken constant along the axial direction z because we assume that both the initial area A_0 and the Young modulus E do not vary in space; so the expression of \mathbf{B} accounts only for the friction term depending on K_R .

The non-linear form (2.18) for the governing system may be transformed into a *conservation form* as

$$\frac{\partial \mathbf{U}}{\partial t} + \frac{\partial \mathbf{F}(\mathbf{U})}{\partial z} - \mathbf{S}(\mathbf{U}) = 0, \quad z \in (0, L), \quad t > 0 \quad (2.20)$$

where

$$\mathbf{F}(\mathbf{U}) = \begin{bmatrix} Q \\ \alpha \frac{Q^2}{A} + C_1 \end{bmatrix} \quad (2.21)$$

is the flux vector, and

$$\mathbf{S}(\mathbf{U}) = -\mathbf{B}(\mathbf{U}) - \begin{bmatrix} 0 \\ \frac{\partial C_1}{\partial A_0} \frac{dA_0}{dz} + \frac{\partial C_1}{\partial \beta} \frac{d\beta}{dz} \end{bmatrix} \quad (2.22)$$

accounts for the source term of the system. C_1 is a primitive of the wave speed c_1 , given by

$$C_1(A; A_0, \beta) = \int_{A_0}^A c_1^2(\tau; A_0, \beta) d\tau$$

Applying the relationships (2.16) and (2.17), we obtain

$$c_1 = \sqrt{\frac{\beta_1}{2\rho A_0}} A^{\frac{1}{4}} \quad \Rightarrow \quad C_1 = \frac{\beta_1}{3\rho A_0} A^{\frac{3}{2}} \quad (2.23)$$

2.4 Characteristic analysis

One of the methods for solving nonlinear systems of partial differential equations, like our one-dimensional model, is the *characteristic analysis* [22][17]; considering (2.18), we can calculate the eigenvalues for the matrix $\mathbf{H}(\mathbf{U})$

$$\lambda_{1,2} = \alpha \frac{Q}{A} \pm c_\alpha \quad (2.24)$$

where

$$c_\alpha = \sqrt{c_1^2 + \alpha(\alpha - 1) \frac{Q^2}{A^2}}$$

Since the Coriolis coefficient $\alpha \geq 1$, c_α is a real number; besides, under the assumption that $A > 0$, indeed a necessary condition to have physical relevant solution, $c_1 > 0$; therefore we have $c_\alpha > 0$ which means \mathbf{H} has two real distinct eigenvalues and so, by definition, the system (2.18) is *strictly hyperbolic*. For typical values of velocity, vessel section and mechanical parameter β_1 encountered in main arteries under physiological conditions, we find that $\lambda_1 > 0$ and $\lambda_2 < 0$.

Indicating with $(\mathbf{l}_1, \mathbf{l}_2)$ and $(\mathbf{r}_1, \mathbf{r}_2)$ the two couples of left and right eigenvectors of \mathbf{H} , we may define the matrices \mathbf{R} , \mathbf{L} and $\mathbf{\Lambda}$ as

$$\mathbf{L} = \begin{bmatrix} \mathbf{l}_1^T \\ \mathbf{l}_2^T \end{bmatrix}, \quad \mathbf{R} = \begin{bmatrix} \mathbf{r}_1 & \mathbf{r}_2 \end{bmatrix}, \quad \mathbf{\Lambda} = \begin{bmatrix} \lambda_1 & 0 \\ 0 & \lambda_2 \end{bmatrix}. \quad (2.25)$$

Here we considered, for simplicity, $\alpha = 1^3$; since left and right eigenvectors are mutually orthogonal, we choose them so that $\mathbf{LR} = \mathbf{I}$, being \mathbf{I} the identity matrix, without loss of generality. The matrix \mathbf{H} becomes

$$\mathbf{H} = \mathbf{RAL}$$

and the system (2.18) takes the equivalent form

$$\mathbf{L} \frac{\partial \mathbf{U}}{\partial t} + \mathbf{\Lambda L} \frac{\partial \mathbf{U}}{\partial z} + \mathbf{LB}(\mathbf{U}) = 0, \quad z \in (0, L), \quad t > 0 \quad (2.26)$$

We introduce a change of variables such that

$$\frac{\partial W_1}{\partial \mathbf{U}} = \mathbf{l}_1, \quad \frac{\partial W_2}{\partial \mathbf{U}} = \mathbf{l}_2 \quad (2.27)$$

W_1 and W_2 are called *characteristic variables* of the hyperbolic system. By setting $\mathbf{W} = [W_1 \ W_2]^T$ the system (2.26) may be elaborated into

$$\frac{\partial \mathbf{W}}{\partial t} + \mathbf{\Lambda} \frac{\partial \mathbf{W}}{\partial z} + \mathbf{G} = 0, \quad z \in (0, L), \quad t > 0 \quad (2.28)$$

with

$$\mathbf{G} = \mathbf{LB} - \frac{\partial \mathbf{W}}{\partial A_0} \frac{dA_0}{dz} - \frac{\partial \mathbf{W}}{\partial \beta} \frac{d\beta}{dz}$$

Under the assumption that A_0 and β_1 are constant in space and taking \mathbf{B} negligible⁴, the equation (2.28) becomes

$$\frac{\partial \mathbf{W}}{\partial t} + \mathbf{\Lambda} \frac{\partial \mathbf{W}}{\partial z} = 0, \quad z \in (0, L), \quad t > 0$$

which is a system of decoupled scalar equations written as

$$\frac{\partial W_i}{\partial t} + \lambda_i \frac{\partial W_i}{\partial z} = 0, \quad z \in (0, L), \quad t > 0, \quad i = 1, 2. \quad (2.29)$$

³The value of α usually varies between 1 and 4/3

⁴Assuming $\mathbf{B} \approx 0$ is consistent with the fact that, in the case of 1D models, the viscous source term in the momentum equation is negligible under the physiological conditions concerning main arteries.

From (2.29) we have that W_1 and W_2 are constant along the two *characteristic curves* in the (z, t) plane (fig. 2.5) described by

$$\frac{dz}{dt} = \lambda_1 \quad \text{and} \quad \frac{dz}{dt} = \lambda_2$$

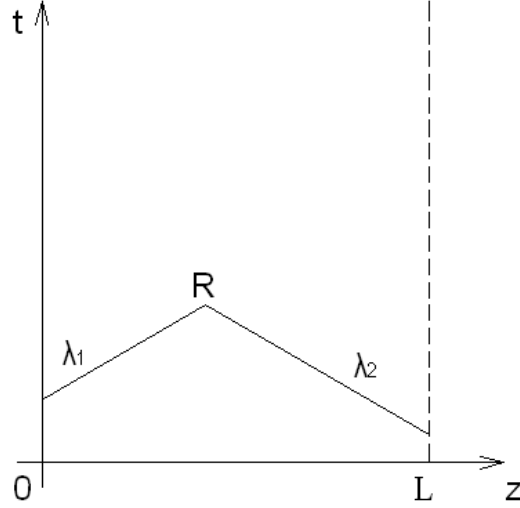


Figure 2.5: Diagram of characteristics in the (z, t) plane. The solution on the point R is obtained by the superimposition of the two characteristics W_1 and W_2

The expression for the left eigenvectors \mathbf{l}_1 and \mathbf{l}_2 is given by

$$\mathbf{l}_1 = \varsigma \begin{bmatrix} c_\alpha - \alpha \bar{u} \\ 1 \end{bmatrix}, \quad \mathbf{l}_2 = \varsigma \begin{bmatrix} -c_\alpha - \alpha \bar{u} \\ 1 \end{bmatrix},$$

where $\varsigma = \varsigma(A, \bar{u})$ is any arbitrary smooth function of its arguments with $\varsigma > 0$. Here we have expressed \mathbf{l}_1 and \mathbf{l}_2 as functions of (A, \bar{u}) instead of (A, Q) in order to simplify the next developments.

For an hyperbolic system of two equations is always possible to find the characteristic variables locally, that is in a small neighbourhood of any point \mathbf{U} [5], yet the existence of global characteristics is not in general guaranteed. Assuming $\alpha = 1$ the relationships (2.27) take the form

$$\frac{\partial W_1}{\partial A} = \varsigma c_1, \quad \frac{\partial W_1}{\partial \bar{u}} = \varsigma A \tag{2.30a}$$

$$\frac{\partial W_2}{\partial A} = -\varsigma c_1, \quad \frac{\partial W_2}{\partial \bar{u}} = \varsigma A \tag{2.30b}$$

We now show that a set of global characteristic variables exist for the problem at hand. Since we note, from 2.30, that $W_{1,2}$ are exact differentials being

$$\frac{\partial^2 W_i}{\partial A \partial \bar{u}} = \frac{\partial^2 W_i}{\partial \bar{u} \partial A}$$

for any value of A and \bar{u} ; we also have that c_1 does not depend on \bar{u} and then, from the above relationships we obtain

$$c_1 \frac{\partial \varsigma}{\partial \bar{u}} = \varsigma + A \frac{\partial \varsigma}{\partial A}$$

In order to satisfy this relation we have to choose $\varsigma = \varsigma(A)$ such that $\varsigma = -A \frac{\partial \varsigma}{\partial A}$. To do this we can take $\varsigma = A^{-1}$.

As a consequence we can write

$$\partial W_1 = \frac{c_1}{A} \partial A + \partial \bar{u}, \quad \partial W_2 = -\frac{c_1}{A} \partial A + \partial \bar{u} \quad (2.31)$$

Taking $(A_0, 0)$ as a reference state for our variables (A, \bar{u}) , we can integrate the above relationships obtaining

$$W_1 = \bar{u} + \int_{A_0}^A \frac{c_1(\epsilon)}{\epsilon} d\epsilon, \quad W_2 = \bar{u} - \int_{A_0}^A \frac{c_1(\epsilon)}{\epsilon} d\epsilon$$

Introducing the expression (2.23) for c_1 we have

$$W_{1,2} = \frac{Q}{A} \pm 4 \left(\sqrt{\frac{\beta_1}{2\rho A_0}} A^{\frac{1}{4}} - c_0 \right) \quad (2.32)$$

with c_0 is the wave speed related to the reference state.

We finally can write the variables (A, Q) in terms of the characteristic ones,

$$A = \left(\frac{2\rho A_0}{\beta_1} \right)^2 \left(\frac{W_1 - W_2}{8} \right)^4, \quad Q = A \frac{W_1 + W_2}{2} \quad (2.33)$$

2.5 Boundary conditions

By the characteristic analysis of the one-dimensional model we pointed out the hyperbolic nature of one-dimensional system for blood flow in arteries; consequently the solution is given by the superimposition of two waves whose eigenvalues $\lambda_{1,2}$ represent the propagation speeds of such waves. As we have seen previously, they always have opposite sign and so blood flow is *sub-critical*; under this condition, we

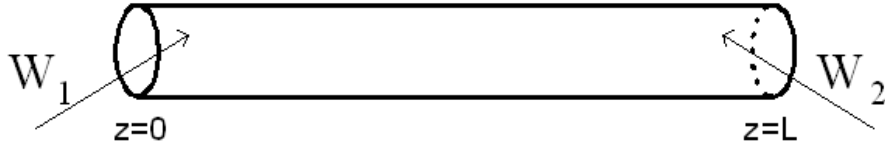


Figure 2.6: Sketch of the two characteristics entering the domain.

need two boundary conditions to close the governing system: one at the inlet section $z = 0$ and the other at the outlet $z = L$ (fig. 2.6).

An important class of boundary conditions is represented by the so-called *non-reflecting* or *absorbing conditions* [30][6], which allow the simple wave associated with the characteristics to enter or leave the domain without spurious reflections.

Absorbing boundary conditions can be imposed by defining values for the wave entering the domain; in our case $\lambda_1 > 0$ and $\lambda_2 < 0$ so W_1 is the entering characteristic in $z = 0$ and W_2 the inlet characteristic in $z = L$. We have

$$\begin{cases} W_1(t) = g_1(t), & \text{for } z = 0 \text{ and } t > 0, \\ W_2(t) = g_2(t), & \text{for } z = L \text{ and } t > 0, \end{cases} \quad (2.34)$$

being $g_1(t)$ and $g_2(t)$ two given functions.

This kind of boundary conditions is suitable when we consider the outlet, or distal, section of the vessel, where the values of area or flow rate are not known before the computation. On the contrary for inlet section we often impose conditions on the physical variables of the system, as pressure or flow rate. Such values can be taken, for example, from experimental measurements.

2.6 Numerical discretization

The system (2.20) has been discretized using both a straightforward Galerkin and a Taylor-Galerkin scheme [1]. The latter is the finite element counterpart of the Lax-Wendroff [10] finite difference scheme.

Considering the equation (2.20) and having $\mathbf{H} = \frac{\partial \mathbf{F}}{\partial \mathbf{U}}$ we may write

$$\frac{\partial \mathbf{U}}{\partial t} = \mathbf{S} - \frac{\partial \mathbf{F}}{\partial z} \quad (2.35)$$

$$\begin{aligned} \frac{\partial^2 \mathbf{U}}{\partial t^2} &= \frac{\partial \mathbf{S}}{\partial \mathbf{U}} \frac{\partial \mathbf{U}}{\partial t} - \frac{\partial}{\partial z} \left(\mathbf{H} \frac{\partial \mathbf{U}}{\partial t} \right) = \\ &= \frac{\partial \mathbf{S}}{\partial \mathbf{U}} \left(\mathbf{S} - \frac{\partial \mathbf{F}}{\partial z} \right) - \frac{\partial \mathbf{H} \mathbf{B}}{\partial z} + \frac{\partial}{\partial z} \left(\mathbf{H} \frac{\partial \mathbf{F}}{\partial z} \right) \end{aligned} \quad (2.36)$$

For simplicity, the dependence of \mathbf{S} and \mathbf{F} from \mathbf{U} is dropped. Starting from the above equations, we now consider the time intervals (t_n, t_{n+1}) , for $n = 0, 1, \dots$ with $t_n = n\Delta t$, being Δt the time step; then we discretize the equation in time using a Taylor series which includes first and second order derivatives of \mathbf{U} ; for the straightforward Galerkin scheme only first order terms will be considered, while for the Taylor-Galerkin scheme we will account for both terms. Therefore we obtain the following *semi-discrete* schemes for the approximation \mathbf{U}^{n+1} of $\mathbf{U}(t_{n+1})$, respectively:

- **Straightforward Galerkin scheme:**

$$\mathbf{U}^{n+1} = \mathbf{U}^n - \Delta t \left(\frac{\partial \mathbf{F}^n}{\partial z} - \mathbf{S}^n \right), \quad n = 0, 1, \dots \quad (2.37)$$

- **Taylor-Galerkin scheme:**

$$\begin{aligned} \mathbf{U}^{n+1} &= \mathbf{U}^n - \Delta t \frac{\partial}{\partial z} \left[\mathbf{F}^n + \frac{\Delta t}{2} \mathbf{H}^n \mathbf{S}^n \right] - \frac{\Delta t^2}{2} \left[\mathbf{S}_U \frac{\partial \mathbf{F}^n}{\partial z} - \frac{\partial}{\partial z} \left(\mathbf{H}^n \frac{\partial \mathbf{F}^n}{\partial z} \right) \right] \\ &+ \Delta t \left(\mathbf{S}^n + \frac{\Delta t}{2} \mathbf{S}_U \mathbf{S}^n \right), \quad n = 0, 1, \dots \end{aligned} \quad (2.38)$$

where $\mathbf{S}_U = \frac{\partial \mathbf{S}^n}{\partial \mathbf{U}}$ and \mathbf{F}^n , stands for $\mathbf{F}(\mathbf{U}^n)$, just as \mathbf{H}^n , \mathbf{S}^n and \mathbf{S}_U^n ; the value \mathbf{U}^0 is given by the initial conditions.

For each time interval (t_n, t_{n+1}) we apply a spatial discretization carried out using the Galerkin finite element method [12][11]. To this purpose we subdivide the domain $\Omega = \{z : z \in (0, L)\}$, which is the 1D counterpart of the 3D domain Ω_c , into a finite number N_{el} of linear elements having length l (fig. 2.7).

Moreover we introduce a trial function space, \mathcal{T} , and a weighting function space, \mathcal{W} . These spaces are both defined to consist of all suitably smooth functions and to be such that

$$\mathcal{T} = \{ \mathbf{U}(z, t) | \mathbf{U}(z, 0) = \mathbf{U}^0(z) \text{ on } \Omega_c \text{ at } t = t^0 \}, \quad \mathcal{W} = \{ \mathbf{W}(z) \}$$

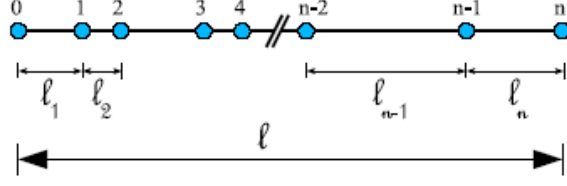


Figure 2.7: One-dimensional linear mesh

Considering the case of a straightforward Galerkin scheme, we multiply the equation (2.37) for the weight function \mathbf{W} and we integrate it over the domain Ω_c obtaining, for $\forall t > t^0$

$$\int_{\Omega} \mathbf{W} (\mathbf{U}^{n+1} - \mathbf{U}^n) d\Omega = \Delta t \left[\int_{\Omega} \frac{\partial \mathbf{W}}{\partial z} \mathbf{F}^n d\Omega + \int_{\Omega} \mathbf{S}^n \mathbf{W} d\Omega \right] + \Delta t [\mathbf{W} \bar{\mathbf{F}}_r^n |_{z=L} - \mathbf{W} \bar{\mathbf{F}}_l^n |_{z=0}] \quad (2.39)$$

The flux term \mathbf{F}^n has been integrated by parts so we must account for boundary terms at the inlet ($z = 0$) and at the outlet ($z = L$) of the domain. Equation (2.39) must be verified for every \mathbf{W} in \mathcal{W} .

Starting from the weak form of the problem (2.39) we build the subspaces \mathcal{T}^h and \mathcal{W}^h for the trial and weighting function spaces \mathcal{T} and \mathcal{W} defining them as

$$\begin{aligned} \mathcal{T}^h &= \{ \hat{\mathbf{U}}(z, t) | \hat{\mathbf{U}}(z, t) = \sum_{j=1}^N \mathbf{U}_j(t) N_j(z); \quad \mathbf{U}(t^0) = \bar{\mathbf{U}}(z_j) = \mathbf{U}_j^0 \} \\ \mathcal{W}^h &= \{ \mathbf{W}(z) | \mathbf{W}(z) = \sum_{j=1}^N W_j N_j(z) \} \end{aligned} \quad (2.40)$$

where N_j is the standard linear finite element shape function (fig. 2.8) associated with the j -th node, located at $z = z_j$, and \mathbf{U}_j the value of $\hat{\mathbf{U}}$ at the node j . Since we are using the Galerkin method, the base shape functions defined above are used as weighting.

Adopting the following notation

$$(W, U)_{\Omega_c} = \int_{\Omega_c} W \cdot U d\Omega,$$

and considering the sum of each element contribution

$$\int_{\Omega} \cdots = \sum_{el} \int_{\Omega_e} \cdots,$$

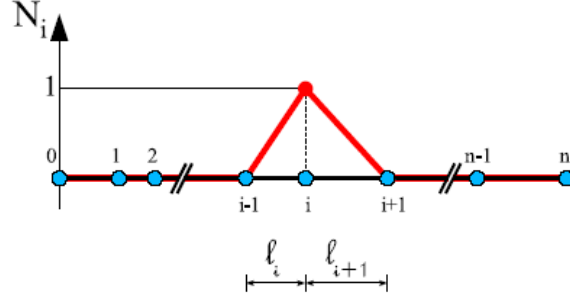


Figure 2.8: Sketch of a 1D shape function

the equation (2.39) becomes

$$\begin{aligned}
 \sum_{el} (N_i, N_j)_{\Omega_e} (\mathbf{U}_j^{n+1} - \mathbf{U}_j^n) &= \Delta t \sum_{el} [(N_{i,z}, N_j)_{\Omega_e} \mathbf{F}_j^n + (N_i, N_j)_{\Omega_e} \mathbf{S}_j^n] - \\
 &\quad - \Delta t [N_i \bar{\mathbf{F}}_r^n|_{z=L} - N_i \bar{\mathbf{F}}_l^n|_{z=0}] \\
 i, j &= 1, 2
 \end{aligned} \tag{2.41}$$

Now we focus on a simple mesh composed by two element, i and $i+1$, and three nodes; then we highlight the contribution made by each single node defining, in a matrix form

$$\mathbf{M}_c = (N_i, N_j)_{\Omega_e} = \frac{l}{6} \begin{bmatrix} 2 & 1 \\ 1 & 2 \end{bmatrix} \tag{2.42}$$

$$\mathbf{M}_f = (N_{i,z}, N_j)_{\Omega_e} = \frac{1}{2} \begin{bmatrix} -1 & -1 \\ 1 & 1 \end{bmatrix} \tag{2.43}$$

\mathbf{M}_c is the so-called *consistent mass matrix*. Afterwards we assembly the 2-element mesh:

$$\begin{aligned}
\frac{l}{6} \begin{bmatrix} 2 & 1 & \\ 1 & 4 & 1 \\ & 1 & 2 \end{bmatrix} \cdot \begin{bmatrix} U_{i-1}^{n+1} - U_{i-1}^n \\ U_i^{n+1} - U_i^n \\ U_{i+1}^{n+1} - U_{i+1}^n \end{bmatrix} &= \frac{\Delta t}{2} \begin{bmatrix} -1 & -1 & \\ 1 & 0 & -1 \\ & 1 & 1 \end{bmatrix} \begin{bmatrix} F_{i-1}^n \\ F_i^n \\ F_{i+1}^n \end{bmatrix} + \\
&+ \frac{l\Delta t}{6} \begin{bmatrix} 2 & 1 & \\ 1 & 4 & 1 \\ & 1 & 2 \end{bmatrix} \begin{bmatrix} S_{i-1}^n \\ S_i^n \\ S_{i+1}^n \end{bmatrix} + \\
&+ \text{(b.c.)} \tag{2.44}
\end{aligned}$$

where (b.c.) means *boundary conditions* and represents the two boundary terms in equation (2.41). It is possible to adopt a simplified or *lumped* form for the matrix M_c [11], summing up the rows into the diagonal, obtaining

$$\mathbf{M}_l = \frac{l}{6} \begin{bmatrix} 3 & 0 \\ 0 & 3 \end{bmatrix} = \frac{l}{2} \mathbf{I} \tag{2.45}$$

For a generic internal node i we finally have

$$U_i^{n+1} = U_i^n + \frac{\Delta t}{l} (F_{i+1}^n - F_{i-1}^n) + \frac{\Delta t}{3} (S_{i-1}^n + 4S_i^n + S_{i+1}^n) \tag{2.46}$$

For what concerns the border nodes, we have to consider also the contribution given by boundary conditions; starting from the equation (2.44), we have the term (b.c.), represented by

$$\Delta t [N_i \bar{\mathbf{F}}_r^n|_{z=L} - N_i \bar{\mathbf{F}}_l^n|_{z=0}], \quad i = 1, 2$$

which implies the knowledge of the flux terms depending from the values of A and Q at inlet and outlet sections. To extract them we need the two characteristic variables W_1 and W_2 at each border to recover $\mathbf{U}(A, Q)$ using the equation (2.33). To this purpose we adopted a technique based on the extrapolation of the outgoing characteristics [21]. Having the friction parameter K_R small with respect to the other equation terms in (2.20), we assume that in the vicinity of the boundaries the flow is governed by the characteristic system (2.29). At the generic time step n we have \mathbf{U}^n known and we linearise the eigenvalues $\lambda_{1,2}$ of (2.20) by taking their values respectively at section $z = L$ and $z = 0$ for $t = t_n$. Then we derive a first order approximation of the outgoing characteristics at time t_{n+1} , which is

$$W_2^{n+1}(0) = W_2^n(-\lambda_2^n(0)\Delta t)$$

$$W_1^{n+1}(L) = W_1^n(-\lambda_1^n(L)\Delta t)$$

By using these information together with the values of $W_1(0)^{n+1}$ and $W_2(L)^{n+1}$ already given by (2.34), we are able to compute $\mathbf{U}(0)^{n+1}$ and $\mathbf{U}(L)^{n+1}$, through (2.33), and in this way we derive the flux terms at boundaries.

Analogously to what we have done for the straightforward Galerkin scheme, it is possible to derive the discretized form of the one-dimensional system in the case we employ a Taylor-Galerkin scheme. Starting from the equation (2.38) and proceeding in the same way as before, we obtain the following expression:

$$\begin{aligned} \sum_{el} (N_i, N_j)_{\Omega_e} (\mathbf{U}_j^{n+1} - \mathbf{U}_j^n) &= \Delta t \sum_{el} [(N_{i,z}, N_j)_{\Omega_e} \mathbf{F}_{LW}^n(\mathbf{U}_j) + (N_i, N_j)_{\Omega_e} \mathbf{S}_{LW}^n(\mathbf{U}_j)] - \\ &\quad - \frac{\Delta t^2}{2} \sum_{el} \left((N_i, N_j)_{\Omega_e} \mathbf{S}_U(\mathbf{U}_j^n) \frac{\partial \mathbf{F}_j^n}{\partial z} \right) - \\ &\quad - \frac{\Delta t^2}{2} \sum_{el} \left((N_{i,z}, N_j)_{\Omega_e} \mathbf{H}_j^n \frac{\partial \mathbf{F}_j^n}{\partial z} \right) - \\ &\quad - \Delta t [N_i \bar{\mathbf{F}}_r^n|_{z=L} - N_i \bar{\mathbf{F}}_l^n|_{z=0}] \\ &\quad i, j = 1, 2 \end{aligned} \tag{2.47}$$

where we have assumed

$$\mathbf{F}_{LW}^n(\mathbf{U}_j) = \mathbf{F}^n + \frac{\Delta t}{2} \mathbf{H}^n \mathbf{F}^n$$

and

$$\mathbf{S}_{LW}^n(\mathbf{U}_j) = \mathbf{S}^n + \frac{\Delta t}{2} \mathbf{B}_U^n \mathbf{F}^n$$

We choose to use, for time integration, both a second and a fourth order explicit Runge-Kutta scheme; such methods are diffused in computational fluid dynamics [7], and show good properties, e.g. ease of programming, simple treatment of boundary conditions and good stability [11]. About this last concept, Galerkin and Taylor-Galerkin require a time step limitation in order to keep the solution stable. Referring to a linear stability analysis, as in reference [16], we indicate that the following condition should be satisfied

$$\Delta t \leq \text{CFL} \min_{0 \leq i \leq N} \left[\frac{l_i}{\max(\lambda_{1,i}, \lambda_{2,i})} \right], \quad (2.48)$$

where $\lambda_{1,i}$ indicates the eigenvalue λ_1 at the mesh node i and CFL is the so-called *Courant-Friedrichs-Levy number*; for the case of a second-order Taylor Galerkin scheme we assume $\text{CFL} = \frac{\sqrt{3}}{3}$ [16]

2.7 Bifurcation treatment

The one-dimensional model of a single artery can be extended to handle the vascular network by imposing suitable conditions at the bifurcations between vessels. In order to manage a branching zone, when using a 1D formulation, we adopt the technique called *domain bifurcation*[19]. As showed in figure 2.9, we divide the domain Ω into three partitions Ω_1 , Ω_2 and Ω_3 ; doing this we have 3 sub-problems which must be coupled imposing adequate boundary conditions. Then we have to evaluate six variable, (A_i, Q_i) with $i = 1 : 3$, corresponding to the problem unknowns, area and flow rate, for each one of the vessels composing the branching.

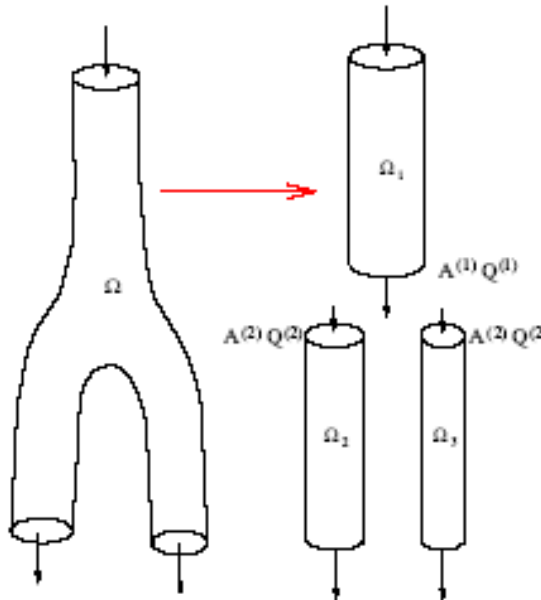


Figure 2.9: Domain decomposition for a generic bifurcation containing one inlet vessel and two outgoing vessels.

The simplest condition we can impose is to require the mass conservation through the bifurcation and therefore the flow rate balance can be written

$$Q_1 = Q_2 + Q_3$$

remembering that the flow moves from the subdomain Ω_1 to the subdomains Ω_2 and Ω_3 . Other two assumptions can be obtained from the requirement of continuity of the momentum flux at the bifurcation. This lead to consider the *total pressure* term continuous at the boundary. So we may write

$$P_1 + \frac{1}{2}\rho \left(\frac{Q_1}{A_1}\right)^2 = P_2 + \frac{1}{2}\rho \left(\frac{Q_2}{A_2}\right)^2$$

$$P_1 + \frac{1}{2}\rho \left(\frac{Q_1}{A_1}\right)^2 = P_3 + \frac{1}{2}\rho \left(\frac{Q_3}{A_3}\right)^2$$

The remaining three relationships can be derived using the characteristic variables. Since we have a hyperbolic system, each bifurcation vessel has one characteristic associated with that section belonging to the branching. So we will consider W_1 for the inlet artery while we will take W_2^1 and W_2^2 for the two outgoing vessels. The final system we obtain for as single bifurcation is the following:

$$\left\{ \begin{array}{l} W_1 = \frac{Q_1}{A_1} + 4\sqrt{\frac{\beta_1}{2\rho A_{01}}} A_1^{\frac{1}{4}} \\ W_2^1 = \frac{Q_2}{A_2} - 4\sqrt{\frac{\beta_2}{2\rho A_{02}}} A_2^{\frac{1}{4}} \\ W_2^2 = \frac{Q_3}{A_3} - 4\sqrt{\frac{\beta_3}{2\rho A_{03}}} A_3^{\frac{1}{4}} \\ Q_1 = Q_2 + Q_3 \\ P_1 + \frac{1}{2}\rho \left(\frac{Q_1}{A_1}\right)^2 = P_2 + \frac{1}{2}\rho \left(\frac{Q_2}{A_2}\right)^2 \\ P_1 + \frac{1}{2}\rho \left(\frac{Q_1}{A_1}\right)^2 = P_3 + \frac{1}{2}\rho \left(\frac{Q_3}{A_3}\right)^2 \end{array} \right. \quad (2.49)$$

We can solve it through the Newton-Raphson technique for differential systems of non-linear equations.

Chapter 3

Implementation of the numerical solver

In the previous chapter we introduced the mathematical formulation concerning the one-dimensional model of blood flow in arteries; we have defined the set of governing equations and boundary conditions whose numerical integration provides an approximated solution for our hemodynamic problem.

In this chapter we deal with the creation of a computation tool necessary to solve such a one-dimensional system and display the obtained results which, as already described, are related to the propagation of blood pressure and flow rate waves into the cardiovascular system.

We can divide the creation process of this solver module, or *problem type*, into two phases:

- Implementation of the numerical solver;
- Coupling of the solver with a graphical interface for data management and visualization of results;

The computational core of the problem type is represented by a finite element code programmed in FORTRAN90¹; then the graphical user interface is provided by GiD², which is a pre-post process finite element software developed at CIMNE³. GiD allows to define, prepare and visualize all the data related to a numerical solution;

¹See appendix B for a more detailed treatment

²See appendix A for details

³Ciéntro Internátional de Metodos Numéricos en Ingeniería, Barcelona, Spain

these data include the definition of the geometry, materials, conditions, solution informations and other parameters. The software can also generate a mesh for finite element, finite volume or finite difference analysis and write the informations for a numerical simulation program in its desired format.

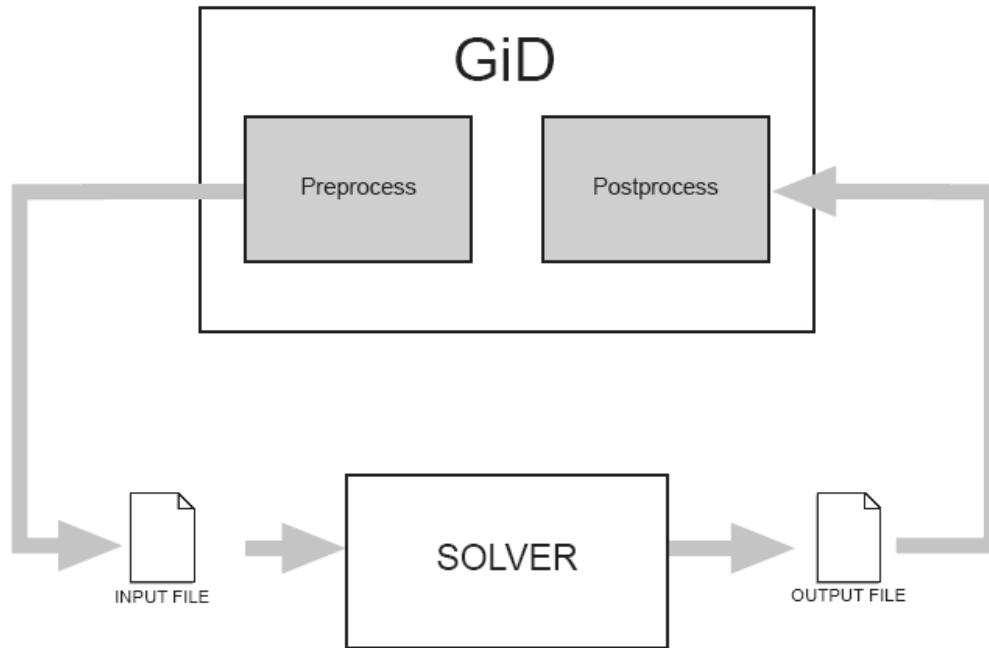


Figure 3.1: Flowchart describing the execution of a GiD problem type

Figure (3.1) shows the general scheme adopted by GiD for the preparation and the execution of a standard problem type; we note that the pre and post process phases, respectively for what concerns the creation of the *INPUT FILE* and the visualization of results, are both supported by the graphical interface. Instead the computation section (represented by the box *SOLVER*), where the numerical solution is calculated, can be seen as a component external to GiD; so it is possible, on the one hand, to customize the pre-post process interface, modifying the files composing GiD problem type (see Appendix A) and, on the other hand, to program any solver and couple it with the rest of the computation tool, just controlling that the *OUTPUT FILE* does respect the GiD format for reading results.

We now briefly present the various parts composing the problem type we created for the one-dimensional model of blood flow in arteries, following a certain number of steps organized as follows

1. Starting the problem, with the creation of the model geometry;

2. Creation of the material definition file;
3. Creation of the condition definition file;
4. Creation of the general configuration file;
5. Creation of the calculation program file and the execution files;
6. Execution of the calculation module and visualizing the results through GiD;

The point 1-4 can be referred to the pre-process phase, which provides the *INPUT FILE* (fig. 3.1) entering the *SOLVER* (point 5). The last point, which deals with the visualization of results, is referable to the post-process phase and will be considered in next chapter.

3.1 Geometry of the model

First of all the geometry of the objects composing the problem at hand must be defined; afterwards this operation has been completed, we can proceed imposing necessary conditions and other properties over the model and finally calculate the solution of our hemodynamic problem.

In GiD a generic geometry can be realized, in a way similar to a CAD (Computer Aided Design) system, through the definition of the points and lines composing the object we want draw.

Since we are considering a one-dimensional model, the problem variables are functions only of the longitudinal coordinate z in space, while the sectional components can be neglected; for this reason we can make two assumption about the vessel representation adopted into GiD interface. For a simplification purpose we first replace the three-dimensional vessel geometry with a single line, having the same length as the 3D tube and representing its longitudinal axis. Furthermore, it is useful to define a local reference system for each vessel of the model, in order to consider only the axial z component when we work with the finite element code. The origin of each local axis system is positioned on the inlet node of the corresponding vessel (the inlet section in a 3D representation), and the z -coordinate has the same direction as the blood flow one.

A single vessel is considered in figure 3.2 where we note the two mentioned assumptions; if we work with models containing more than one arterial vessel, a local axis must be created for each artery (fig. 3.3).

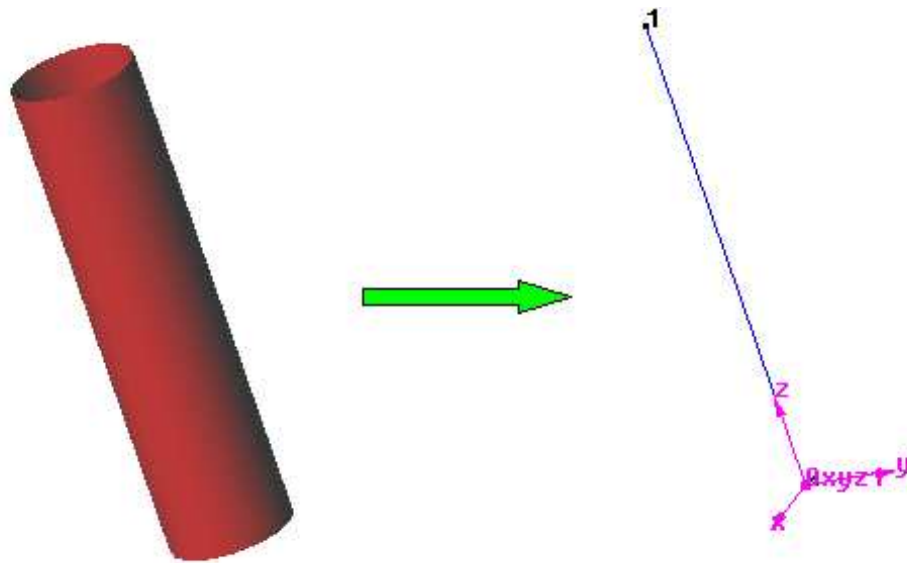


Figure 3.2: Comparison between a 3D vessel geometry and the 1D representation used in GiD problem type

3.2 Definition of materials

For the one-dimensional model of the arterial network, the definition of materials concerns the mechanical and geometrical characterization of the arterial wall surrounding each vessel.

It is possible to assign such properties selecting between those arteries whose parameters are included in tables 3.2 and 3.2. These data are referred to a simplified arterial network containing the 55 largest arteries in the human body (fig. 3.5); it was proposed and modelled using electrical circuits for the first time by Westerhof [34]. This reference provides data for diameters, wall thickness, length and elastic moduli for each of the 55 arteries. As we can see from the figure 3.4, the left window contains the mechanical and geometrical values defined into tables. The user has the possibility to modify such quantities, either changing only some of the listed properties or creating a new vessel with a completely different characterization (fig. 3.4, the right window).

3.3 Boundary and bifurcation conditions

The boundary conditions for a one-dimensional model, as written in the previous chapter, have to be defined both at inlet and outlet sections of the arterial

No.	Name of the vessel	l (cm)	r (cm)	h (cm)	E ($10^6 Pa$)	c ($\frac{m}{s}$)
1	Ascending Aorta	4.0	1.470	0.163	0.4	4.67
2	Aortic Arch I	2.0	1.263	0.126	0.4	4.43
3	Brachiocephalic	3.4	0.699	0.080	0.4	4.47
4	R. Subclavian I	3.4	0.541	0.067	0.4	4.93
5	R. Carotid	17.7	0.473	0.063	0.4	5.11
6	R. vertebral	14.8	0.240	0.045	0.8	8.58
7	R. Subclavian II	42.2	0.515	0.067	0.4	5.05
8	R. radius	23.5	0.367	0.043	0.8	6.78
9	R. ulnar I	6.7	0.454	0.046	0.8	6.31
10	R. interosseus	7.9	0.194	0.028	1.6	10.64
11	R. ulnar II	17.1	0.433	0.046	0.8	6.45
12	R. int. carotid	17.6	0.382	0.045	0.8	6.80
13	R. ext. carotid	17.7	0.382	0.043	0.8	6.57
14	Aortic arch II	3.9	1.195	0.115	0.4	4.35
15	L. carotid	20.8	0.413	0.063	0.4	5.47
16	L. int. carotid	17.6	0.334	0.045	0.8	7.27
17	L. ext. carotid	17.7	0.334	0.042	0.8	7.02
18	Thoracic aorta I	5.2	1.120	0.110	0.4	4.39
19	L. Subclavian I	3.4	0.474	0.066	0.4	5.23
20	L. vertebral	14.8	0.203	0.045	0.8	9.23
21	L. Subclavian II	42.2	0.455	0.067	0.4	5.38
22	L. radius I	23.5	0.324	0.043	0.8	7.21
23	L. ulnar I	6.7	0.401	0.046	0.8	6.71
24	L. interosseous	7.9	0.172	0.028	1.6	11.23
25	L. ulnar II	17.1	0.383	0.046	0.8	6.87
26	Intercostals	8.0	0.317	0.049	0.4	5.51
27	Thoracic aorta II	10.4	1.071	0.100	0.4	4.28
28	Abdominal aorta I	5.3	0.920	0.090	0.4	4.38
29	Celiac I	2.0	0.588	0.064	0.4	4.62

Table 3.1: Physiological data of the 55 main arteries used in the one-dimensional model. From [34][25] and [33]. Part 1 of 2, vessels from 1 to 29

No.	Name of the vessel	l (cm)	r (cm)	h (cm)	E ($10^6 Pa$)	c ($\frac{m}{s}$)
30	Celiac II	1.0	0.200	0.064	0.4	7.93
31	Hepatic	6.6	0.458	0.049	0.4	4.58
32	Gastric	7.1	0.375	0.045	0.4	4.85
33	Splenic	6.3	0.386	0.054	0.4	5.24
34	Sup. mesenteric	5.9	0.499	0.069	0.4	5.21
35	Abdominal aorta II	1.0	0.843	0.080	0.4	4.32
36	L. renal	3.2	0.350	0.053	0.4	5.45
37	Abdom. aorta III	1.0	0.794	0.080	0.4	4.45
38	R. renal	3.2	0.350	0.053	0.4	5.45
39	Abdominal aorta IV	10.6	0.665	0.075	0.4	4.70
40	Inf. mesenteric	5.0	0.194	0.043	0.4	6.60
41	Abdominal aorta V	1.0	0.631	0.065	0.4	4.50
42	R. com. iliac	5.9	0.470	0.060	0.4	5.00
43	L. com. iliac	5.8	0.470	0.060	0.4	5.00
44	L. ext. iliac	14.4	0.482	0.053	0.8	6.57
45	L. int. iliac	5.0	0.301	0.040	1.6	10.21
46	L. femoral	44.3	0.361	0.050	0.8	7.37
47	L. deep femoral	12.6	0.356	0.047	0.8	7.20
48	L. post tibial	32.1	0.376	0.045	1.6	9.69
49	L. ant. tibial	34.3	0.198	0.039	1.6	12.44
50	R. ext. iliac	14.5	0.482	0.053	0.8	6.57
51	R. int. iliac	5.0	0.301	0.040	1.6	10.21
52	R. femoral	44.4	0.361	0.050	0.8	7.37
53	R. deep femoral	12.7	0.356	0.047	0.8	7.20
54	R. post tibial	32.2	0.375	0.045	1.6	9.71
55	R. ant. tibial	34.3	0.197	0.039	1.6	12.46

Table 3.2: Physiological data of the 55 main arteries used in the one-dimensional model. From [34][25] and [33]. Part 2 of 2, vessels from 30 to 55

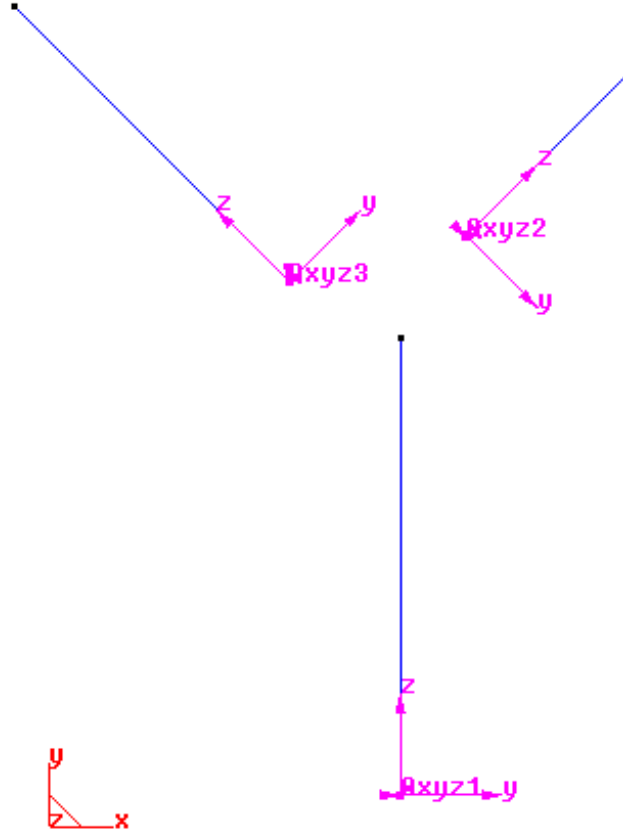


Figure 3.3: Scheme of a bifurcation containing three vessels. As we note each vessel has its own local reference axis (pink color), rotated with respect to the global reference system (red color).

network; moreover, since we also consider the presence of bifurcations between vessels, it is necessary to identify those arteries composing the branching and apply the compatibility conditions over them (see section 2.7 of chapter 2).

For what concerns boundary conditions, at the inlet we can choose the type of known variable, pressure or flow rate, and modify a certain number of parameters related to the entering waveform (fig. 3.6): if we select a half sine wave profile (fig. 3.8 right), we can modify the initial and the maximum amplitude value of the curve, while if we use a physiological-type known function (fig. 3.8 left), no parameters needs to be modified.

The boundary conditions at the outlet section depend upon the applied value of terminal resistance R_T . If we assume the case of absorbing condition, then $R_T = 0$ and there should not be any wave reflection at the outlet section. In the other situation, that is consider a certain contribution of terminal resistance which simulates the distal part of the arterial network, then $R_T \neq 0$. The value of R_T can be settled

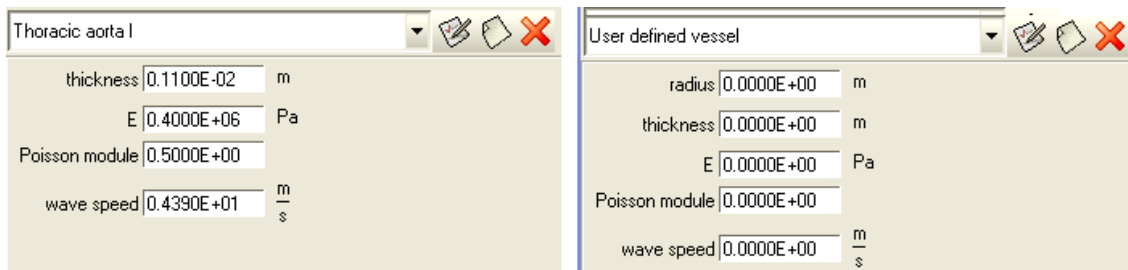


Figure 3.4: GiD windows containing material properties. Left window: vessel types belonging to arterial network defined [25],[34] and [33]. Right window: customizable vessel with user-defined properties

by the user through the GiD window shown in fig. 3.6.

The presence of a bifurcation in the arterial network must be defined indicating those vessels composing the selected branching; we have to follow the 55 artery model in order to select the correct vessels. Figure 3.7 shows the list of bifurcation and the arteries belonging to each of them.

3.4 General configuration of the problem

The configuration of a problem type in GiD, besides the attribution of boundary conditions and material properties, also needs the definition of several parameters related to:

- The general data (e.g. blood rheologic parameters, graphical visualization parameters);
- Data concerning the numerical solution (tolerance parameters for iterative schemes, integration period);

3.4.1 General data

As shown in figure 3.9, such informations include the problem title, the unit system, the density and viscosity of blood, the initial pressure in the aortic root⁴, the Coriolis coefficient and the type of velocity profile (fig. 2.3) adopted for the 1D formulation. For the last parameter we can choose between a flat velocity profile ($\gamma = 0$), a parabolic profile ($\gamma = 2$) and power-law profile [24] ($\gamma = 9$).

⁴With the term *aortic root* we refer to the section of aorta closest to the semilunar valve out of the left ventricle

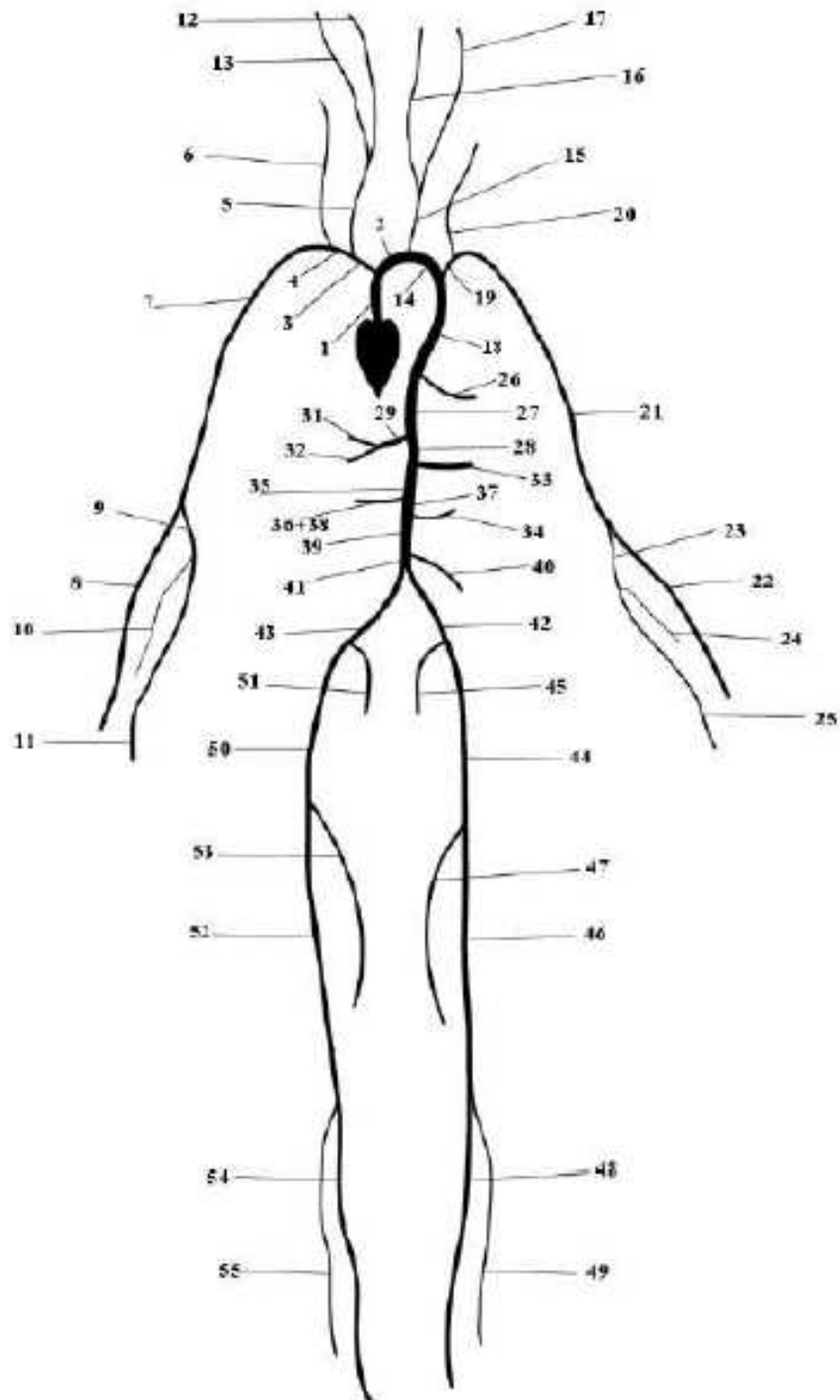


Figure 3.5: Connectivities between the 55 main arteries of the human body. From [22]

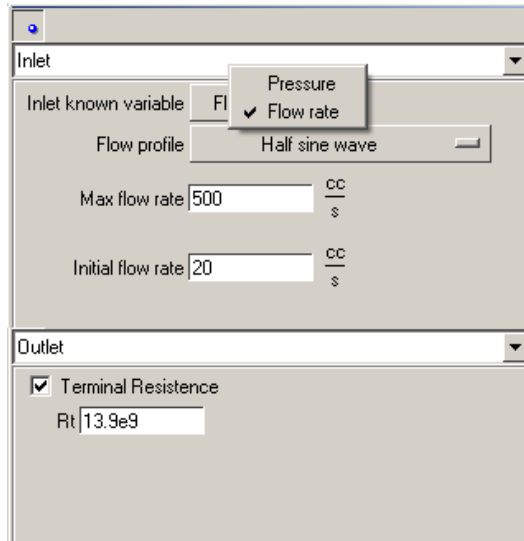


Figure 3.6: GiD window for boundary conditions assignment.

Beyond such informations, the GiD problem type allows the user to choose which results show during the post-process and how many temporal step write, and subsequently display, into the output file.

The visualization of results into GiD post-process is done transforming the 1D representation of the model geometry, adopted during the pre-process phase, into a three-dimensional mesh, used only for graphical purposes, which gives a representation of results clearer than the one we may have by means of the one-dimensional sketch. For this reason the user must set, through the parameter *Section contour nodes* (fig. 3.9), the number of nodes lying on the border of each section in order to build the 3D mesh composed by triangular elements (fig. 3.10).

3.4.2 Numerical integration data

The process of numerical integration involves the configuration of several parameters, some of them concerning the tolerances for approximation errors and others related to the integration period. Figure 3.11 shows the list of parameter whose values can be inserted by the user. We have:

- The number of cardiac cycles considered for the simulation. The user can choose between three classes of cardiac frequency: *Standard*, with a generic value of 72 bpm, *Tachycardia*, with 110 bpm and *Brachycardia* with 55 beats per minute. It is also possible to change the time duration of the cardiac cycle,

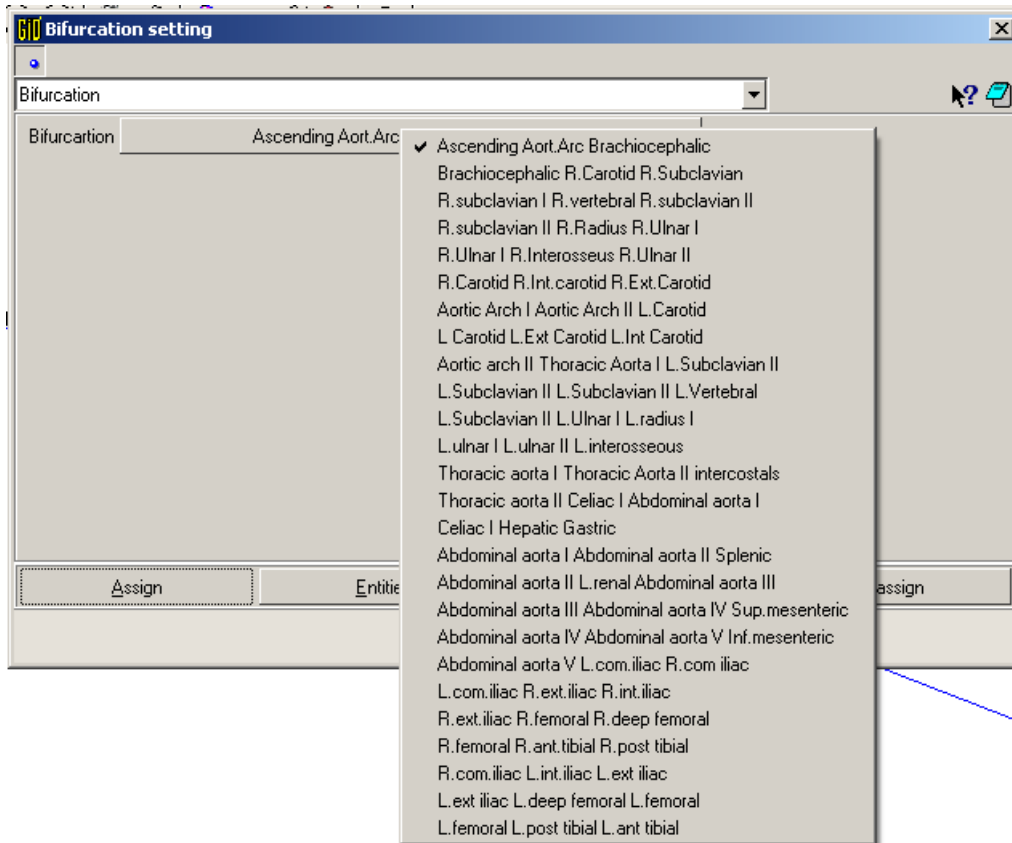


Figure 3.7: Bifurcation assignment window

paying attention not to insert too low values; if we decrease under a period of 0.3 seconds, which represents the duration of heart systole phase, the complete simulation of a heart beat would not be accomplished.

- The space-time integration scheme to use; the choice is between straightforward Galerkin - Taylor Galerkin and 2nd - 4th Runge Kutta (R-K) schemes.
- The maximum number of steps to calculate using R-K schemes;
- The CFL parameter, defined by (2.48), for the maximum time step definition;
- The α_s stabilization parameter (for straightforward Galerkin only);
- In the case we use the adaptive step size control for Runge-Kutta schemes, it is possible to define the minimum time step and the error tolerance;
- The error tolerance of Newton-Raphson iterative scheme for the solution of non-linear equations related to the compatibility relationships at bifurcations

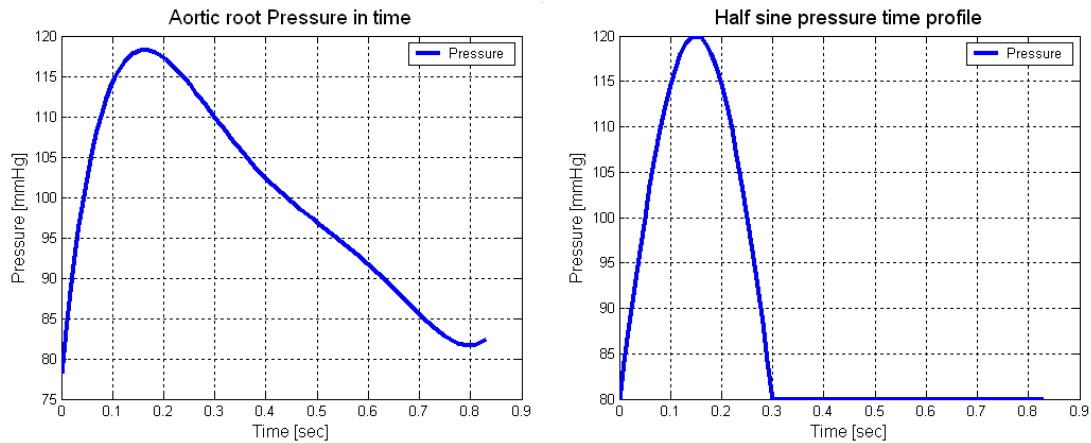


Figure 3.8: Inlet known pressure profiles. Left graph: polynomial-interpolated function based on physiological data. Right graph: half-sine wave profile. Data referred to a single cardiac cycle.

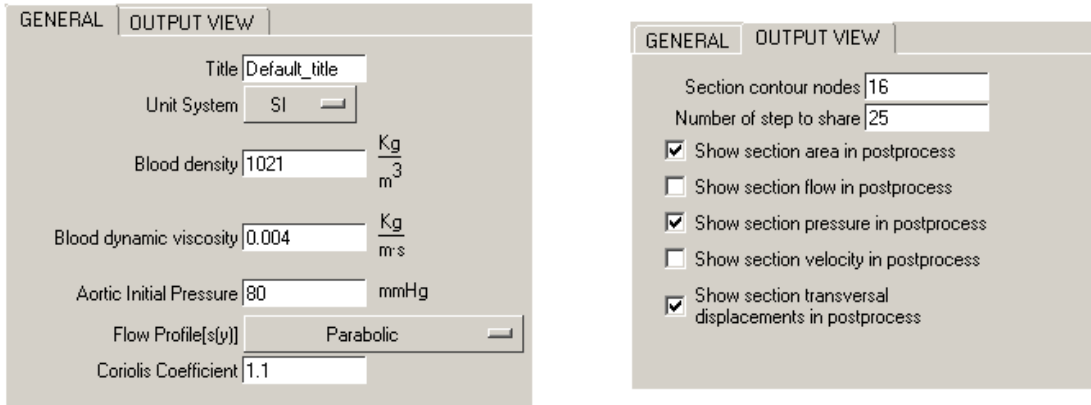


Figure 3.9: GiD general data window

and the pseudo-characteristic evaluation at the outlet boundaries;

3.5 The numerical solver

All the informations related to finite element mesh, material and geometrical properties, and problem general parameters are assembled together by GiD in a *calculation file*, which is indicated by the *INPUT FILE* in fig. 3.1; these data represent the starting point of the numerical solver.

The finite element code we programmed (see Appendix B) first reads the information coming from this calculation file, then starts solving the numerical problem following this general scheme:

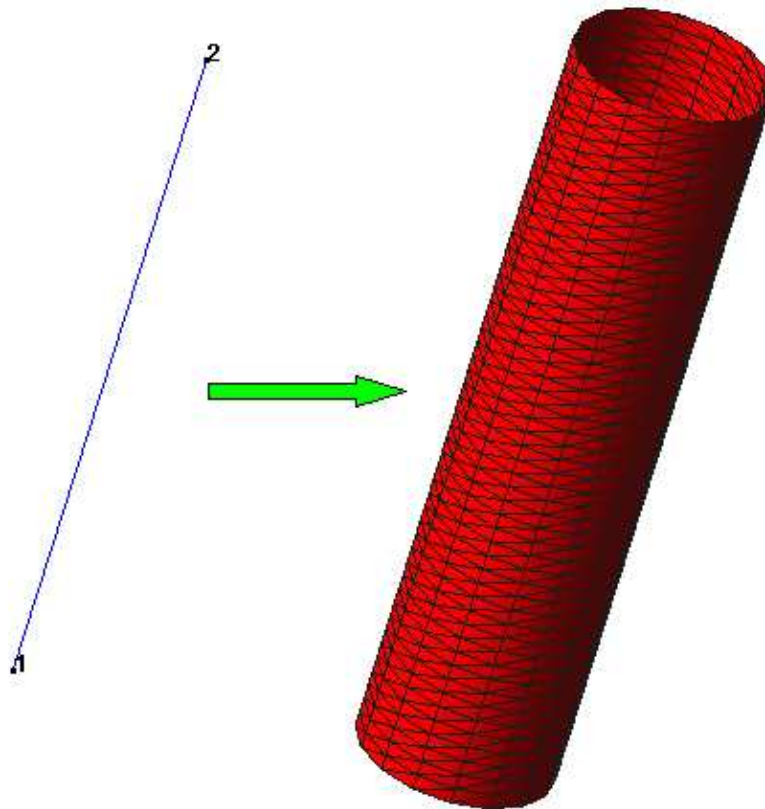


Figure 3.10: Correspondence between 1D and 3D representation of a single vessel into GiD problem type.

START

(1) **Input data reading;**

$t=t_0$; \Rightarrow Initial time

$U=U_0$; \Rightarrow Initial values

(2) WHILE ($t < T$)

Evaluate $\Delta t < CFL \frac{l}{\max(\lambda_{1,2})}$;

(3) FOR ($i=1$:Number of elements)

calculate rhs-element;

rhs-global = rhs-global + rhs-element;

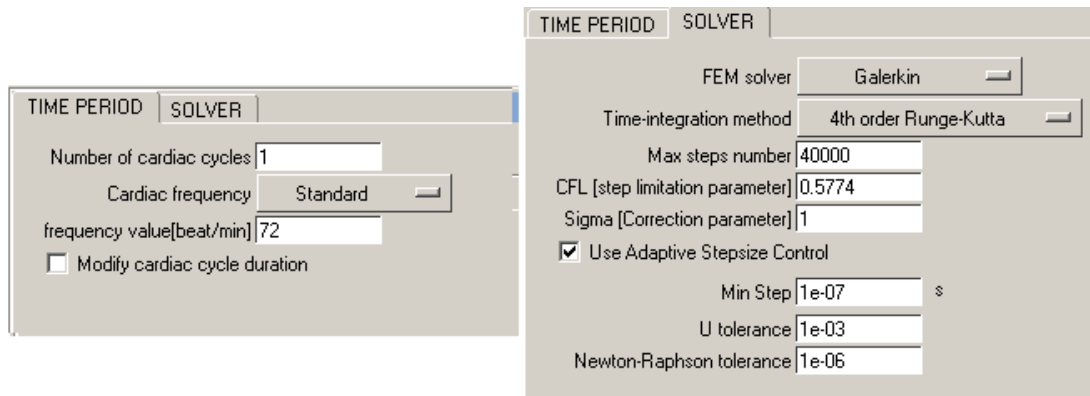


Figure 3.11: Windows for the assignment of numerical analysis parameters.

END

(4) Apply boundary and bifurcation conditions

$$U(t + \Delta t) = U(t) + \Delta t(\text{rhs-global});$$

$$t = t + \Delta t;$$

END

(5) write output results

STOP

In order to briefly explain the scheme above, we focus on five points, enumerated from 1 to 5:

1. **Input data reading:** from GiD pre-process, the problem data are loaded and read by the program;
2. WHILE loop: main temporal loop which provides the solution array \mathbf{U} , as defined in (2.19), for each temporal step; the number of step is not a priori defined, because at each iteration we have to calculate the maximum step following the relationship (2.48). For this reason we employed a WHILE loop instead of a FOR one;
3. FOR loop: secondary loop which calculates, for each linear mesh element, the

contribution given by the right-hand side (*rhs-element* in the scheme above) of equation (2.41) or (2.47), depending if we use straightforward Galerkin or Taylor-Galerkin scheme respectively.

4. **Apply boundary and bifurcation conditions:** all the element contributions are assembled into a global right-hand side (*rhs-global* in the scheme) to which boundary and bifurcation conditions are applied;
5. **(5) write output results:** The results are written in an *OUTPUT FILE* (fig. 3.1) following the indications, given during pre-process (fig. 3.9), about the type of variables (pressure, vessel section, flow rate or blood velocity) and the number of temporal steps to be saved for post-process visualization.

During the execution of the program, the user can control the development of the calculus through a window (fig. 3.12) displaying some general informations, e.g. the number of nodes and elements related to the liner 1D mesh, and the number of iterations already computed. In the case of interruptions, e.g. due to not convergence or exceeded limit of maximum iterations, a message to screen will appear.

```

output info for 'current' Sun Feb 26 13.43.02
Program started at: 13:43:03
Project name   Carotid_validation
1D arterial network modelling
Mesh composed by:
      401 Nodes and      400 Elements
Time integration interval 0.8333330000000000 seconds
 1000 iterations calculated. t= 0.147290252418953
 2000 iterations calculated. t= 0.290137986586796
 3000 iterations calculated. t= 0.441072142366871
 4000 iterations calculated. t= 0.593081443998162
 5000 iterations calculated. t= 0.745120887817474
Total number of iterations =      5581
Computation time      0 minutes      16 seconds
  
```

Figure 3.12: GiD window for monitoring numerical calculation

Chapter 4

Numerical results

The computational tool we implemented coupling the GiD interface with a finite element code allows to numerically simulate the blood flow in the arterial network through a one-dimensional formulation. In this chapter we will show the results obtained by the approximated solution of such a hemodynamic problem; first we consider a simple geometry composed by one single vessel in order to validate the model and also compare the various space-time schemes that we programmed. Afterwards we will deal with the vascular network composed by the 55 main human arteries, whose structure and properties have been presented respectively in fig. 3.5 and in tables 3.2 and 3.2.

4.1 Inlet profiles

The correct imposition of a suitable perturbation which enters the problem domain is fundamental for the correct development of pressure or flow rate waves through the arteries. At the inlet section of our model we have to impose, in order to satisfy the mathematical requirements for hyperbolic models, exactly one boundary condition related to the entering characteristic $W1$ (see eq. 2.34). In the majority of cases we use to express such a condition in terms of physical variables, like area or flow rate; doing this we have the possibility, using such quantities, to configure a certain type of profiles similar to a physiological ones, obtained for example by experimental data.

When we presented the configuration of the GiD problem type, we introduced in figure 3.8 two inlet profiles of pressure in time. Through the pressure-area relationship, derived by the elastic model (see eq. 2.13) of the arterial wall, it is possible

to obtain the corresponding value of area. The other possibility is to introduce a function expressing the flow rate variation at the inlet of the arterial network. This relationship, taken as an approximation of a real physiological profile, can be written as

$$\left\{ \begin{array}{ll} Q = Q_0 & \text{if } 0 \leq t < 0.05s \\ Q = Q_0 + \Delta Q \sin\left(\pi \frac{t - 0.05}{0.21}\right) & \text{if } 0.05s \leq t < 0.26s \\ Q = Q_0 - \frac{\Delta Q}{10} \sin\left(\pi \frac{t - 0.26}{0.03}\right) & \text{if } 0.26s \leq t \leq 0.29s \\ Q = Q_0 & \text{if } t > 0.29s \end{array} \right. \quad (4.1)$$

where Q_0 is the initial flow rate and ΔQ represents the peak of flow rate reached by the half sine wave. The above function follows the trend given by of the physiological Q profile, in proximity of the semilunar valve out of the left ventricle, as showed in figure 4.1. Here we assumed the duration of 0.83 seconds, for this single cycle, considering a standard cardiac frequency of 72 bpm, typical of a normal healthy person. For different values of frequency, e.g. in the case of pathologic situations (bradycardia, tachycardia) it is possible to modify the duration of the diastolic phase, which comes after the half sine wave propagation and is the only heart-rate dependent part of the cardiac cycle, as explained in figure 4.1.

The imposition of this kind of profile, or equally a pressure known function, allows to evaluate the wave propagation through arteries, first imposing a no-reflecting output condition for the case of a single vessel, then comparing such an 'absorbing behaviour' of the outlet section with the imposition of a terminal resistance for the case of an artery network. Beyond this aspect it is also possible to observe the distribution of the flux into the vascular system, comparing numerical values with experimental data.

4.2 Case I: model of a single artery

We consider the modelling of a single artery having mechanical and geometrical properties referred to the *Thoracic aorta I* in table 3.2. Here we resume such properties:

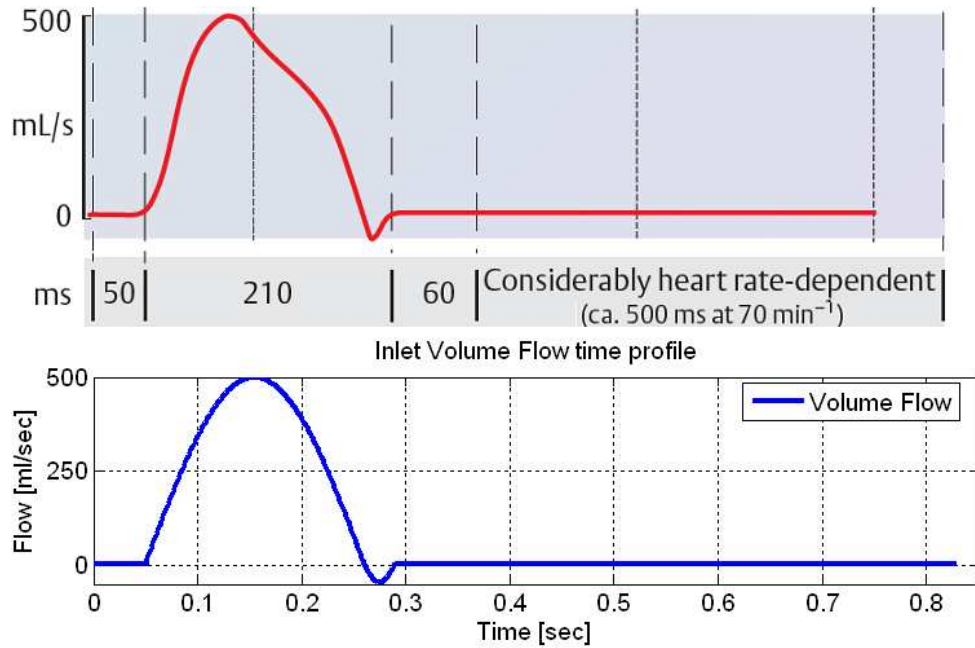


Figure 4.1: Lower image: input flow rate profile for the 1D model. Upper image: flow rate profile out of the left ventricle. From <http://www.zoo.ufl.edu/courses/pcb4723/>.

Name	Thoracic aorta I
Radius	1.120 cm
Length	80 cm
Wall thickness	0.110 cm
Elastic modulus	400000 Pa

In this case we assume a length of 80 cm in order to better evaluate the wave propagation through the artery. We simulated our one-dimensional problem imposing both pressure and flow rate at the inlet section, and adopting a no-reflecting condition at the outlet. The time period considered is 1.66 seconds, corresponding to the duration of two complete cardiac cycles in standard frequency conditions (72 bpm).

Through the evaluation of the results we can outline some considerations about the numerical schemes we implemented into our finite element code. Figure 4.3 shows the flow rate in time related to a single vessel, the thoracic aorta, calculated using both a straightforward Galerkin and a Taylor-Galerkin scheme. Analyzing the wave profiles we note that the Galerkin obtained solution has a positive flow rate increasing, after the main pulse has passed. This behaviour does not conform with the physiological flow trend (fig. 4.1), which presents a small decrease of flow

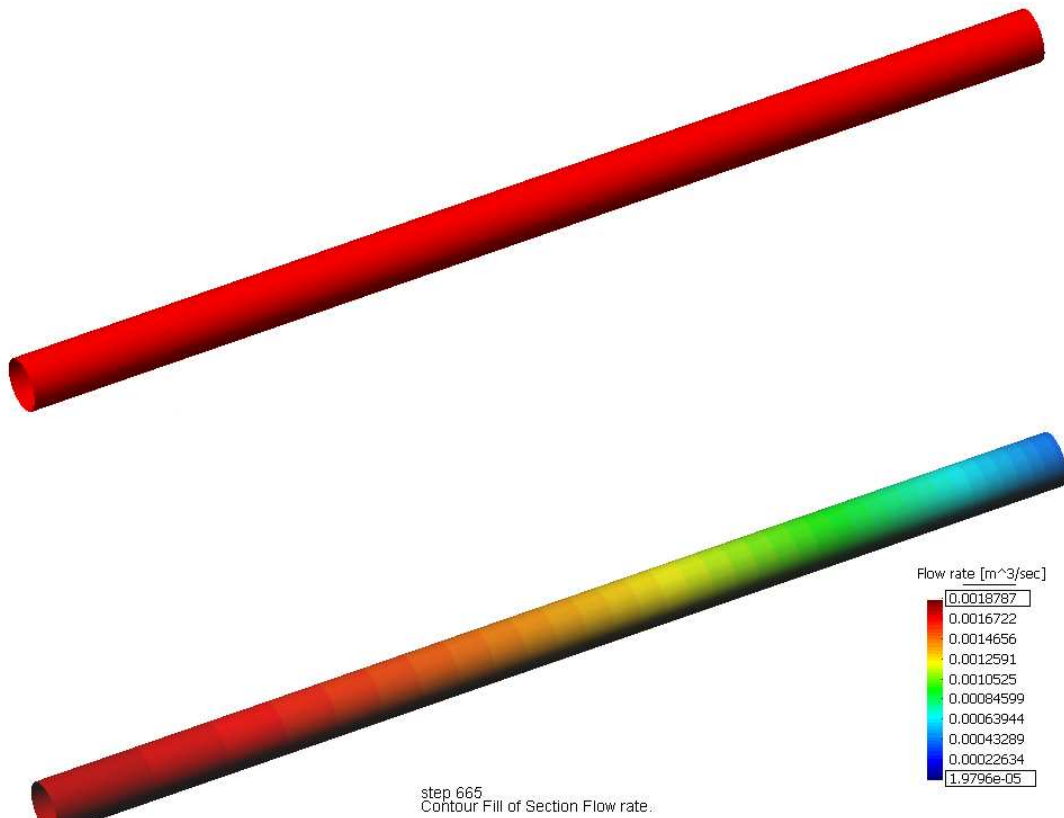


Figure 4.2: Result visualization through GiD post-process interface. In this case we consider mean sectional values of flow rate in a certain time instant.

rate due to the pressure drop at the end of the systolic phase. On the contrary the profile resulting from the simulation with a Taylor-Galerkin scheme seem to better reproduce the physiological trend for Q in time.

Another aspect that we can evaluate is the variation of the solution when considering different velocity profiles. We can change the slope of the function (2.7) through the modification of the coefficient γ , so we compare the two most common profiles which are the parabolic one ($\gamma = 2$) and the power-law one ($\gamma = 9$).

As we can see in figure 4.4, the flow rate trend does not significantly change with respect to the applied profile. This behaviour of the numerical solution accords with the assumption that, for one-dimensional modellings of blood flow in main arteries, the viscous term gives an inferior contribution with respect to the other terms. Therefore we do not properly consider it, especially when we work with characteristic variables, because we can decouple the characteristic system (2.29), as already discussed in section 2.4.

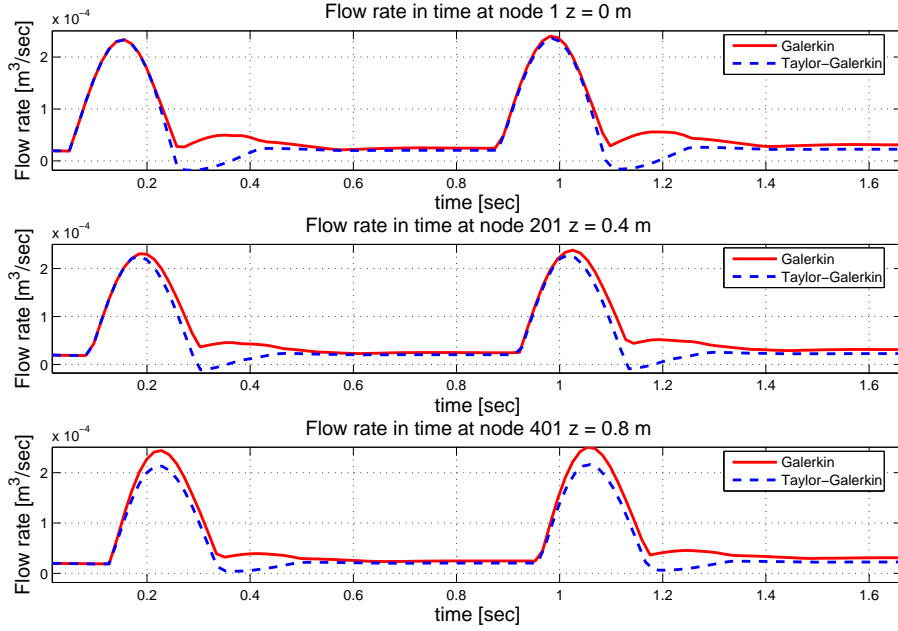


Figure 4.3: Comparison between the solutions, related to blood flow propagation into a 80 cm length Thoracic aorta, obtained using straightforward Galerkin and Taylor-Galerkin schemes. We imposed a known pressure profile at the inlet and no terminal resistance has been applied.

4.3 Case II: 55 artery network

The simplified vascular network (scheme in fig. 3.5) has been represented, through the GiD interface, as we can see from figure 4.6. The orientation of vessels in the model does not influence the computation of the numerical solution, first because we defined a local reference system for each artery, in order to work always with only an axial component, and second because we do not consider, at bifurcations, that blood flow changes depending on the value of the angles formed by the branching vessels. This assumption is coherent since the solution of our problem, does not significantly change if we consider or not a certain dependence from the branching degree of a bifurcation; for details see [4].

4.3.1 Terminal resistance

In the previous model of a single vessel we applied only an absorbing condition at the outlet section. For a more realistic simulation of blood flow, the contribution given by the distal components of the cardiovascular system, which are not part of the 55 artery network, must be considered.

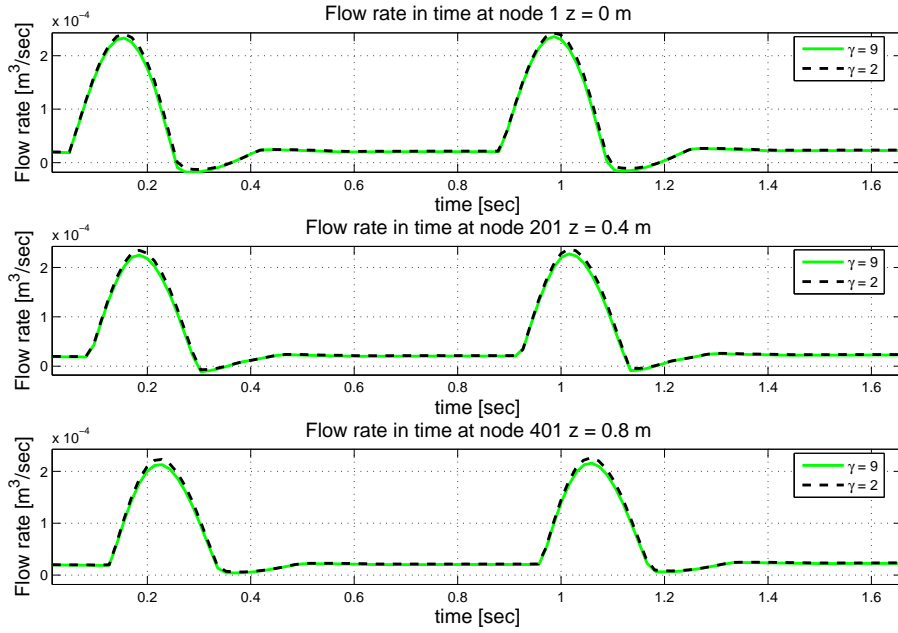


Figure 4.4: Comparison between flow rate waveforms obtained using different velocity profiles; $\gamma = 2$ the parabolic one and $\gamma = 9$ for the power law profile. Taylor-Galerkin scheme applied. Again we imposed a known pressure profile at the inlet and no terminal resistance has been applied.

For this reason we assumed that the downstream micro-circulation acts as an 'obstacle' to the blood flow coming from the main arteries; this resistive effect can be expressed, using an analogy with electric circuits (4.5), with a relationship between pressure and flow rate of the type

$$P = Q \cdot R_T,$$

where R_T represents *terminal resistance*. The magnitude of this term is different depending on the position we consider over the vascular network; table 4.3.1 shows the different values of R_T corresponding to the terminal vessels of our model. Such

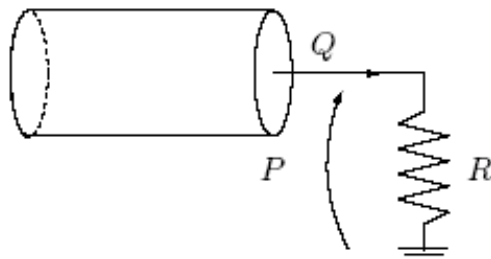


Figure 4.5: Scheme of the resistive model adopted to simulate reflecting outlet conditions

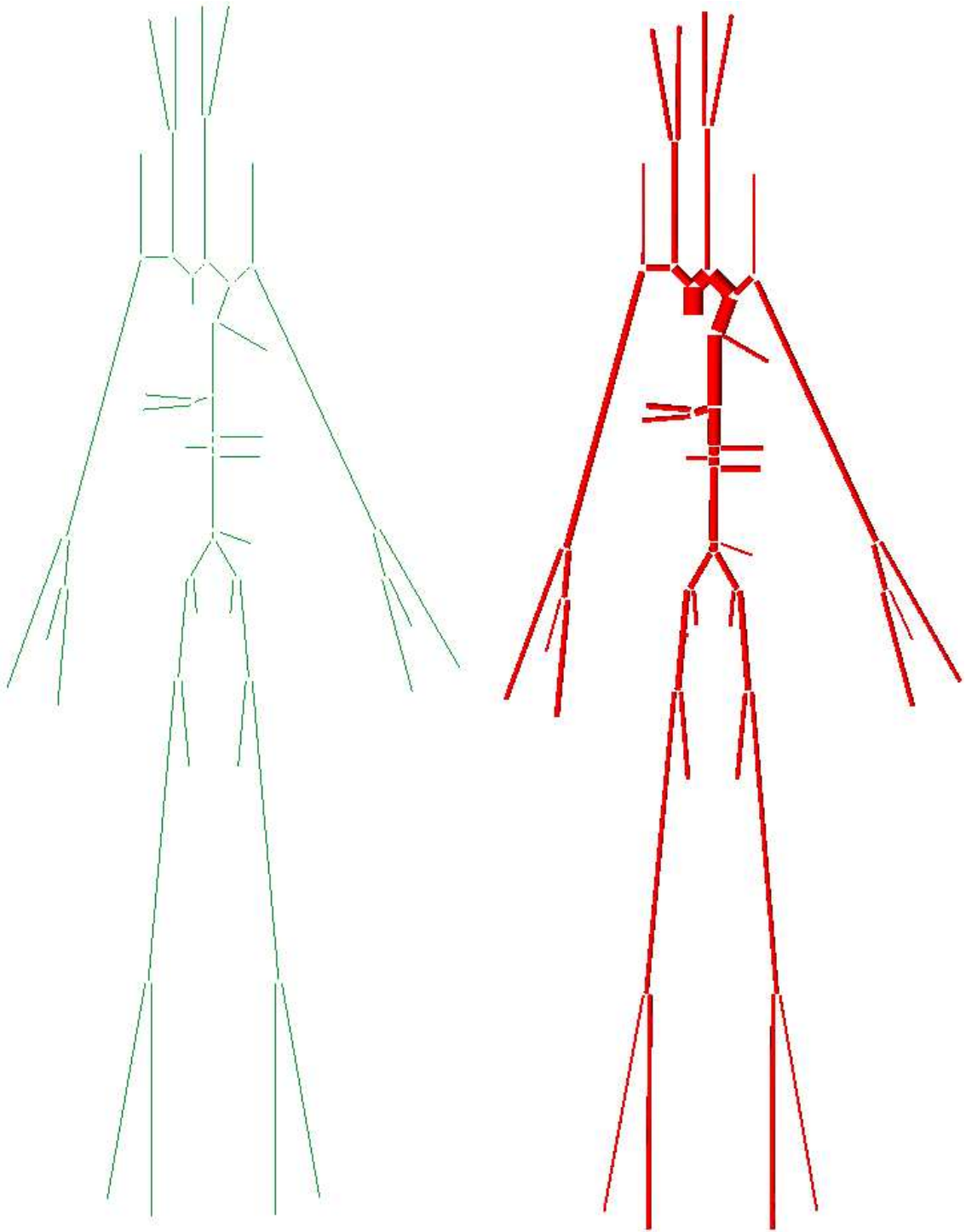


Figure 4.6: GiD representation of the 55 artery network

quantities have been calculated by Stergiopoulos and Parker [25]; here we adopt the values modified by Wang and Parker [33].

No.	Artery	$R_T \left(10^9 \frac{Pa \cdot s}{m^3} \right)$	No.	Artery	$R_T \left(10^9 \frac{Pa \cdot s}{m^3} \right)$
6	Right vertebral	6.01	32	Gastric	5.41
8	Right radius	5.28	33	Splenic	2.32
10	Right interosseous	84.3	34	Sup. mesenteric	0.93
11	Right ulnar II	5.28	36	Left renal	1.13
12	Right int. carotid	13.9	40	Inf. mesenteric	6.88
13	Right ext. carotid	13.9	45	Left ext. Iliac	7.94
16	Left int. carotid	13.9	47	Left deep femoral	4.77
17	Left ext. carotid	13.9	48	Left post. tibial	4.77
19	Left vertebral	6.01	49	Left ant. tibial	5.59
22	Left radius	5.28	51	Right int. iliac	7.94
24	Left interosseous	84.3	52	Right deep. femoral	4.77
25	Left ulnar II	5.28	54	Right post. tibial	4.77
26	Intercostals	1.39	55	Right ant. tibial	5.59
31	Hepatic	3.63			

Table 4.1: Values of terminal resistance for the 55 artery model. Data taken from [33].

4.3.2 Ascending-descending aorta

The numerical solution of the arterial network model provides values of section area and flow rate at each node of the 1D linear mesh generated by GiD. In order to validate the finite element code which calculates such results, we have compared the mean profiles of flow rate derived from our model with the ones obtained through magnetic resonance imaging (MRI).

Thanks to the collaboration with the Santa Creu I Sant Pau Hospital of Barcelona, we have available a set of high-resolution MR images corresponding to several sections of the ascending-descending aorta segments; by means of a software for image

elaboration, the *FLOW MEDIS 4.1*,¹ we are able to extract a time profile for the mean flow rate over the considered sections. Figure 4.7 shows, taking as reference our GiD model of the artery network, the disposition of the four section corresponding to the ones whose experimental MRI data are available.

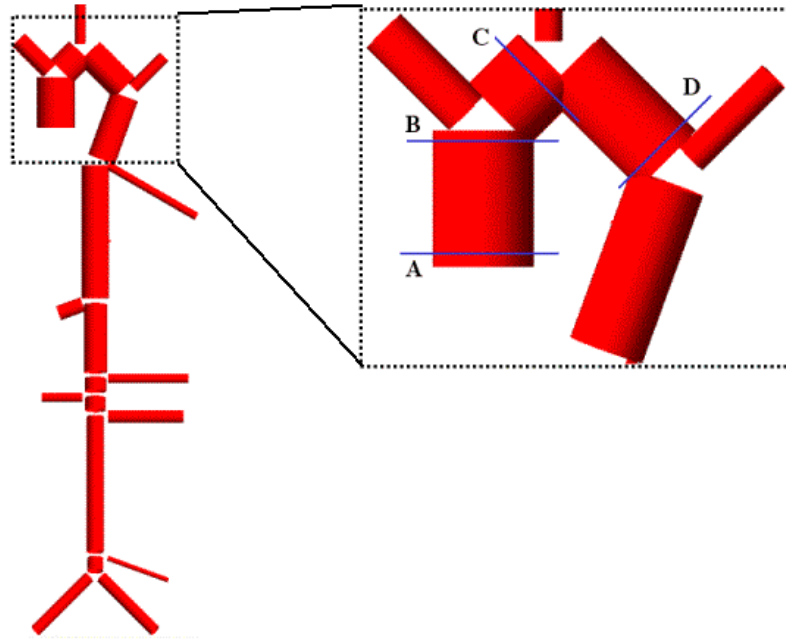


Figure 4.7: Flow rate values at four locations (A,B,C,D sections) in the aorta. Comparison between 1D-model profiles, obtained applying/not applying terminal resistance, and MRI imaging data.

The following graphics contain the trend of different flow rate profiles, related both to the numerical results and the magnetic resonance values, at sections A,B,C and D of the figure 4.7.

As we can note, the flow rate in the ascending aorta, which is the artery segment directly linked to the left ventricle, is not modified by the presence of terminal resistances in distal vessel with respect to the totally absorbing configuration of the network; when the distance from the heart increases, the influence of such terms begins revealing through a decrease of the flow rate, due to the 'obstacle' created by the peripheral tissues and acting on the flowing blood.

¹FLOW MEDIS - MRI Volume Analysis. Manufacturer: Philips Medical Systems. For more informations: www.medical.philips.com

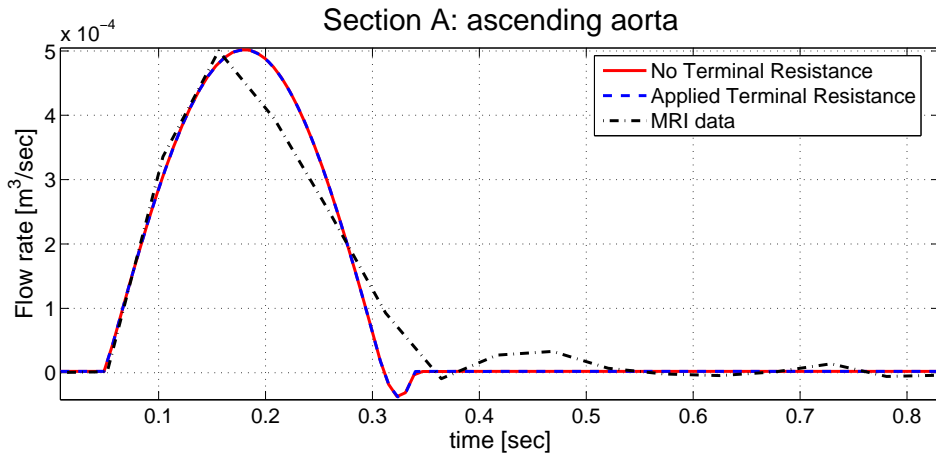


Figure 4.8: Flow rate profiles at the root of the ascending aorta (section **A**).

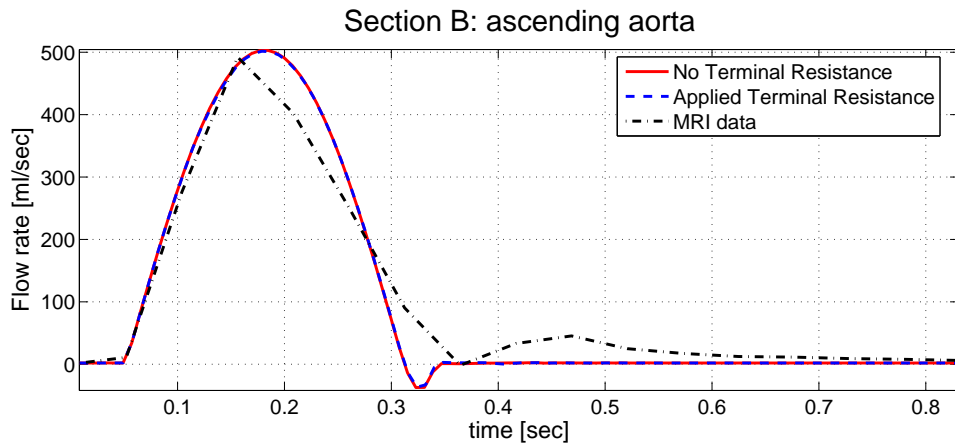


Figure 4.9: Flow rate profiles at the top of the ascending aorta (section **B**).

The profiles extracted by numerical simulations accords with the flow rate trend characteristic of MRI data, both for what concerns the peak values and the time progress, above all in the phase of initial systole, when blood comes out from the heart and begin propagating into the systemic circulation; for what concerns the late systole, we note small differences between numerical and experimental profiles. This may be due to the fact that the inlet flow rate we imposed at the inlet decreased faster if compared with the smoother profile related to the physiological data (see fig. 4.1).

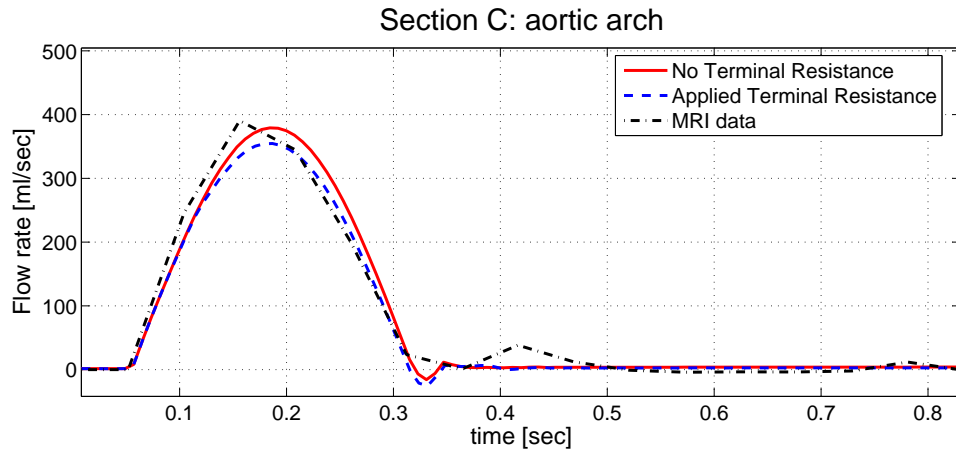


Figure 4.10: Flow rate profiles in the aortic arch (section **C**).

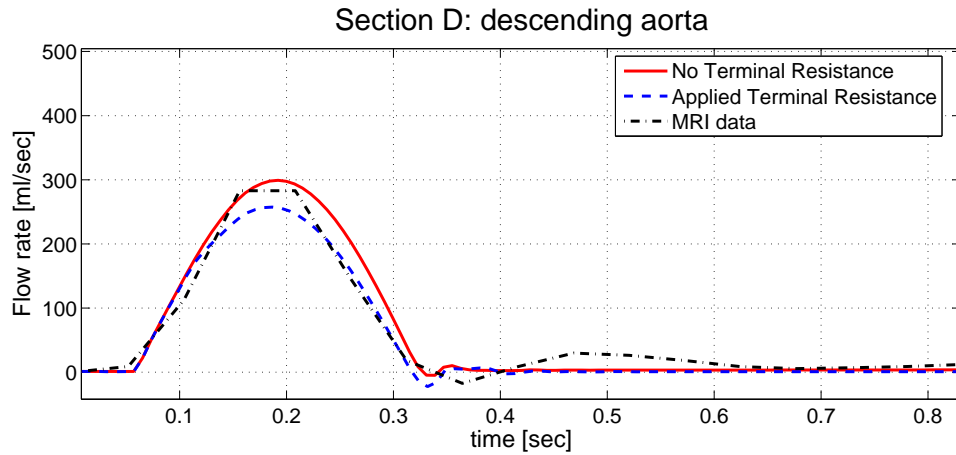


Figure 4.11: Flow rate profiles in the beginning of the descending aorta (section **D**).

4.3.3 Flow distribution

In order to validate the numerical solution of the one-dimensional problem concerning the blood flow into cerebral and limb circulation, we can demonstrate that the cardiac output is distributed in a correct way following typical physiological values². At rest conditions, approximately 1/3 of the volume flow coming out from the heart is directed into the upper-aortic circulation, which includes the cerebral and upper limbs vessels; the remaining 2/3 pass through the aorta and reaches the central and lower circulation, including e.g. renal and mesenteric arteries, and the lower limb vessels.

²The physiological considerations which follow are taken from the website <http://users.rcn.com//jkimball.ma.ultranet/BiologyPages/C/Circulation2.htm>

Vessel name	Q ($\frac{ml}{sec}$)	% of total flow
Brachiocephalic	105	
Left carotid	26	
Left subclavian I	40	
	171	34%
Thoracic aorta I	350	66%
<i>total flow</i>	521	

Table 4.2: Table containing flow rate values for those arteries involved in the evaluation of blood distribution.

We evaluated the flow rate values measured in those arteries which bifurcate from the aortic segment to go into the upper circulation together with the profile related to the thoracic aorta, which on the contrary drives blood to the central and lower arteries. We have taken values respectively from the *brachiocephalic* (fig. 4.12), *left carotid* (fig. 4.13), *left subclavian* (fig. 4.14) and *thoracic* (fig. 4.15) arteries; the global blood flow passing into the first three vessels, during a standard cardiac cycle, really represents the 2/3 of the total volume flow pumped out by the heart, while the remaining 1/3 is driven through the aorta. Table 4.3.3 shows such results.

Another situation that can be considered is the flow into the lower limbs. Figure 4.16 shows the profile related to the terminal segment of abdominal aorta which bifurcates into the left (fig. 4.18) and right (fig. 4.17) common iliac arteries. As we can note the flow divides exactly in two parts, according with the fact that, in each lower limbs the blood flow rate must be the same.

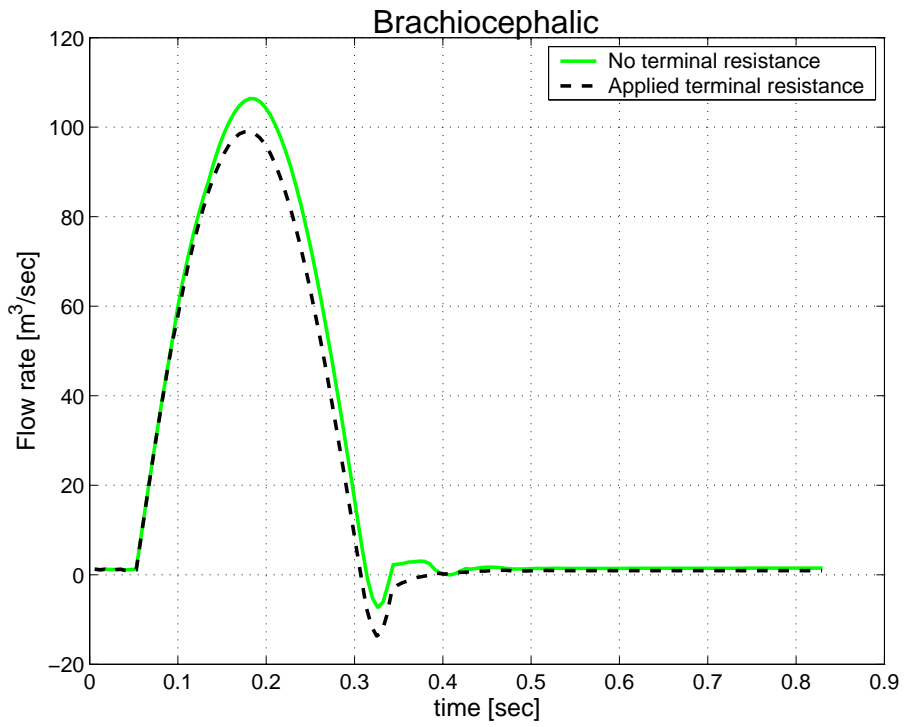


Figure 4.12: Flow rate profiles in Brachiocephalic artery (No. 3 in table 3.2).

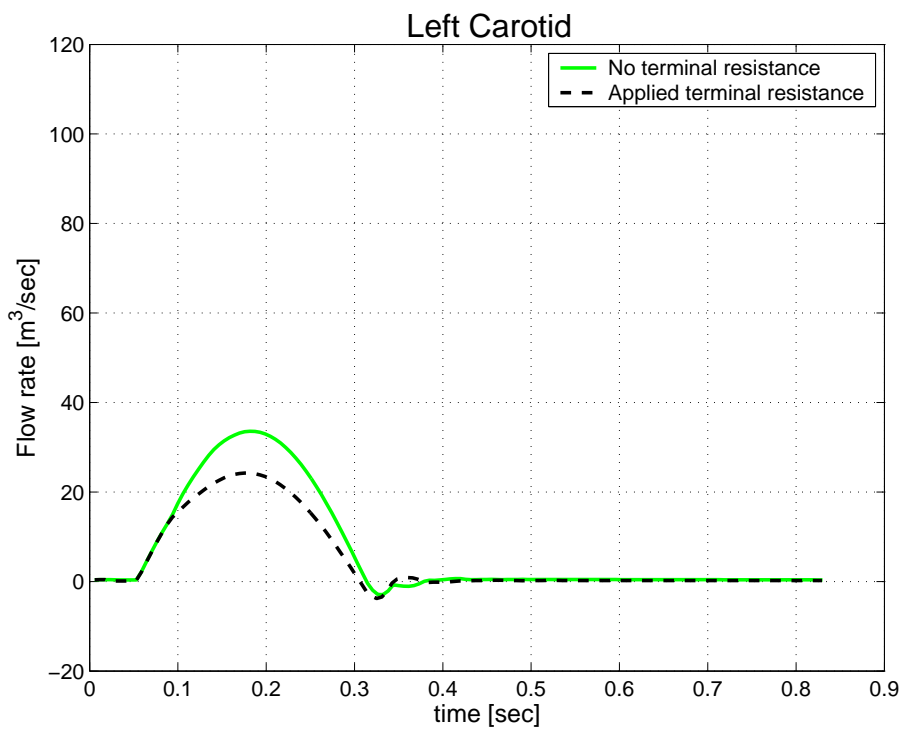


Figure 4.13: Flow rate profiles in left carotid artery (No. 15).

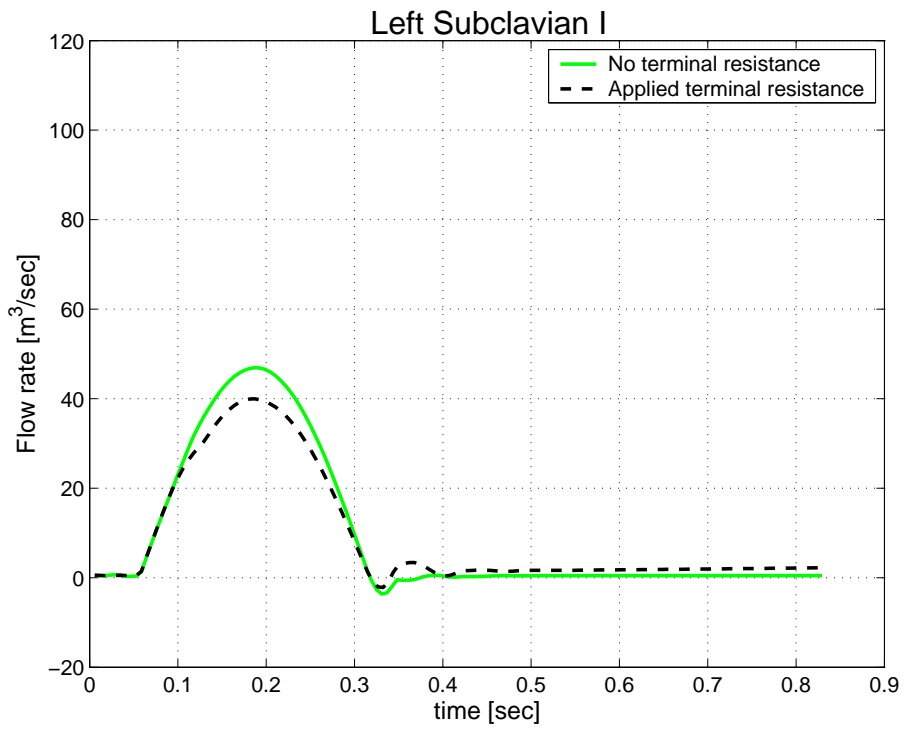


Figure 4.14: Flow rate profiles in left subclavian artery I (No. 9).

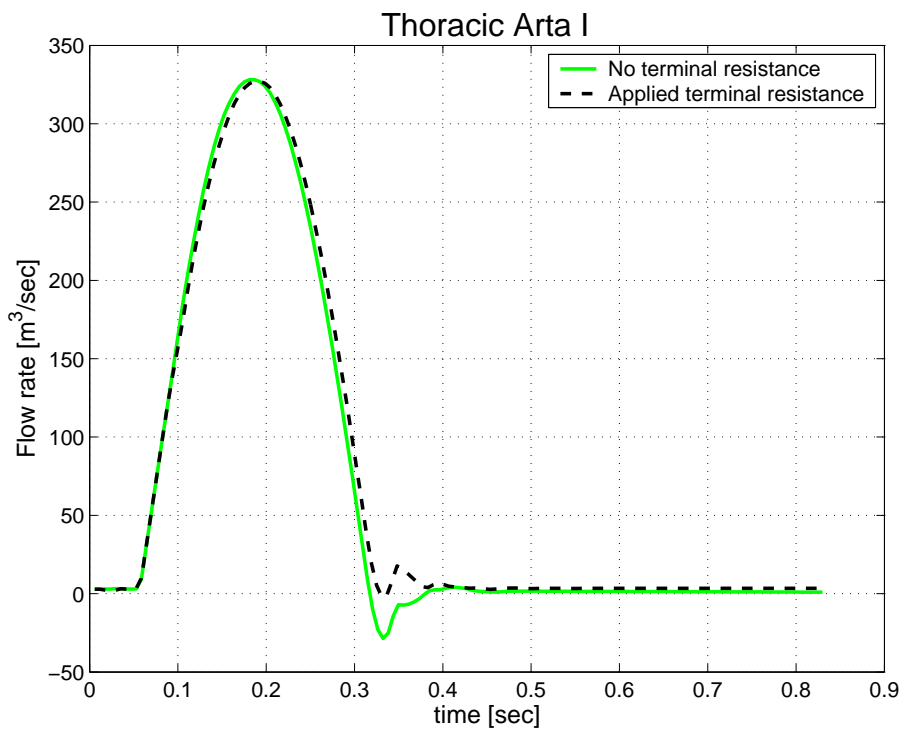


Figure 4.15: Flow rate profiles in Thoracic Aorta (No. 18).

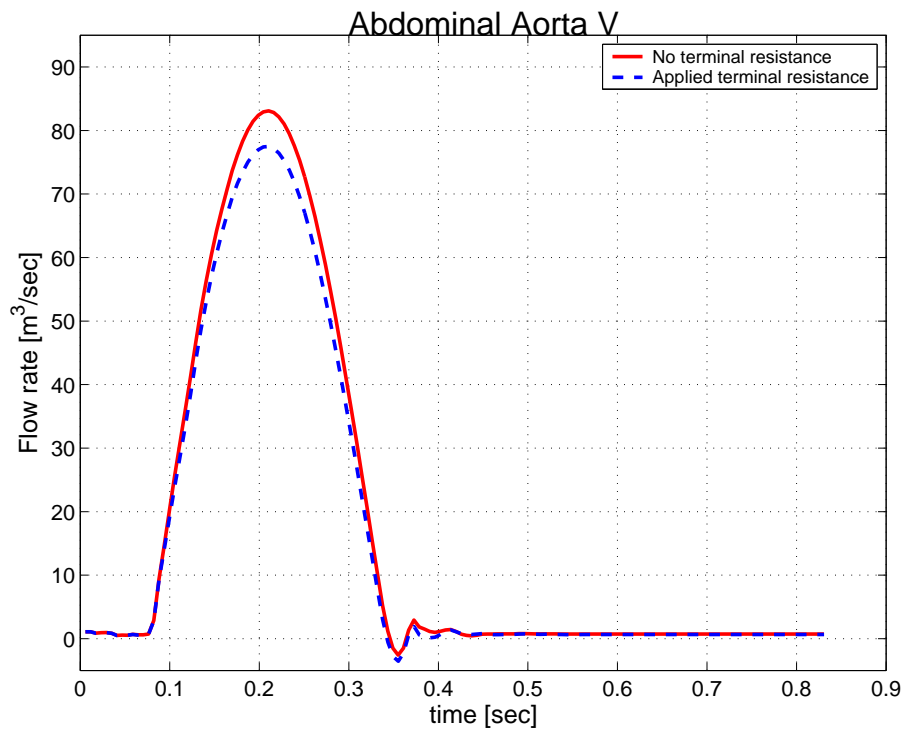


Figure 4.16: Flow rate profiles in abdominal aorta V (No. 41).

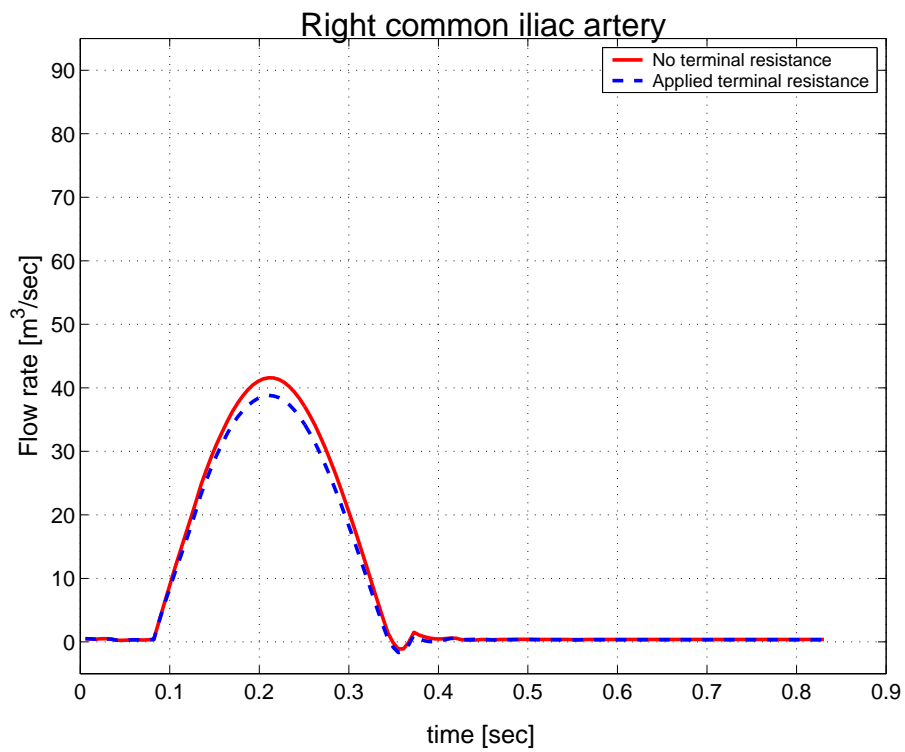


Figure 4.17: Flow rate profiles in right common iliac artery (No. 43).

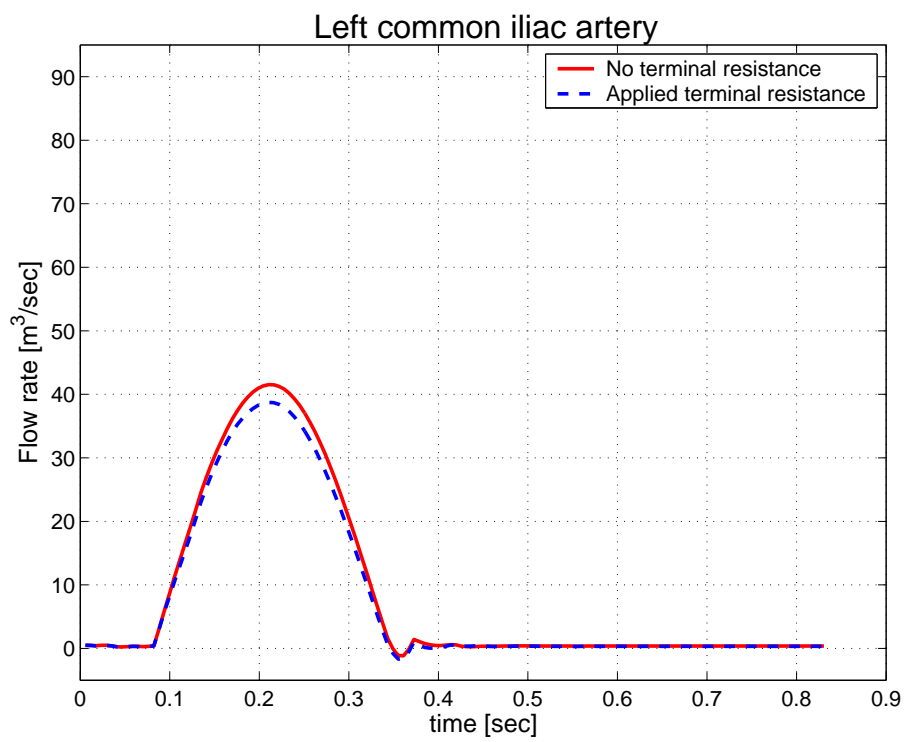


Figure 4.18: Flow rate profiles in left common iliac artery (No. 42).

Chapter 5

Conclusion and future prospects

In this project we developed a computational tool, already called *problem type*, for solving the one-dimensional problem for blood flow in arteries. We coupled a finite element code programmed in FORTRAN together with a graphical interface, suitably modified for our hemodynamic model, which has been provided by GiD, a pre-post process software for finite elements problems. Finally we applied our computational tool to a simplified vascular network containing the main human arteries.

As we already explained in the introduction chapter, one-dimensional models give useful informations about the evolution of averaged quantities along the arterial tree; as we demonstrated in the previous chapter, they allow a good description of flow rate waves in arteries at a reasonable computational cost. In fact, for what concerns our numerical solver, the calculation times and the memory used for data allocation are widely supported by a common personal computer; for example, a complete simulation of the whole 55 artery network lasts about 20 minutes, a time which is several order of magnitude lower than three-dimensional fluid dynamic models.

Regarding to 3D models, the employ of a one-dimensional formulation can be useful when we consider a multi-scale approach for the blood flow problem in arteries [3]; the simplified 1D model allows the imposition of more realistic boundary conditions for three dimensional calculations.

The problem type we developed, as well as the correct mean flow simulation, gives the opportunity to configure several parameters directly from the graphical user interface (as explained in chapter 3) without the necessity to modify the finite element code; to this purpose one of the further applications for this 1D model is the simulation of the arterial network in pathologic conditions, e.g. the presence

of stenosis, or considering the introduction of mechanical devices, e.g a stent. In these cases we can modify the geometrical and mechanical properties of the involved arteries in order to account for the contribution of such external components inserted in the vascular system.

The natural evolution of this model, starting from the 55 artery network, is on the one hand the employment of more complex formulations for what concerns both the arterial wall modelling and the type of inlet profiles, which could be as much realistic as possible with respect to the simplified waveforms used in this project. On the other hand there is the possibility to couple our network with other models of vascular sub-systems; for example we could consider the Willis circle¹ in order to expand the 1D model including also the cerebral micro-circulation. Doing so we can improve the quality of obtained results mainly for two reasons: first, the simple resistance models used to replace the distal components of the cardiovascular system cannot reproduce their hemodynamic behaviour as properly as a direct numerical simulation. Second the effects of flow redistribution, as observed from numerical tests, outline that blood flow, in a certain zone of the network, is not independent from the whole circulation in the remaining part.

¹The circle of anastomosed arteries (roughly pentagonal in outline) at the base of the brain, with the posterior communicating artery on either side joining posterior cerebral (branches of the basilar artery) to the anterior cerebral (branches of the internal carotid artery) arteries. By this full circulation to all parts of the brain can be maintained even when the carotid or vertebral arteries are blocked.

Appendix A

The GiD software

GiD is an interactive graphical user interface used for the definition, preparation and visualization of all the data related to a numerical simulation. This data includes the definition of the geometry, materials, conditions, solution information and other parameters. The program can also generate a mesh for finite element, finite volume or finite difference analysis and write the information for a numerical simulation program in its desired format. It is also possible to run the numerical simulation from within GiD and to visualize the results of the analysis.

GiD can be customized and configured by users so that the data required for their own solver modules may be generated. These solver modules may then be included within the GiD software system.

The program works, when defining the geometry, similar to a CAD (Computer Aided Design) system but with some differences. The most important one is that the geometry is constructed in a hierarchical mode. This means that an entity of higher level (dimension) is constructed over entities of lower level; two adjacent entities will then share the same lower level entity.

All materials, conditions and solution parameters can also be defined on the geometry without the user having any knowledge of the mesh: the meshing is done once the problem has been fully defined. The advantages of doing this are that, using associative data structures, modifications can be made to the geometry and all other information will automatically be updated and ready for the analysis run.

Full graphic visualization of the geometry, mesh and conditions is available for comprehensive checking of the model before the analysis run is started. More comprehensive graphic visualization features are provided to evaluate the solution results after the analysis run. This post-processing user interface is also customizable

depending on the analysis type and the results provided.

A.1 GiD basics

GiD is a geometrical system in the sense that, having defined the geometry, all the attributes and conditions (i.e., material assignments, loading, conditions, etc.) are applied to the geometry without any reference or knowledge of a mesh. Only when everything is defined, the meshing of the geometrical domain is carried out. This methodology facilitates alterations to the geometry while maintaining the attributes and conditions definitions. Alterations to the attributes or conditions can simultaneously be made without the need of reassigning to the geometry. New meshes can also be generated if necessary and all the information will be automatically assigned correctly.

GiD also provides the option of defining attributes and conditions directly on the mesh once this has been generated. However, if the mesh is regenerated, it is not possible to maintain these definitions and therefore all attributes and conditions must be then redefined.

In general, the complete solution process can be defined as:

1. Define geometry - points, lines, surfaces, volumes;
 - Use other facilities;
 - Import geometry from CAD;
2. Define attributes and conditions;
3. Generate mesh;
4. Carry out simulation;
5. View results;

Depending upon the results in step (5) it may be necessary to return to one of the steps (1), (2) or (3) to make alterations and rerun the simulations.

Building a **geometrical domain** in GiD is based on the following four geometrical levels of entities: points, lines, surfaces and volumes. Entities of higher level are constructed over entities of lower level; two adjacent entities can therefore share the same level entity. A few examples are given:

1. **example 1:** One line has two lower level entities (points), each of them at an extreme of the line. If two lines are sharing one extreme, they are really sharing the same point, which is a unique entity;
2. **example 2:** When creating a new line, what is being really created is a line plus two points or a line with existing points created previously;
3. **example 3:** When creating a volume, this is created over a set of existing surfaces which are joined to each other by common lines. The lines are, in turn, joined to each other by common points;

All domains are considered in 3-dimensional space but if there is no variation in the third coordinate (into the screen) the geometry is assumed to be 2-dimensional for analysis and results visualization purposes. Thus, to build a geometry with GiD, the users must first define points, join these together to form lines, create closed surfaces from the lines and define closed volumes for the surfaces. Many other facilities are provided for creating the geometrical domain; these include: copying, moving points, automatic surface creation, etc.

The geometrical domain can be created in a series of layers where each one is a separate part of the geometry. Any geometrical entity (points, lines, surfaces or volumes) can belong to a particular layer. It is then possible to view and manipulate some layers and not others. The main purpose of the use of layers is to offer a visualization and selection tool, but they are not used in the analysis. An example of the use of layers might be a chair where the four legs, seat, backrest and side arms are the different layers.

GiD has the option of importing a geometry or a mesh that has been created by an external CAD program. At present, this can be done via a DXF, IGES, Parasolid, ACIS, VDA, STL or NASTRAN interfaces available inside GiD.

Attributes and conditions are applied to the geometrical entities (points, lines, surfaces and volumes) using the data input dialog box. These menus are specific to the particular solver that will be utilized for the simulation and, therefore, the solver needs to be defined before attributes are defined.

Once the geometry and attributes have been defined, the mesh can be generated using the mesh generation tools supplied within the system. Structured and unstructured meshes containing triangular and quadrilateral surface meshes or tetrahedral and hexahedral volume meshes may be generated. The automatic mesh generation

facility utilizes a background mesh concept for which the users are required to supply a minimum number of parameters.

Simulations are carried out from within GiD by using the **calculate** menu. Indeed, specific solvers require specific data that must have been prepared previously. A number of solvers may be incorporated together with the correct pre-processing interfaces.

The final stage of **graphic visualization** is flexible in order to allow the users to critically evaluate the results quickly and easily. The menu items are generally determined by the results supplied by the solver module. This not only reduces the amount of information stored but also allows a certain degree of user customization. One of the major strengths of GiD is the ability for the users to define and configure their own graphic user interface within GiD. This is done by creating some configuration files which define new windows, where the final user will enter data, such as materials or conditions. The format that GiD uses to write a file containing the necessary data in order to run the numerical simulation program must also be defined in a similar way. This pre-processor or data input interface will thus be tailored specifically for the users simulation program, but using the facilities and functionality of the GiD system.

The user's simulation program can then be included within GiD so that it may be run utilizing the calculate menu option.

The third step consists of writing an interface program that provides the results information in the format required by the GiD graphic visualizer, thereby configuring the post-processing menus. This post analysis interface may be included fully into the GiD system so that it runs automatically once the simulation run has terminated.

A.2 Problem type customization

When GiD is to be used for a particular type of analysis, it is necessary to predefine all the information required from the user and to define the way the final information is given to the solver module. To do so, some files are used to describe conditions, materials, general data, units systems, symbols and the format of the input file for the solver. We call **problem type** to this collection of files used to configure GiD for a particular type of analysis.

Due to the vocation of GiD as general purpose pre and post processor, the configuration for the different analysis must be performed according to the particular

specifications of every solver. This implies the necessity of creating specific data input files for every solver. However, GiD allows to perform this configuration process inside itself without any change in the solver and without having to program any independent utility.

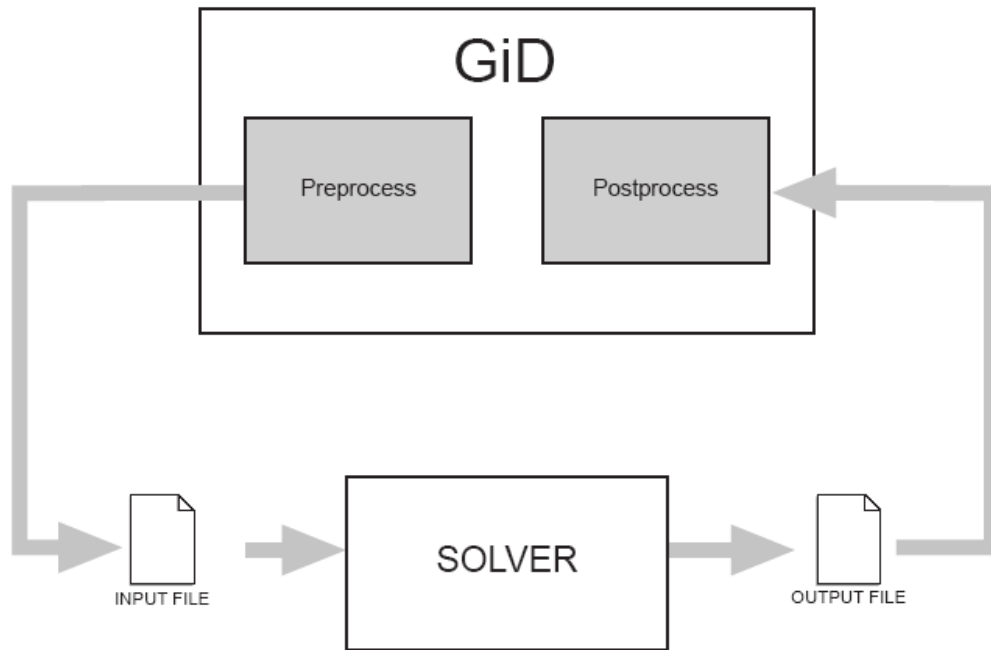


Figure A.1: Flowchart describing the execution of a GiD problem type

To configure these files means to define the data that must be input by the user, as well as the materials to be implemented and other geometrical and time-dependent conditions. It is also possible to add some symbols or drawings to represent the defined conditions. GiD gives the opportunity of working with units when defining the properties of the mentioned data, but there must be a configuration file where it could be found the definition of the units systems. It must be also defined the way that all this data must be written inside a file that will be the input file to be read by the corresponding solver.

The definition of a **problem type** implies the creation of a directory with the problem type name and the extension `.gid`. The series of files must be inside the problem type directory. The name for most of them will be composed by the same problem type's name and an extension referring to their function. Considering `problem_type_name` to be the name of the problem type and `project_name` the name of the project, the diagram of the file configuration is the following:

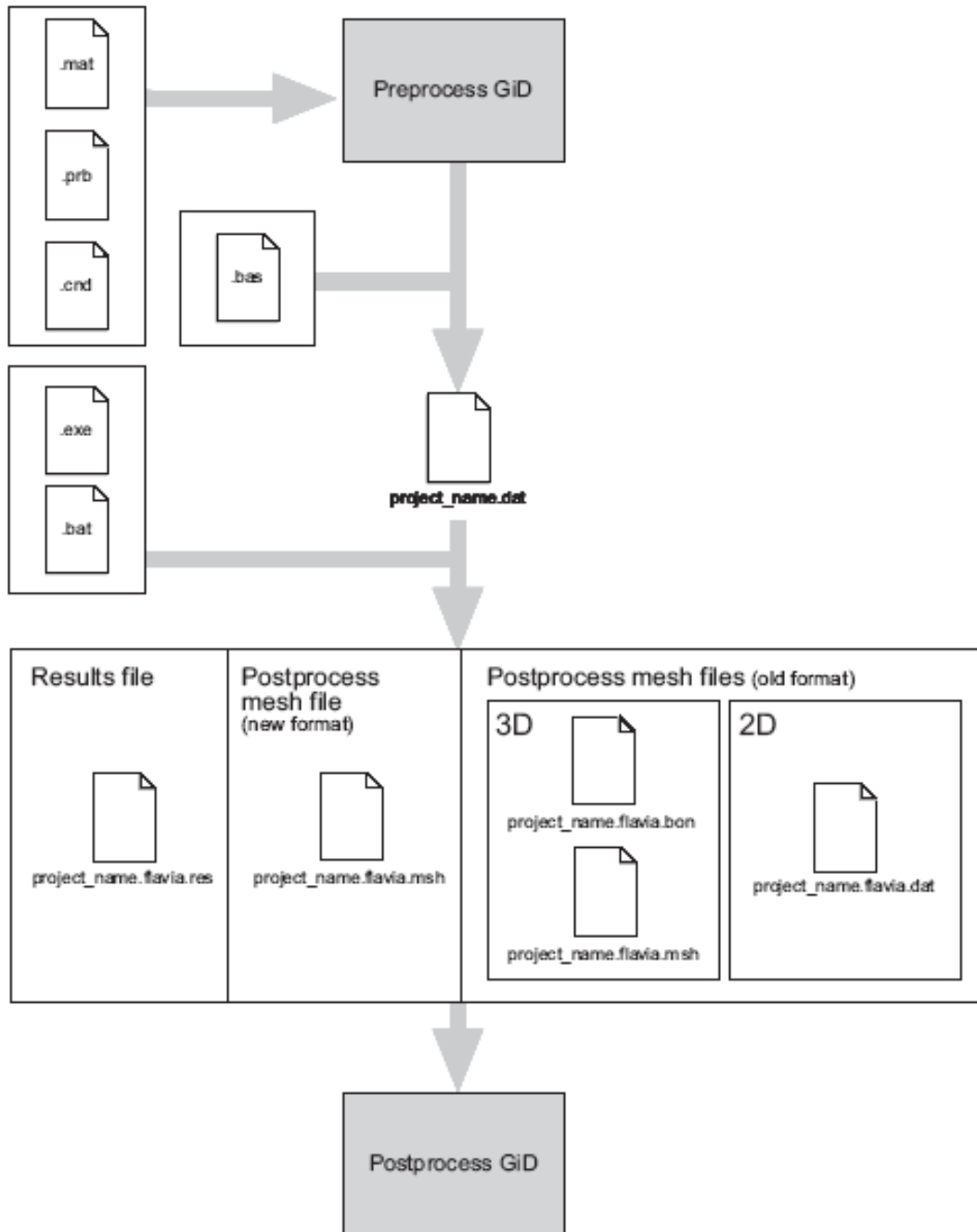


Figure A.2: Problem type flowchart including file configuration.

A.2.1 Configuration files

These files, whose location into the problem type structure is showed in figure A.2, generate the conditions and material properties, as well as the proper general problem and intervals data to be transferred to the mesh, giving at the same time the chance to define geometrical drawings or symbols to represent some conditions on the screen. Now a brief description is given related to those files which play an important role into the problem type structure.

Condition file (.cnd)

The file with extension's name `.cnd` contains all the information about the conditions that can be applied to different entities. The condition can adopt different field values for every entity. This type of information includes, for instance, all the displacement constraints and applied loads in a structural problem or all the prescribed and initial temperatures in a thermal analysis.

A **condition** can be considered as a group of fields containing the name of the referred condition, the geometric entity over which it is applied, the mesh entity over which it will be transferred, its corresponding properties and their values.

Material file (.mat)

This file `projectname.mat` include originally the definition of different materials through their properties. These are base materials as they can be used as templates during the pre-processing step for the creation of newer ones.

The user can define as many materials as desired and with a variable number of fields. All the unused materials will not be taken in consideration when writing the data input files for the solver. Alternatively, they can be useful to generate a materials library.

Conversely to the case of conditions, the same material can be assigned to different geometrical entities levels (lines, surfaces or volumes) and even can be assigned directly to the mesh elements. In a similar way as a condition was defined, a material can be considered as a group of fields containing its name, its corresponding properties and their values.

Problem and interval data (.prb)

The file `projectname.prb` contains all the information about the general problem and intervals data. The general problem data is all the information required for performing the analysis and it does not concern any particular geometrical entity. This differs from the previous definitions of conditions and materials properties, which are assigned to different entities. Example of general problem data can be the type of solution algorithm used by the solver, the value of the various time steps, convergence conditions and so on.

Within this data, the user may consider the definition of specific problem data (for the whole process) and intervals data (variable values along the different solution intervals). An interval would be the subdivision of a general problem that contains its own particular data. Typically, one can define a different load case for every interval or, in dynamic problems, not only variable loads, but also changing the various time steps, convergence conditions and so on.

Template file (.bas)

Once the user has generated the mesh, assigned the conditions and the materials properties, as well as the general problem and intervals data for the solver, it is necessary to produce the data input files to be processed by that program.

To manage this reading, GiD employs a file called `problem_type_name.bas`, where `problem_type_name` is the name of the working directory of the problem type without the `.bas` extension.

This template file describes the format and structure of the required data input file for the solver that is used in a particular case.

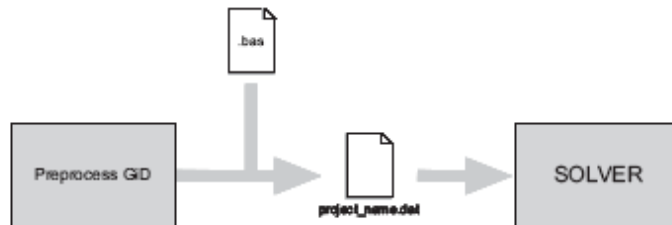


Figure A.3: Interaction between pre process and solver by means of the template `.bas` file

These files work as interface from GiD standard results to the specific data input for any individual solver module. This allows to complete the process of running

the analysis as one step more within the system, and to visualize results during post-process.

A.3 Post-process data files

In the GiD postprocess you can study the results obtained from a solver program. The communication between the solver and the GiD Postprocess is made using files. The solver program has to write the results in a file that must have the extension `.flavia.res` and its name must be the project name.

The solver program can also (it is not mandatory) give to GiD the postprocess mesh, and should have the extension `.flavia.msh`. If this mesh is not provided by the solver program, GiD uses in the post-process, the preprocess mesh.

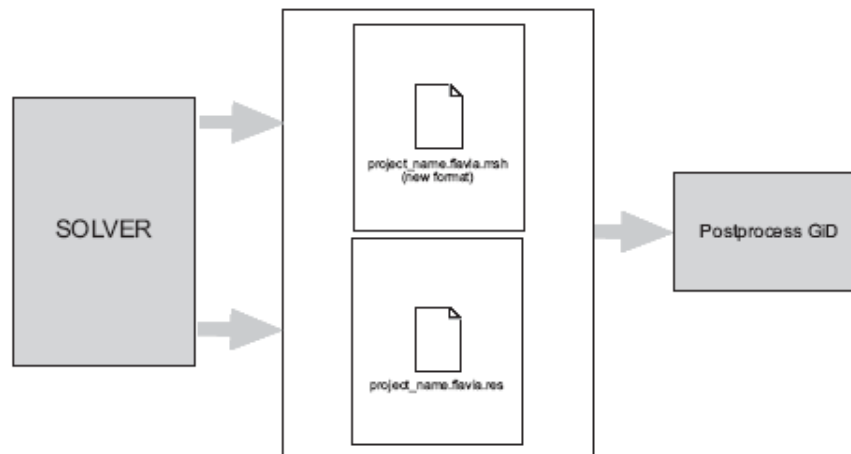


Figure A.4: Post-process file creation

So, post-processing files are ASCII files and can be separated into two categories:

- Mesh Data File: `projectname.flavia.msh` for volume and surface (3D or 2D) mesh informations; it should contain nodal coordinates of the 3D mesh, and its nodal connectivities and the material of each element;
- Result Data File: `projectname.flavia.res` for nodal variables. GiD allows the user to define as many nodal variables as desired, as well as several steps and analysis cases (limited only by the memory of the machine).

Appendix B

Finite element code *Arteries-1D.exe*

Here we present a general scheme concerning the finite element code which represents the computational core of our GiD problem type. This program, developed in Fortran 90, links together pre and post process phases, as it receives input data configured through the graphical interface and creates an output result file that will be used during postprocess.

B.1 Input-output data files

Considering a generic problem related to 1D blood flow model, the input informations, required by the solver, are provided by two different files whose structure is the following

1. "**projectname**".**dat**, is the *computation file* created by GiD after the pre-process phase is terminated; it contains, in order:
 - Finite mesh parameters: the number and coordinates of mesh nodes together with the number and connectivities of mesh elements;
 - Geometrical and mechanical properties of each vessel: length, wall thickness, Young Modulus, Poisson Ratio and initial wave speed;
 - General properties, e.g. project name, type of velocity profile, blood density and viscosity;
 - Numerical parameters, e.g. error tolerances, selection of space-time scheme and maximum number of iterations;
 - List of boundary nodes, each one with its applied conditions;

For more informations, chapter 3 contains all the interface windows in which such parameters can be configured and modified.

2. **bifurcations.dat**: this file contains the list of all bifurcations belonging to the arterial network, and for each one of them are indicated, in order, the entering and the outgoing vessels;

The program creates two *output* files, one accounting for 3D mesh properties and the other containing the results. Briefly they are structured as follows:

1. **"projectname".flavia.msh**: contains both the node coordinates and the element connections of the three-dimensional mesh used for the postprocess visualization of results;
2. **"projectname".flavia.res**: It is the result file which GiD reads during post-process and can contain values of Area, Flow rate, pressure and velocity on each node belonging to the 3D output mesh. The user, during pre-process, can select how many time steps write in such a file and also establish which quantities share during post-process (also see figure 3.9 in chapter 3);

B.2 Finite element code flowchart

The finite element code is composed by a main routine whose structure is schematized in table B.2. We start with the data acquisition from the input files previously described, first reading the bifurcation list and then the pre-process informations provided by GiD; once that all these data are allocated in memory, we are ready to compute the numerical solution. To do this, we need, on the one hand, to transform 3D coordinates of the pre-process geometry into a 1D reference system for each vessel in the model, in order to work only with the axial quantity z and neglect the other cylindrical components (r, θ) . On the other hand we must impose initial data which allow to start calculating the approximated solution of our hemodynamic problem. Two routines, external to the main structure, are used to carry out such operations:

1. *OMOG_TRANSF*:
 - Input variables: *trans_type*.
 - Output variables: *omog*.

This routine applies a homogeneous transformation to each node coordinate from 3D pre-process to 1D format. Both the rotation matrix and the center coordinates for each vessel reference system are read from GiD input file and assembled into a 4x4 *homogeneous transformation matrix*. For the generic i-th artery we have:

$$A_t^i = \begin{bmatrix} \mathbf{R}^i & \mathbf{d}^i \\ 0 & 1 \end{bmatrix},$$

being R^i the i-th rotation matrix and d^i the (x, y, z) center components. The output variable *omog* represents the matrix A_t^i and, depending on the value of *trans_type*, we may have:

- *trans_type* = 1: pass from 3D to 1D notation. Then

$$\mathbf{P}_{1D} = \mathbf{A}_t^T \mathbf{P}_{3D} \implies \text{omog} = \mathbf{A}_t^T$$

- *trans_type* = 2: pass from 1D to 3D notation. Then

$$\mathbf{P}_{3D} = \mathbf{A}_t \mathbf{P}_{1D} \implies \text{omog} = \mathbf{A}_t$$

with P_{1D} and P_{3D} defined as 4x1 arrays containing node coordinates in 1D and 3D notation respectively:

$$P_{1D} = \begin{bmatrix} \mathbf{d}_{1D} \\ 0 \end{bmatrix} \quad P_{3D} = \begin{bmatrix} \mathbf{d}_{3D} \\ 0 \end{bmatrix}$$

2. INITIAL_VALUES(2):

- Output variables: A_{t0}, Q_{t0}

Through this routine we evaluate initial values of area A_{t0} and flow rate Q_{t0} into each vessel of our network; by default we have values of A_0 related to the reference configuration of the arterial tree in rest conditions (see also chapter 2). For what concerns the flow rate we know that, at rest, blood velocity is the same in every network location so it is true the relationship

$$u_i = u_0 \implies \frac{Q_i}{A_i} = \frac{Q_0}{A_0} \implies Q_i = Q_0 \frac{A_i}{A_0}$$

between the vessel 0, where we apply an initial condition on blood flow, and the generic vessel i belonging to the network.

Now we have 1D coordinates and initial solution values, it is possible to apply the numerical space-time scheme for solving the problem. Before doing this, we generate the 3D mesh for post-process visualization of results; to this purpose we use the meshing routine indicated into the scheme B.2 with the number 3:

3. *MESHING*: this routine allows the creation of a 3D mesh simply considering 1D nodes lying on vessel axial directions; each one of these nodes becomes the center of a new circular section, with reference radius R_0 , which has a certain number of points projected, along radial direction, from the center to the border circumference (fig. B.1).

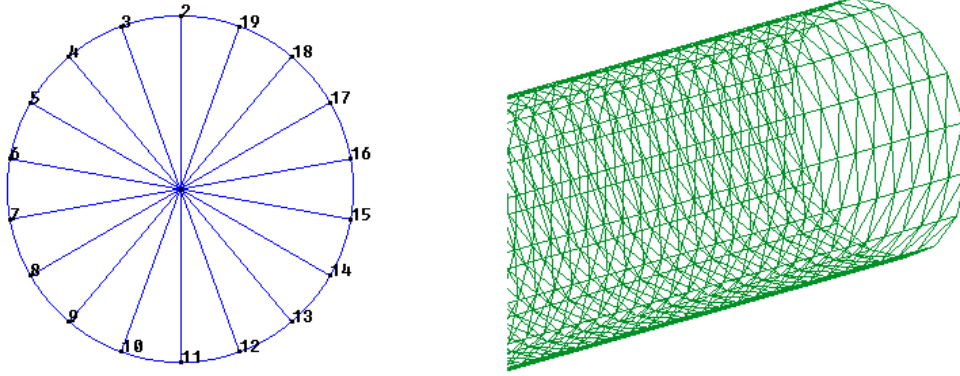


Figure B.1: Left figure: sketch of a 3D-mesh section. The number of radial nodes can be settled into GiD preprocess (see fig. 3.9 in chapter 3). Right figure: side wall meshing for a generic vessel. The element are triangular and link nodes belonging to different radial sections.

Moreover these nodes are connected to form a cylindrical surface of triangular elements over the side walls of each artery (fig. B.1);

The computation core of our finite element code is represented in the scheme B.2 by the block **SOLVER (L1)**. When the program execution arrives at this point, it enters a **WHILE** loop which iterates in time from t_0 to $t_{end} = t_0 + T$, where T is the integration period of our problem. As shown in table B.2, we move step by step evaluating the solution matrix \mathbf{U}^1 for each time instant i .

The block **RK L(2)** represent the point in the **WHILE** loop where \mathbf{U} is computed. As explained in chapter 2, we employ an explicit Runge-Kutta (RK) scheme for time integration; the program allows to choose between a 2nd and a 4th order

¹For every time step, the solution is composed by values of A and Q at each 1D mesh node. So the dimension of \mathbf{U} , and also the *rhs* term used further, is 2 x number of nodes.

RK, while for our schematization we consider only the 4th order one, whose structure is

$$\begin{aligned}
U^{n+1} &= U^n + \frac{\Delta t}{6}(K_1 + 2K_2 + 2K_3 + K_4) \\
K_1 &= f^n, \\
K_2 &= f(t^n + \frac{\Delta t}{2}, U^n + \frac{\Delta t}{2}K_1), \\
K_3 &= f(t^n + \frac{\Delta t}{2}, U^n + \frac{\Delta t}{2}K_2), \\
K_4 &= f(t^{n+1}, U^n + \Delta t K_3).
\end{aligned} \tag{B.1}$$

The 2nd order Runge-Kutta scheme has a structure similar the 4th order one, which consider only two intermediate evaluation for each step Δt :

$$\begin{aligned}
U^{n+1} &= U^n + \frac{\Delta t}{2}K_2 \\
K_1 &= f^n, \\
K_2 &= f(t^n + \frac{\Delta t}{2}, U^n + \frac{\Delta t}{2}K_1),
\end{aligned}$$

The scheme RK L(2) in table B.2 shows the numerical scheme: first we set the time step Δt^i in order to satisfy the CFL convergence condition (see the relationship (2.48) in chapter 2), then we proceed with the RK routine. The discrete equation to evaluate can be expressed, simplifying the (2.46) we derived in chapter 2, as follows

$$\frac{U^{n+1} - U^n}{\Delta t} = rhs(t^n, U^n) \tag{B.2}$$

For each intermediate *rhs* evaluation K_i , $i = 1 : 4$, we use the finite element routine **RHS L(3)**; by means of a loop over the linear elements of the 1D mesh, we first evaluate the single contribution provided by each element and little by little we assembly it into the global right hand side matrix² for the whole mesh. Once this operation is terminated, we have to complete the *rhs* term with the boundary conditions not introduced during the element loop. The flowchart RHS L(3) from table B.2 schematize all these operations, and includes the following block:

4. *UPDATE BOUNDARY VALUES*: It is an updating routine for boundary nodes including inlet, outlet and branching points. For each one of these conditions we act in the following ways

²Analogously to U , also the term *rhs* has dimension 2 x number of 1D mesh nodes.

- **Inlet nodes:** here we impose the known value of area or flow rate depending on the inlet profile considered (see chapter 2);
- **Bifurcation nodes:** in this case we have to solve the six equation system (see (2.49) in chapter 2) in order to obtain (A, Q) values at vessel interfaces belonging to each bifurcation. Such quantities must respect the compatibility relationships defined in the non-linear equations contained into (2.49);
- **Outlet nodes:** we have two possible outlet conditions: the first is the absorbing one, and we use the pseudo-characteristic evaluation (see section 2.6) to extract values of area and flow rate. The other condition accounts for the resistive term R_T and in this case we apply the relationship between flow and pressure:

$$P = QR_T.$$

Now the *rhs* term is complete, we can use it to evaluate the corresponding intermediate step into the RK scheme; proceeding in this way we finally obtain the solution of equation (B.2) for the current *i*-th step. Then the program exits from the **RK L(2)** routine and returns into the **SOLVER L(1)** block. Here we have the writing phase of the obtained result:

5. *OUTPUT*: creates the postprocess file, whose format is recognized by GiD, and writes the results which can be showed through the software graphical interface. This routine is not executed at each time step, but with a certain frequency in order to finally write the approximated number of iteration defined during pre-process (see figure 3.9 in chapter 3);

MAIN

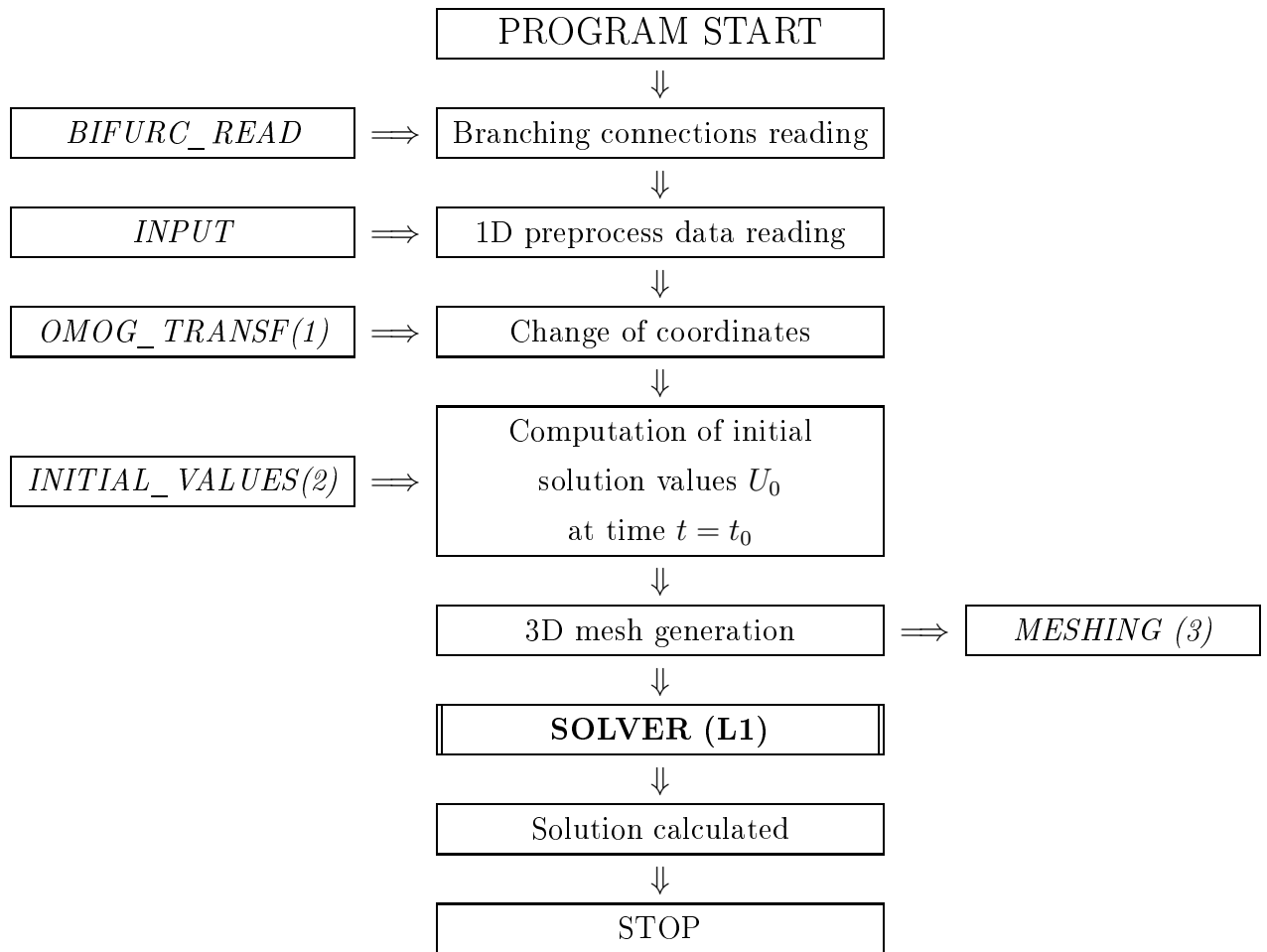


Table B.1: Main program flowchart: input data are read and allocated in memory, while the definition of initial conditions allow to start calculating the approximated solution.

SOLVER L(1)

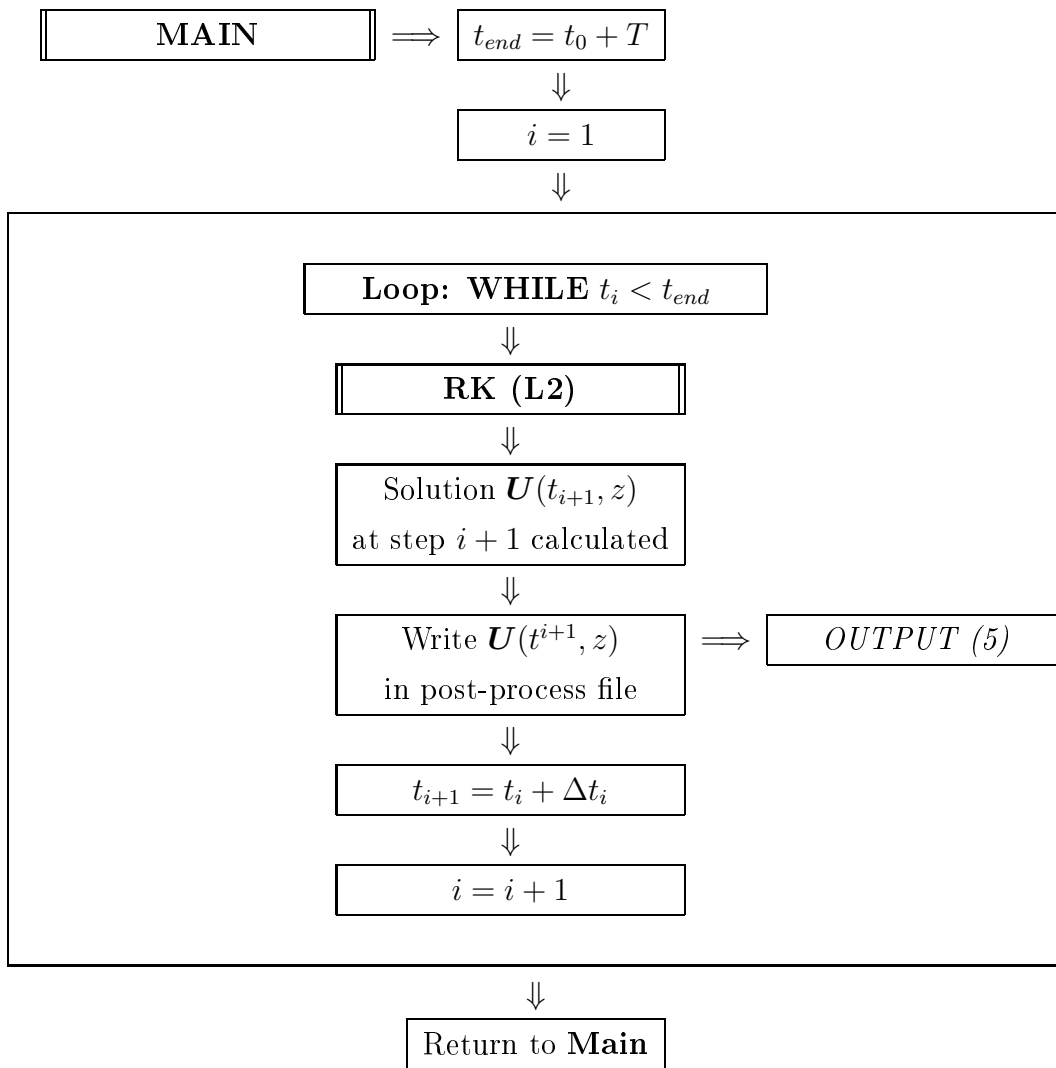
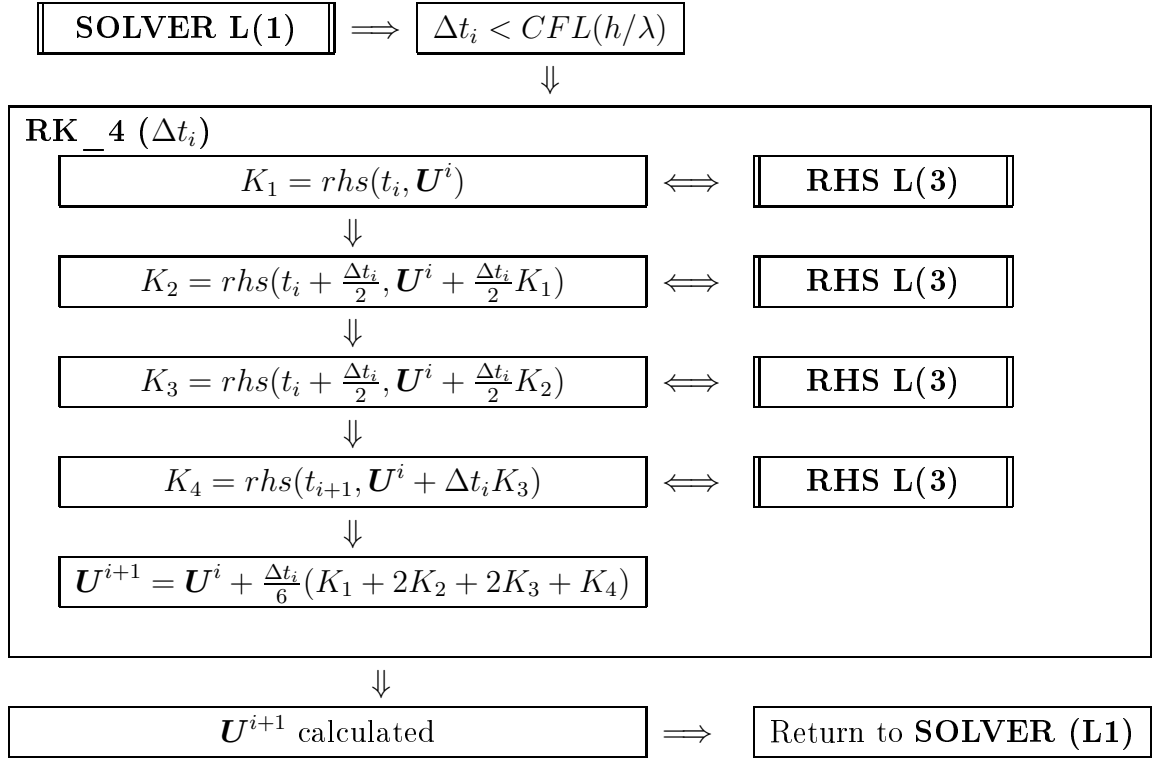


Table B.2: Solver routine flowchart.

RK L(2)



RHS L(3)

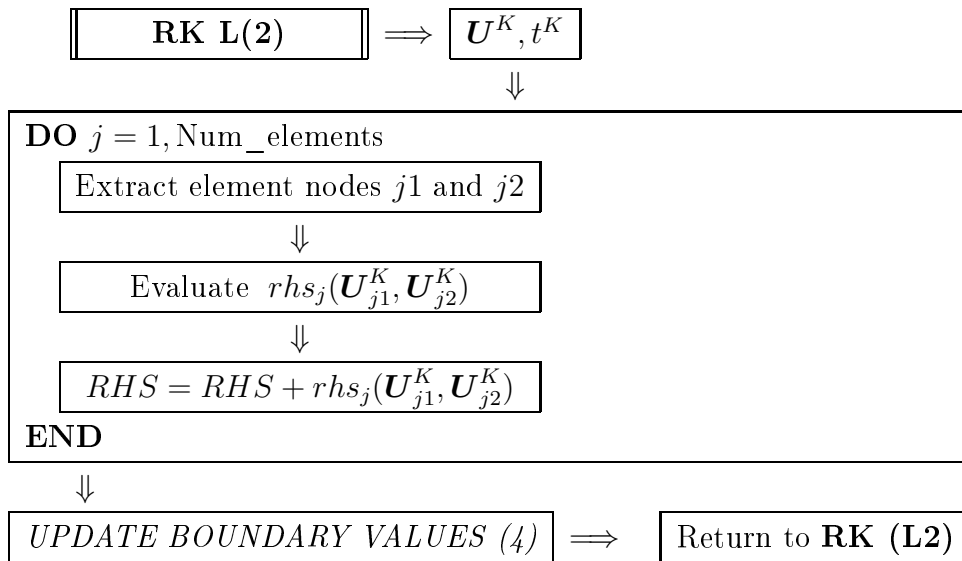


Table B.3: Runge-Kutta and FEM routines

Bibliography

- [1] J. Donea, S. Giuliani, H. Laval, and L. Quartapelle. Time-accurate solutions of advection-diffusion problems by finite elements. *Comp. Meth. Appl. Mech. Engrng*, 71:93–122, 1984.
- [2] L. Euler. Principia pro motu sanguinis per arteries determinando. *Opera posthuma mathematica et physica anno 1884 detecta*, 2:814–823, 1775.
- [3] L. Formaggia, J.F. Gerbau, F. Nobile, and A. Quarteroni. On the coupling of 3D and 1D Navier-Stokes equation for flow problems in compliant vessels. *Comput. Methods Appl. Mech. Engrg.*, 191:561–582, 2001.
- [4] L. Formaggia, D. Lamponi, and A. Quarteroni. One dimensional model for blood flow in arteries. *Journal of Engineering mathematics*, 47:251–276, 2003.
- [5] E. Godlewski and P.A. Raviart. *Numerical approximation of hyperbolic systems of conservation laws*, volume 118 of *Applied mathematical sciences*. Springer-Verlag, New York, USA, 1996.
- [6] G.W. Hedstrom. Nonreflecting boundary conditions for nonlinear hyperbolic systems. *Journal of Computational Physics*, 30:222–237, 1979.
- [7] A. Jameson, W. Schmidt, and E. Turkel. Numerical solution of the Euler equations by Finite Volume Methods using Runge-Kutta time-stepping schemes. *AIAA*, pages 81–1259, 1981.
- [8] D.J. Korteweg. Uber die fortpflanzungesgeschwindigkeit des schalles in elastischen rohern. *Ann. Phys. Chem. (NS)*, 5:525–527, 1878.
- [9] G.J. Langewouters, K.H. Wesseling, and W.J. Goedhard. The elastic properties of 45 human arteries and 20 abdominal aortas in vitro and the parameters of a new model. *J. Biomech.*, **17**(6):425–435, 1984.

- [10] P.D. Lax and B. Wendroff. Difference schemes for hyperbolic equations with high order accuracy. *Comm. Pure Appl. Math.*, 17:381, 1964.
- [11] R. Löhner. *Applied computational fluid dynamics techniques: An introduction based on finite element methods*. John Wiley & Sons Ltd, School of computational Sciences, George Mason University, Fairfax, Virginia, USA, 2001.
- [12] P.R.M. Lyra and K. Morgan. A review and comparative study of upwind biased schemes for compressible flow computation. part i: 1-D first-order schemes. *Arch. Comp. Meth. Engng*, 7(1):19–55, 2000.
- [13] A.I. Moens. Over de voortplantingssnelheid von den pols (on the speed of propagation of the pulse. Technical report, Leiden, 1877.
- [14] M. Olufsen, H. Tran, and Johnny Ottesen. Modeling cerebral blood flow control during posture change from sitting to standing. *Cardiovascular Engineering: An International Journal*, 4:47–58, 2004.
- [15] F. Phythoud, N. Stergiopoulos, and J.J. Meister. Forward and backward waves in the arterial system: non-linear separation using riemann invariants. *Technology and Health Care*, 3:201–207, 1995.
- [16] L. Quartapelle. *Numerical solution of the incompressible Navier-Stokes equations*. Birkhäuser Verlag, Basel, 1993.
- [17] A. Quarteroni and L. Formaggia. *Modelling of living systems*, volume Handbook of Numerical Analysis, chapter Mathematical modelling and numerical simulation of the cardiovascular system. Elsevier, Amsterdam, 2001.
- [18] A. Quarteroni, M. Tuveri, and Veneziani A. Computational vascular fluid dynamics: Problems, models and methods. *Computing and Visualization in Science*, 2:163–197, 2000.
- [19] A. Quarteroni and A. Valli. *Domain decomposition methods for partial differential equations*, volume 118 of *Applied mathematical sciences*. The Clarendon Press Oxford University Press, New York, USA, 1999.
- [20] B. Riemann. Gesammelte mathematische werke und wissenschaftlicher nachlass. *Leipzig, B.G. Teubner (ed.)*, pages 145–164, 1876. originally published as

"Ueber die Fortpflanz ebener luftwellen von endlicher Schwingungsweite. Technical report, Gottingen 8 (1860) 43.

- [21] S.J. Sherwin, L. Formaggia, J. Peiró, and V. Franke. Computational modelling of 1D blood flow with variable mechanical properties and its application to the simulation of wave propagation in the human arterial system. *Int. J. Numer. Meth. Fluids*, pages 673–700, 2003.
- [22] S.J. Sherwin, V. Franke, J. Peiró, and Parker K. One-dimensional modelling of a vascular network in space-time variables. *J. Engng. Math.*, 47:217–250, 2003.
- [23] R. Skalak. The synthesis of a complete circulation. in: D. bergel (ed.). *Cardiovascular Fluid Dynamics*, vol 2:341–376, 1972. London: Academic Press.
- [24] N.P. Smith, A.J. Pullan, and P.J. Hunter. An anatomically based model for transient coronary blood flow in the heart. *SIAM J. Appl. Math.*, 62:990–1018, 2003.
- [25] N. Stergiopoulos, D.F. Young, and T.R. Rogge. Computer simulation of arterial flow with application to arterial and aortic stenoses. *J. Biomech.*, 25:1477–1488, 1992.
- [26] J.C. Stettler, P. Niederer, and M. Anliker. Theoretical analysis of arterial hemodynamics including the influence of bifurcations part i: Mathematical model and prediction of normal pulse patterns. *Ann. Biomed. Eng.*, 9:145–164, 1981.
- [27] J.C. Stettler, P. Niederer, and M. Anliker. Theoretical analysis of arterial hemodynamics including the influence of bifurcations part ii: Critical evaluation of theoretical model and comparison with noninvasive measurements of flow patterns in normal and pathological cases. *Ann. Biomed. Eng.*, 9:165–175, 1981.
- [28] V.L. Streeter, W.F. Keitzer, and D.F. Bhor. Pulsatile pressure and flow through distensible vessels. *Circulation Research*, 13:3, 1963.
- [29] C.A. Taylor, T.J.R. Hughes, and C.K. Zarins. Finite element modeling of blood flow in arteries. *Comput. Methods Appl. Mech. Engrg.*, 158:155–196, 1998.
- [30] K.W. Thompson. Time dependent boundary conditions for hyperbolic systems. *Journal of Computational Physics*, 68:1–24, 1987.

- [31] I.E Vignon and C.A. Taylor. Outflow boundary conditions for one-dimensional finite element modeling of blood flow and pressure waves in arteries. *Wave Motion*, 39:361–374, 2004.
- [32] J. Wan, B. Steele, A.S. Spicer, S. Strohband, G.R. Feijoo, T.J.R. Hughes, and C.A. Taylor. A one-dimensional finite element method for simulation-based medical planning for cardiovascular disease. *Comp. Meth. Boimech. Biomed. Engng*, 5(3):195–206, 2002.
- [33] J.J. Wang and K.H. Parker. Wave propagation in a model of the arterial circulation. *J. Biomech.*, 37:457–470, 2004.
- [34] N. Westerhof and A. Noordergraaf. Arterial viscoelasticity: a generalized model. Effect on input impedance and wave travel in the systemic tree. *J. Biomech.*, 3:357–379, 1970.
- [35] J.R. Womersley. An elastic tube theory of pulse transmission and oscillatory flow in mammalian arteries. *Technical Report WADC Technical Report TR*, pages 56–614, 1957. Wright Air Development Center.
- [36] T. Young. Hydraulic investigations, subservient to an intended croonian lecture on the motion of the blood. *Phil. Trans. Roy. Soc., London*, 98:164–186, 1808.

First of all, I want to thank Prof. Eugenio Oñate and Prof. Ferdinando Auricchio for giving me the opportunity to prepare my thesis at CIMNE. I want to thank as well all the researchers who helped me during the realization of this project, in particular Eng. Eduardo Soudah (mi jefe), Eng. Enrique Ortega for the fluid-dynamic part and Eng. Carlos Labra for the programmation part.

Sincere thanks to Dr. Francesc Carreras at Santa Creu I Sant Pau Hospital of Barcelona for having provided experimental MRI blood flow profiles.

Quiero agradecer también todo los chicos de la Mazmorra (Adrian, Hiram, Xavi, Bego, Elke, Alex, Jordi, Dani, Cruchi, Esteffen y Claudio) por sus disponibilidad durante toda mi permanencia en CIMNE.

E un ultimo, ma non meno importante, ringraziamento va a tutte quelle persone che in questi anni mi hanno salvato dalla pazzia: in primis la 'cumpa' (Die, Teo, Biste, Mes, Pato, Beppe, Mone, Gire, Marghe, Silvia), Maurizio e gli altri bioamici (Giò, Ste, Curo, Nocci, Deborah, Matteo, Carmelo, Simona, Noemi e Leo), la Pallavolo Casteggio (Fabio, Marchino, Lore, Fara, Mago, Garba, Jesus, Pasto, Della, Simo, Ciccio, Cico) e poi Ale Reali, Fugo, Dario, Mauro, Marzia, Paolo Jonny, Rocco, Maddy, Paolo Ronda, Ste Piazza e tutti quelli che ho dimenticato...